USING HDG+ TO COMPUTE SOLUTIONS OF THE 3D LINEAR ELASTIC AND POROELASTIC WAVE EQUATIONS

by

Allan Hungria

A dissertation submitted to the Faculty of the University of Delaware in partial fulfillment of the requirements for the degree of Doctor of Philosophy in Mathematics

Summer 2019

USING HDG+ TO COMPUTE SOLUTIONS OF THE 3D LINEAR ELASTIC AND POROELASTIC WAVE EQUATIONS

by

Allan Hungria

Approved: ____

Dr. Louis Rossi, Ph.D.
Chair of the Department of Mathematics

Approved: ____

Dr. John Pelesko, Ph.D.
Interim Dean of the College of Arts and Sciences

Approved: ____

Dr. Doug Doren, Ph.D.
Interim Vice Provost for Graduate and Professional Education and
Dean of the Graduate College

I certify that I have read this dissertation and that in my opinion it meets the academic and professional standard required by the University as a dissertation for the degree of Doctor of Philosophy.

Signed: ____

Dr. Francisco-Javier Sayas, Ph.D.
Professor in charge of dissertation

I certify that I have read this dissertation and that in my opinion it meets the academic and professional standard required by the University as a dissertation for the degree of Doctor of Philosophy.

Signed: ____

Dr. Peter Monk, Ph.D.
Co-chair of dissertation committee

I certify that I have read this dissertation and that in my opinion it meets the academic and professional standard required by the University as a dissertation for the degree of Doctor of Philosophy.

Signed: ____

Dr. Constantin Bacuta, Ph.D.
Member of dissertation committee

I certify that I have read this dissertation and that in my opinion it meets the academic and professional standard required by the University as a dissertation for the degree of Doctor of Philosophy.

Signed: ____

Dr. Bernardo Cockburn, Ph.D.
Member of dissertation committee

ACKNOWLEDGEMENTS

Neither this dissertation, nor, indeed, my continued existence, would have been possible without the love and sacrifice of my wife, Christina.

As I dance across my living room floor with Rosa (my service dog), I cannot but be reminded of the generosity, wisdom, guidance, and support of my advisor, Francisco-Javier;

Or of the faith and (and in) intellectual curiosity imparted to me by my parents, Ivan and Marcelina;

Nor the many friends that I have made here at the University of Delaware, in particular Thomas Brown, Hasan Eruslu, Shukai Du, and Hugo Diaz-Norambuena;

Thank you all, from the bottom of my heart, for tonight, at least, I feel truly blessed.

-Allan Hungria, December 29th, 2018

Research partially supported by the NSF grant DMS-1818867.

TABLE OF CONTENTS

LIST OF TABLES . . . . **vii**
LIST OF FIGURES . . . . **x**
ABSTRACT . . . . **xiii**

Chapter

1 INTRODUCTION **1**

2 FUNDAMENTALS OF LINEAR ELASTICITY **5**

2.1 Notation 5
2.2 Key quantities in transient linear elasticity 7
2.3 Transient linear elasticity 9
2.4 Quasi-static linear elasticity 9
2.5 Time-harmonic linear elasticity 10
2.6 Laplace domain formulation 11
2.7 Convolution Quadrature 11
2.8 CQ and elasticity 14

3 HDG FOR THE TIME-HARMONIC PROBLEM **15**

3.1 Introduction 15
3.2 HDG+ discretization 19
3.3 Main results 21
3.4 Local solvability and energy identity 23
3.5 Dual problem and bootstrapping process 27
3.6 Variants and insights 33
3.7 Numerical experiments 38
3.8 Some additional proof 44

4 HDG+ AND EXTENDED HDG+ FOR TRANSIENT LINEAR ELASTICITY **47**

4.1 Transient Waves 47

4.2 Numerical Experiments 49
4.3 Extended HDG+ for Linear Elasticity 66
4.4 Numerical Experiments 67

5 HDG+ FOR BIOT'S MODEL OF LINEAR POROELASTICITY 79

5.1 Introduction 79
5.2 Model Equations 81
5.3 HDG+ semidiscretization 84
5.4 Numerical Experiments in the Frequency Domain 88
5.5 Numerical Experiments in the Time Domain 100

6 CONCLUSIONS 119

BIBLIOGRAPHY 121

Appendix

PERMISSIONS 125

LIST OF TABLES

3.1 Comparison of dimensions of global solution spaces 43

4.1 Time-Dependent Elasticity: Dirichlet Conditions at $k = 1$ 55

4.2 Time-Dependent Elasticity: Dirichlet Conditions at $k = 2$ 55

4.3 Time-Dependent Elasticity: Dirichlet Conditions at $k = 3$ 56

4.4 Time-Dependent Elasticity: Dirichlet Conditions at $k = 4$ 56

4.5 Time-Dependent Elasticity: Neumann Conditions at $k = 1$ 57

4.6 Time-Dependent Elasticity: Neumann Conditions at $k = 2$ 57

4.7 Time-Dependent Elasticity: Neumann Conditions at $k = 3$ 58

4.8 Time-Dependent Elasticity: Neumann Conditions at $k = 4$ 58

4.9 Time-Dependent Elasticity: Mixed Conditions at $k = 1$ 59

4.10 Time-Dependent Elasticity: Mixed Conditions at $k = 2$ 59

4.11 Time-Dependent Elasticity: Mixed Conditions at $k = 3$ 60

4.12 Time-Dependent Elasticity: Mixed Conditions at $k = 4$ 60

4.13 Time-Dependent Extended Elasticity: Dirichlet Conditions at $k = 1$ 73

4.14 Time-Dependent Extended Elasticity: Dirichlet Conditions at $k = 2$ 73

4.15 Time-Dependent Extended Elasticity: Dirichlet Conditions at $k = 3$ 74

4.16 Time-Dependent Extended Elasticity: Dirichlet Conditions at $k = 4$ 74

4.17 Time-Dependent Extended Elasticity: Neumann Conditions at $k = 1$ 75

4.18 Time-Dependent Extended Elasticity: Neumann Conditions at $k = 2$ 75

4.19 Time-Dependent Extended Elasticity: Neumann Conditions at $k = 3$ 76

4.20 Time-Dependent Extended Elasticity: Neumann Conditions at $k = 4$ 76

4.21 Time-Dependent Extended Elasticity: Mixed Conditions at $k = 1$. 77

4.22 Time-Dependent Extended Elasticity: Mixed Conditions at $k = 2$. 77

4.23 Time-Dependent Extended Elasticity: Mixed Conditions at $k = 3$. 78

4.24 Time-Dependent Extended Elasticity: Mixed Conditions at $k = 4$. 78

5.1 Frequency Domain for Poroelasticity: Dirichlet Conditions at $k = 1$ 94

5.2 Frequency Domain for Poroelasticity: Dirichlet Conditions at $k = 2$ 94

5.3 Frequency Domain for Poroelasticity: Dirichlet Conditions at $k = 3$ 95

5.4 Frequency Domain for Poroelasticity: Dirichlet Conditions at $k = 4$ 95

5.5 Frequency Domain for Poroelasticity: Neumann Conditions at $k = 1$ 96

5.6 Frequency Domain for Poroelasticity: Neumann Conditions at $k = 2$ 96

5.7 Frequency Domain for Poroelasticity: Neumann Conditions at $k = 3$ 97

5.8 Frequency Domain for Poroelasticity: Neumann Conditions at $k = 4$ 97

5.9 Frequency Domain for Poroelasticity: Mixed Conditions at $k = 1$. 98

5.10 Frequency Domain for Poroelasticity: Mixed Conditions at $k = 2$. 98

5.11 Frequency Domain for Poroelasticity: Mixed Conditions at $k = 3$. 99

5.12 Frequency Domain for Poroelasticity: Mixed Conditions at $k = 4$. 99

5.13 Time-Dependent Poroelasticity: Dirichlet Conditions at $k = 1$ . . . 107

5.14 Time-Dependent Poroelasticity: Dirichlet Conditions at $k = 2$ . . . 107

5.15 Time-Dependent Poroelasticity: Dirichlet Conditions at $k = 3$ . . . 108

5.16 Time-Dependent Poroelasticity: Dirichlet Conditions at $k = 4$ . . . 108
5.17 Time-Dependent Poroelasticity: Neumann Conditions at $k = 1$ . . . 109
5.18 Time-Dependent Poroelasticity: Neumann Conditions at $k = 2$ . . . 109
5.19 Time-Dependent Poroelasticity: Neumann Conditions at $k = 3$ . . . 110
5.20 Time-Dependent Poroelasticity: Neumann Conditions at $k = 4$ . . . 110
5.21 Time-Dependent Poroelasticity: Mixed Conditions at $k = 1$ 111
5.22 Time-Dependent Poroelasticity: Mixed Conditions at $k = 2$ 111
5.23 Time-Dependent Poroelasticity: Mixed Conditions at $k = 3$ 112
5.24 Time-Dependent Poroelasticity: Mixed Conditions at $k = 4$ 112

LIST OF FIGURES

3.1 First-order-in-frequency method. Mixed boundary conditions. $\kappa = 1$. Expected order of convergence: $\mathcal{O}(h^{k+2})$ for $\mathbf{u}$ and $\mathcal{O}(h^{k+1})$ for $\boldsymbol{\sigma}$. ($k = 1$ top-left, $k = 2$ top-right, $k = 3$ mid-left, $k = 4$ mid-right, $k = 5$ bottom left, $k = 6$ bottom right) 40

3.2 Second-order-in-frequency method. Mixed boundary conditions. $\kappa = 1$. Expected order of convergence: $\mathcal{O}(h^{k+2})$ for $\mathbf{u}$ and $\mathcal{O}(h^{k+1})$ for $\boldsymbol{\sigma}$.($k = 1$ top-left, $k = 2$ top-right, $k = 3$ mid-left, $k = 4$ mid-right, $k = 5$ bottom-left, $k = 6$ bottom-right 41

4.1 Dirichlet conditions, Time-Dependent Case: Expected order of convergence: $\mathcal{O}(h^{k+2})$ for $\mathbf{u}_h$ and $\mathcal{O}(h^{k+1})$ for $\boldsymbol{\sigma}_h$ (top-left $k = 1$, top-right $k = 2$, bottom-left $k = 3$, bottom-right $k = 4$) 52

4.2 Neumann conditions, Time-Dependent Case: Expected order of convergence: $\mathcal{O}(h^{k+2})$ for $\mathbf{u}_h$ and $\mathcal{O}(h^{k+1})$ for $\boldsymbol{\sigma}_h$ (top-left $k = 1$, top-right $k = 2$,, bottom-left $k = 3$, bottom-right $k = 4$) 53

4.3 Mixed conditions, Time-Dependent Case: Expected order of convergence: $\mathcal{O}(h^{k+2})$ for $\mathbf{u}_h$ and $\mathcal{O}(h^{k+1})$ for $\boldsymbol{\sigma}_h$ (top-left $k = 1$, top-right $k = 2$, bottom-left $k = 3$, bottom-right $k = 4$) 54

4.4 Elastic wave, part I 61

4.5 Elastic wave, part II 62

4.6 Elastic wave, part III 63

4.7 Elastic wave, part IV 64

4.8 Elastic hippo 65

4.9 Dirichlet Conditions for the Extended Elastic Problem, Time-Dependent Case: Expected order of convergence: $\mathcal{O}(h^{k+2})$ for $\mathbf{u}_h$ and $\mathcal{O}(h^{k+1})$ for $\boldsymbol{\eta}_h$ and $\boldsymbol{\sigma}_h$. $\beta = 0.75, c = 2, \kappa/\gamma = 2$ (top-left $k = 1$, top-right $k = 2$, bottom-left $k = 3$, bottom-right $k = 4$) . . . 70

4.10 Neumann Conditions for the Extended Elastic Problem, Time-Dependent Case: Expected order of convergence: $\mathcal{O}(h^{k+2})$ for $\mathbf{u}_h$ and $\mathcal{O}(h^{k+1})$ for $\boldsymbol{\eta}_h$ and $\boldsymbol{\sigma}_h$. $\beta = 0.75, c = 2, \kappa/\gamma = 2$, (top-left $k = 1$, top-right $k = 2$, bottom-left $k = 3$,bottom-right $k = 4$) . . . 71

4.11 Mixed Conditions for the Extended Elastic Problem, Time-Dependent Case: Expected order of convergence: $\mathcal{O}(h^{k+2})$ for $\mathbf{u}_h$ and $\mathcal{O}(h^{k+1})$ for $\boldsymbol{\eta}_h$ and $\boldsymbol{\sigma}_h$. $\beta = 0.75, c = 2, \kappa/\gamma = 2$, (top-left $k = 1$, top-right $k = 2$, bottom-left $k = 3$, bottom-right $k = 4$)) . . 72

5.1 Dirichlet Conditions for the Poroelastic Problem, Frequency Domain: Expected order of convergence: $\mathcal{O}(h^{k+2})$ for $\mathbf{u}_h$ and p_h and $\mathcal{O}(h^{k+1})$ for $\boldsymbol{\sigma}_h$ and $\mathbf{q}_h$. $s = .5 + .25\imath, \beta = 0.75, c = 2, \kappa/\gamma = 2$ (top-left $k = 1$, top-right $k = 2$, mid-left $k = 3$, mid-right $k = 4$) 91

5.2 Neumann Conditions for the Poroelastic Problem, Frequency Domain: Expected order of convergence: $\mathcal{O}(h^{k+2})$ for $\mathbf{u}_h$ and p_h and $\mathcal{O}(h^{k+1})$ for $\boldsymbol{\sigma}_h$ and $\mathbf{q}_h$. $s = .5 + .25\imath, \beta = 0.75, c = 2, \kappa/\gamma = 2$ (top-left $k = 1$, top-right $k = 2$, bottom-left $k = 3$, bottom-right $k = 4$) 92

5.3 Mixed Conditions for the Poroelastic Problem, Frequency Domain: Expected order of convergence: $\mathcal{O}(h^{k+2})$ for $\mathbf{u}_h$ and p_h and $\mathcal{O}(h^{k+1})$ for $\boldsymbol{\sigma}_h$ and $\mathbf{q}_h$. $s = .5 + .25\imath, \beta = 0.75, c = 2, \kappa/\gamma = 2$ (top-left $k = 1$, top-right $k = 2$, bottom-left $k = 3$, bottom-right $k = 4$) 93

5.4 Dirichlet conditions for the Poroelastic Problem, Time-Dependent Case: Expected order of convergence: $\mathcal{O}(h^{k+2})$ for $\mathbf{u}_h$ and p_h and $\mathcal{O}(h^{k+1})$ for $\boldsymbol{\sigma}_h$ and $\mathbf{q}_h$. $\beta = 0.75, c = 2, \kappa/\gamma = 2$ (top-left $k = 1$, top-right $k = 2$, bottom-left $k = 3$, bottom-right $k = 4$) 104

5.5 Neumann conditions for the Poroelastic Problem, Time-Dependent Case: Expected order of convergence: $\mathcal{O}(h^{k+2})$ for $\mathbf{u}_h$ and p_h and $\mathcal{O}(h^{k+1})$ for $\boldsymbol{\sigma}_h$ and $\mathbf{q}_h$. $\beta = 0.75, c = 2, \kappa/\gamma = 2$, (top-left $k = 1$, top-right $k = 2$, bottom-left $k = 3$,bottom-right $k = 4$) 105

5.6 Mixed conditions for the Poroelastic Problem, Time-Dependent Case: Expected order of convergence: $\mathcal{O}(h^{k+2})$ for $\mathbf{u}_h$ and p_h and $\mathcal{O}(h^{k+1})$ for $\boldsymbol{\sigma}_h$ and $\mathbf{q}_h$. $\beta = 0.75, c = 2, \kappa/\gamma = 2$, (top-left $k = 1$, top-right $k = 2$, bottom-left $k = 3$, bottom-right $k = 4$)) 106

5.7 Poroelastic wave, part I 113

5.8 Poroelastic wave, part II 114

5.9 Poroelastic hippo, part I 115

5.10 Poroelastic hippo, part II 116

5.11 Poroelastic hippo, part III 117

5.12 Poroelastic hippo, part IV 118

ABSTRACT

We are interested in the numerical simulation of elastic and poroelastic waves in three dimensions on polyhedral domains. First we tackle the frequency-domain case for elasticity, proving that our HDG+ method's solution converges at $\mathcal{O}(h^{k+2})$ to the exact displacement solution and $\mathcal{O}(h^{k+1})$ to the exact stress solution, where k is the polynomial degree used in the approximation and h is the maximum length of an edge of our tetrahedra. Next we show numerical experiments to verify these results. We then extend our results to the time-domain, proving that the system is conservative and showing numerical results that match our predictions. Then we introduce an extended method by adding a third variable corresponding to the strain, and show numerical results that match our predictions. We next go on to explore HDG+ for Biot's poroelastic system in 3D, proving dissipativity of our method and showing numerical results of the same convergence rates as well as $\mathcal{O}(h^{k+2})$ for pressure and $\mathcal{O}(h^{k+1})$ for pressure flux in both the frequency domain and the time-domain.

Chapter 1

INTRODUCTION

This dissertation is the culmination of three years of the intensive study of the numerical approximation of linear elastic and poro/thermoelastic waves using the Hybridizable Discontinuous Galerkin method, by Bernardo Cockburn, Jay Gopalakrishnan, and Raytcho Lazarov [9], and extended to what we will call HDG+ by Christophe Lehrenfeld and Joachim Schöberl [31]. Here, the "+" in HDG+ represents the enrichment of the approximating displacement space by one polynomial degree. We will get to the rest of the acronym presently.

Mainly we extend previous work on steady-state elasticity to the frequency domain by mixing the work of Qiu, Shi, and Shen [41] on HDG for steady-state elasticity with that of Griesmaier and Monk [24] on HDG for time-harmonic acoustic waves. Thereupon, we continue our work into the time domain using a time-discretization method called Convolution Quadrature (CQ) developed by Christian Lubich [34] using a MATLAB implementation by Hassell and Sayas [25]. We then briefly analyze and apply our HDG+/CQ framework to the Biot system of poroelasticity equations in three dimensions in both the frequency domain and the time domain.

Throughout this dissertation, we will study four basic models:

1. Time-harmonic elasticity:

$$\begin{aligned} \mathcal{A}\boldsymbol{\sigma} - (\nabla \mathbf{u} + (\nabla \mathbf{u})^\top)/2 &= 0, \\ \rho s^2 \mathbf{u} + \operatorname{div} \boldsymbol{\sigma} &= \mathbf{f}, \end{aligned}$$

2. Fully dynamic elasticity:

$$\begin{aligned} \mathcal{A}\boldsymbol{\sigma}(t) - (\nabla \mathbf{u}(t) + (\nabla \mathbf{u}(t))^\top)/2 = 0, \\ \rho \ddot{\mathbf{u}}(t) + \text{div } \boldsymbol{\sigma}(t) = \mathbf{f}(t), \end{aligned}$$

3. Time-harmonic poroelasticity:

$$\begin{aligned} \mathcal{A}\boldsymbol{\sigma} - (\nabla \mathbf{u} + (\nabla \mathbf{u})^\top)/2 = 0, \\ \rho s^2 \mathbf{u} + \text{div } \boldsymbol{\sigma} - \beta \nabla p = \mathbf{f}_{\mathbf{u}}, \\ \beta \nabla \cdot s\mathbf{u} + csp - \nabla \cdot (\kappa \nabla p) = f_p, \end{aligned}$$

4. Fully dynamic poroelasticity:

$$\begin{aligned} \mathcal{A}\boldsymbol{\sigma}(t) - (\nabla \mathbf{u}(t) + (\nabla \mathbf{u}(t))^\top)/2 = 0, \\ \rho \ddot{\mathbf{u}}(t) + \text{div } \boldsymbol{\sigma}(t) - \beta \nabla p(t) = \mathbf{f}_{\mathbf{u}}(t), \\ \beta \nabla \cdot \dot{\mathbf{u}}(t) + c\dot{p}(t) - \nabla \cdot (\kappa \nabla p(t)) = f_p(t). \end{aligned}$$

all with mixed boundary conditions. Note that many papers deal with the so-called quasistatic model of poroelasticity, which is identical to #4, but eliminating the kinetic term $\rho\ddot{\mathbf{u}}$. The resulting model is purely parabolic and doesn't produce any waves.

So HDG – What is it? Discontinuous Galerkin (DG) methods have evolved from that first introduced by Reed and Hill [42] in 1973, in the context of the neutron transport equation, into a large class of finite element methods designed to find polynomial approximations to solutions of partial differential equations locally, and in particular discontinuously, across each element of a particular triangulation/tetrahedrization of a given domain. Reed and Hill's method was first analyzed by Lesaint and Raviart [33] in 1974, who showed it is strongly A-stable of order $2k + 1$ at mesh points, where k is the polynomial degree used in the approximation. DG methods are in contrast to the more traditional Continuous Galerkin (CG) methods, which provide continuity of the polynomial approximations across element boundaries automatically, but at the cost of flexibility and adaptibility to different meshes.

DG methods and their analyses are now abundant in mathematical and engineering literature. The “Hybridizable” part represents the ability to transfer local information onto a so-called hybrid variable that lives on the “skeleton,” i.e. the union of the faces, of a tetrahedral mesh of the domain, and then solve a (presumably) smaller global system for just that variable, before inverting the local systems to solve, in parallel, for the variables of interest. As is shown below, this process leads to massive static condensation in the global linear system needed to solve for an approximation. In addition, the parallelization of the second part of the method is extremely advantageous computationally, and keeping track of the degrees of freedom is quite easy.

This HDG methodology is applied to the problem of static linear elasticity by Cockburn, Soon, and Stolarski in [13] with numerical results that show both displacement and stress converging at $\mathcal{O}(h^{k+1})$ for any $k \geq 0$ where h is the maximum length of an edge of an element and k is the degree of the approximating polynomials. Moreover, they show $\mathcal{O}(h^{k+2})$ error in the displacement after using an element-by-element post-processing technique whenever $k \geq 2$. Then Fu, Cockburn and Stolarski [17] prove convergence in displacement on the order of h^{k+1} and stress on the order of $h^{k+1/2}$. The topic (for weakly symmetric stress) is revisited by Cockburn and Shi [12], who achieve a proof of $\mathcal{O}(h^{k+2})$ convergence for the displacement and $\mathcal{O}(h^{k+1})$ for the stress for any polynomial degree k. Then Qiu, Shi, and Shen [41] proved the same results for an HDG method which preserves the strong symmetry of the stress tensor.

New challenges arise when we move into the time-harmonic regime. We begin, after this short introduction, by reviewing the basics of linear elasticity–namely, a quick introduction to our notation, a (terse) review of Sobolev spaces, and then some information about the key quantities involved in linear elasticity. Next we move on to explain the frequency-domain case, and then the transient case. We then have an introduction to our time-discretization method, Convolution Quadrature, developed by Christian Lubich [34] for parabolic problems and extended in [35] to hyperbolic problems.

The third chapter consists of a detailed description of the HDG+ discretization for the frequency domain case and a fully rigorous analysis of the convergence of the HDG+ solution to the weak solution of the (frequency domain) elastic system. We prove, under certain specific conditions and full regularity of the exact solution, that the displacement error converges at $\mathcal{O}(h^{k+2})$ and that the error in the stress converges at $\mathcal{O}(h^{k+1})$, where h is identified with the maximum length of an edge of our tetrahedrization $\mathcal{T}_h$ and k is the polynomial degree used in the approximation.

The fourth chapter is about HDG+ for transient elasticity. The theory has been developed by Shukai Du [16]. He uses a new HDG+ projection that simplifies the static and time-harmonic analysis and makes the transient analysis quite doable. This leaves us to simply making sure that the method we use is conservative, and then performing some numerical experiments to show that our method is optimally convergent. We then say a word or two about "extended HDG+," which is a method designed to circumvent the need to invert the elastic law and to calculate the strain directly.

The fifth chapter is devoted to HDG+ for poro/thermoelasticity. We note that the equations for poroelasticity and thermoelasticity are mathematically identical, so we do not distinguish between them. Just read temperature whenever you see pressure and temperature flux whenever you see pressure flux to convert to thermoelasticity. This chapter contains a brief analysis of the diffusive nature of the problem and of the HDG formulation, and numerical experiments to verify our convergence rates.

Chapter 2

FUNDAMENTALS OF LINEAR ELASTICITY

Before we get to the nitty-gritty of theorem and proof, we need to start with a bit of notation. Then we continue with recalling some information about Sobolev spaces: refer to [1] for more on Sobolev spaces and [22] for more on $H(\mathrm{div})$ spaces. Next we will move on to explain some key quantities involved in linear elasticity, and then to a recap of the different versions of linear elasticity that are in the literature–transient, quasi-static, time-harmonic, and Laplace transformed. Finally, we give an introduction to the time-discretization method, Convolution Quadrature, first in an abstract framework, and then as applied to the problem of transient linear elasticity.

2.1 Notation

Let $\Omega \subset \mathbb{R}^d$ be a Lipschitz polyhedron with boundary Γ. We will write

$$(u, v)_\Omega := \int_\Omega u\, v, \quad (\mathbf{u}, \mathbf{v})_\Omega := \int_\Omega \mathbf{u} \cdot \mathbf{v}, \quad (\boldsymbol{\xi}, \boldsymbol{\chi})_\Omega := \int_\Omega \boldsymbol{\xi} : \boldsymbol{\chi} := \int_\Omega \mathrm{trace}(\boldsymbol{\chi}^\top \boldsymbol{\xi}),$$

for real square-integrable scalar, vector-valued, and matrix-valued functions. The three norms induced by the considered inner products will be denoted by $\|\cdot\|_\Omega$. Further, we will assume Γ is divided into two pieces Γ_D and Γ_N such that

$$\overline{\Gamma}_D \cup \overline{\Gamma}_N = \Gamma \text{ and } \Gamma_D \cap \Gamma_N = \emptyset,$$

where we will respectively impose Dirichlet (displacement) and Neumann (normal stress or traction) conditions. For L^2 products on the boundaries, we will write

$$\langle u, v\rangle_{\Gamma_*} := \int_{\Gamma_*} u\, v, \quad \langle \mathbf{u}, \mathbf{v}\rangle_{\Gamma_*} := \int_{\Gamma_*} \mathbf{u} \cdot \mathbf{v}, \quad \langle \boldsymbol{\xi}, \boldsymbol{\chi}\rangle_{\Gamma_*} := \int_{\Gamma_*} \boldsymbol{\xi} : \boldsymbol{\chi} = \int_{\Gamma_*} \mathrm{trace}(\boldsymbol{\chi}^\top \boldsymbol{\xi}),$$

where $*$ runs over D and N.

The symbol $\top$ will be used for real transposition of matrices. When used for complex-valued fields, all brackets will still be defined in the same way, and *will therefore be bilinear and not sesquilinear.* In the same spirit, $\top$ will denote transposition (not conjugation and transposition) and the colon will be defined as above, even when applied to complex matrices. The set of symmetric real $d \times d$ matrices will be denoted $\mathbb{R}^{d\times d}_{\mathrm{sym}}$ and the set of symmetric (not Hermitian) complex $d \times d$ matrices will be denoted $\mathbb{C}^{d\times d}_{\mathrm{sym}}$. Similarly, the set of skewsymmetric real $d \times d$ matrices will be denoted $\mathbb{R}^{d\times d}_{\mathrm{skw}}$ and the set of skewsymmetric (not Hermitian) complex $d \times d$ matrices will be denoted $\mathbb{C}^{d\times d}_{\mathrm{skw}}$.

We will consider the spaces

$$
\begin{aligned}
H^1(\Omega;\mathbb{R}^d) &:= \{\mathbf{u} \in L^2(\Omega;\mathbb{R}^d) : \nabla\mathbf{u} \in L^2(\Omega;\mathbb{R}^{d\times d})\},\\
H(\Omega,\mathrm{div};\mathbb{R}^{d\times d}) &:= \{\boldsymbol{\sigma} \in L^2(\Omega;\mathbb{R}^{d\times d}) : \|\mathrm{div}\ \boldsymbol{\sigma}\|_\Omega < \infty\},\\
H^{1/2}(\widehat{\Gamma};\mathbb{R}^d) &:= \{\mathbf{g} \in L^2(\widehat{\Gamma};\mathbb{R}^d) : \exists \mathbf{u} \in H^1(\Omega;\mathbb{R}^d) \text{ s.t. } \mathbf{g} = \gamma|_{\widehat{\Gamma}}\mathbf{u}\},
\end{aligned}
$$

where the divergence of $\boldsymbol{\sigma}$ is taken by rows and $\gamma|_{\widehat{\Gamma}}$ is the trace operator on some piece of the boundary $\widehat{\Gamma}$ (which will usually be the Dirichlet portion Γ_D of the boundary). We equip these spaces with their natural norms

$$
\|\mathbf{u}\|_{1,\Omega} := \sqrt{\|\mathbf{u}\|^2_\Omega + \|\nabla\mathbf{u}\|^2_\Omega}, \tag{2.1.1}
$$

$$
\|\boldsymbol{\sigma}\|_{\mathrm{div},\Omega} := \sqrt{\|\boldsymbol{\sigma}\|^2_\Omega + \|\mathrm{div}\ \boldsymbol{\sigma}\|^2_\Omega}, \tag{2.1.2}
$$

$$
\|\mathbf{g}\|_{1/2,\widehat{\Gamma}} := \inf\{\|\mathbf{u}\|_{1,\Omega} : \mathbf{u} \in H^1(\Omega,\mathbb{R}^d) \text{ s.t. } \gamma|_{\widehat{\Gamma}}\mathbf{u} = \mathbf{g}\}. \tag{2.1.3}
$$

Since we will be working in the Laplace and frequency domains, we will also need the complexifications of these spaces,

$$
\begin{aligned}
H^1(\Omega;\mathbb{C}^d) &:= \{\mathbf{u} \in L^2(\Omega;\mathbb{C}^d) : \nabla\mathbf{u} \in L^2(\Omega,\mathbb{C}^{d\times d})\},\\
H(\Omega,\mathrm{div};\mathbb{C}^{d\times d}) &:= \{\boldsymbol{\sigma} \in L^2(\Omega;\mathbb{C}^{d\times d}) : \|\mathrm{div}\ \boldsymbol{\sigma}\|_\Omega < \infty\},\\
H^{1/2}(\widehat{\Gamma};\mathbb{C}^d) &:= \{\mathbf{g} \in L^2(\widehat{\Gamma};\mathbb{C}^d) : \exists \mathbf{u} \in H^1(\Omega;\mathbb{C}^d) \text{ s.t. } \mathbf{g} = \gamma|_{\widehat{\Gamma}}\mathbf{u}\},
\end{aligned}
$$

equipped with their natural norms defined as in (2.1.1),(2.1.2), and (2.1.3).

2.2 Key quantities in transient linear elasticity

We will be looking for a displacement field $\mathbf{u} : [0, \infty) \to H^1(\Omega; \mathbb{R}^d)$ and for the associated stress tensor $\boldsymbol{\sigma} : [0, \infty) \to H(\mathrm{div}, \Omega; \mathbb{R}^{d\times d}_{\mathrm{sym}})$. The stress field is given by a general linear non-homogeneous anisotropic law:

$$\boldsymbol{\sigma} = \mathcal{C}\boldsymbol{\varepsilon}(\mathbf{u}), \qquad \boldsymbol{\varepsilon}(\mathbf{u}) := \tfrac{1}{2}(\nabla \mathbf{u} + (\nabla \mathbf{u})^\top),$$

where for almost every $\mathbf{x} \in \Omega$, the linear operator $\mathcal{C}(\mathbf{x})$ transforms real symmetric matrices into real symmetric matrices, satisfies the symmetry condition

$$(\mathcal{C}(\mathbf{x})\boldsymbol{\xi}) : \boldsymbol{\chi} = \boldsymbol{\xi} : (\mathcal{C}(\mathbf{x})\boldsymbol{\chi}) \quad \forall \boldsymbol{\xi}, \boldsymbol{\chi} \in \mathbb{R}^{d\times d}_{\mathrm{sym}},$$

and the positivity condition

$$(\mathcal{C}(\mathbf{x})\boldsymbol{\xi}) : \boldsymbol{\xi} \geq C_0\, \boldsymbol{\xi} : \boldsymbol{\xi} \qquad \forall \boldsymbol{\xi} \in \mathbb{R}^{d\times d}_{\mathrm{sym}},$$

for some $C_0 > 0$. Moreover, we assume that the components of the tensor $\mathcal{C}$ with respect to the canonical basis of $\mathbb{R}^{d\times d}_{\mathrm{sym}}$ are $L^\infty(\Omega)$ functions.

The other physical parameter in the equations to follow is the strictly positive bounded density $\rho : \Omega \to \mathbb{R}$, so that the ρ-weighted norm is equivalent to the $L^2(\Omega)$ norm, i.e., there exist two constants C_1 and C_2 such that

$$C_1 \|\mathbf{u}\|^2_\Omega \leq \|\mathbf{u}\|^2_\rho := (\rho \mathbf{u}, \overline{\mathbf{u}})_\Omega \leq C_2 \|\mathbf{u}\|^2_\Omega \qquad \forall \mathbf{u} \in L^2(\Omega, \mathbb{R}^d).$$

For the HDG formulation, we will first need to invert the elastic law $\mathcal{C}$. With the hypothesis given for $\mathcal{C}$, we can assert that for almost every $\mathbf{x} \in \Omega$, there exists a linear operator $\mathcal{A}(\mathbf{x}) = \mathcal{C}(\mathbf{x})^{-1}$, transforming real symmetric matrices into real symmetric matrices. The tensor $\mathcal{A}$ is often referred to as the *compliance tensor* for the elastic material. From the given hypotheses on $\mathcal{C}$, we know that the $\mathcal{A}$-weighted norm satisfies equivalence to the L^2 norm, i.e., there exist two constants C_1 and C_2 such that

$$C_1 \|\boldsymbol{\xi}\|^2_\Omega \leq \|\boldsymbol{\xi}\|^2_\mathcal{A} := (\mathcal{A}\boldsymbol{\xi}, \overline{\boldsymbol{\xi}})_\Omega = (\mathcal{A}\boldsymbol{\xi}_{\mathrm{re}} + \imath \mathcal{A}\boldsymbol{\xi}_{\mathrm{im}}, \overline{\boldsymbol{\xi}})_\Omega \leq C_2 \|\boldsymbol{\xi}\|^2_\Omega \qquad \forall \boldsymbol{\xi} \in L^2(\Omega, \mathbb{C}^{d\times d}_{\mathrm{sym}}).$$

There is a natural mapping $\mathbb{R}^{d\times d}_{\text{sym}} \to \mathbb{R}^{\frac{d(d+1)}{2}}$ that takes advantage of the symmetry to transform matrices into vectors. It is typically performed by mapping

$$\begin{bmatrix} \sigma_{1,1} & \sigma_{1,2} & \dots & \sigma_{1,d} \\ \sigma_{2,1} & \sigma_{2,2} & \dots & \sigma_{2,d} \\ \vdots & \vdots & \ddots & \vdots \\ \sigma_{d,1} & \sigma_{d,2} & \dots & \sigma_{d,d} \end{bmatrix} \longmapsto \begin{bmatrix} \sigma_1 \\ \sigma_2 \\ \vdots \\ \sigma_{\frac{d(d+1)}{2}} \end{bmatrix} = \begin{bmatrix} \sigma_{1,1} \\ \sigma_{2,2} \\ \vdots \\ \sigma_{d,d} \\ \sigma_{1,2} \\ \vdots \\ \sigma_{d-1,d} \\ \sigma_{1,3} \\ \vdots \\ \sigma_{1,d} \end{bmatrix}.$$

In 3 dimensions for easier visualization, the transformation is

$$\begin{bmatrix} \sigma_{1,1} & \sigma_{1,2} & \sigma_{1,3} \\ \sigma_{2,1} & \sigma_{2,2} & \sigma_{2,3} \\ \sigma_{3,1} & \sigma_{3,2} & \sigma_{3,3} \end{bmatrix} \longmapsto \begin{bmatrix} \sigma_1 \\ \sigma_2 \\ \sigma_3 \\ \sigma_4 \\ \sigma_5 \\ \sigma_6 \end{bmatrix} = \begin{bmatrix} \sigma_{1,1} \\ \sigma_{2,2} \\ \sigma_{3,3} \\ \sigma_{1,2} \\ \sigma_{2,3} \\ \sigma_{1,3} \end{bmatrix}.$$

This mapping does not preserve the scalar invariance of the matrix, but there are adjustments we can make. One such adjustment is to use Voigt notation, so that $\boldsymbol{\sigma} : \boldsymbol{\varepsilon} = \boldsymbol{\sigma} : \widetilde{\boldsymbol{\varepsilon}}$.

$$\boldsymbol{\varepsilon} = \begin{bmatrix} \varepsilon_{1,1} \\ \varepsilon_{2,2} \\ \varepsilon_{3,3} \\ \varepsilon_{1,2} \\ \varepsilon_{1,3} \\ \varepsilon_{2,3} \end{bmatrix} \longmapsto \widetilde{\boldsymbol{\varepsilon}} = \begin{bmatrix} \varepsilon_{1,1} \\ \varepsilon_{2,2} \\ \varepsilon_{3,3} \\ 2\varepsilon_{1,2} \\ 2\varepsilon_{1,3} \\ 2\varepsilon_{2,3} \end{bmatrix}$$

2.3 Transient linear elasticity

The time-dependent case for linear elasticity, which is discussed in Chapter 4, consists of the search for

$$\boldsymbol{\sigma} : [0, \infty) \to H(\mathrm{div}, \Omega; \mathbb{R}^{d \times d}_{\mathrm{sym}}) \qquad \text{and} \qquad \mathbf{u} : [0, \infty) \to H^1(\Omega; \mathbb{R}^d)$$

such that for all $t \geq 0$,

$$\mathcal{A}\boldsymbol{\sigma}(t) - \boldsymbol{\varepsilon}(\mathbf{u}(t)) = \mathbf{0} \qquad \text{in } \Omega, \tag{2.3.1a}$$

$$-\mathrm{div}\ \boldsymbol{\sigma}(t) + \rho\ddot{\mathbf{u}}(t) = \mathbf{f}(t) \qquad \text{in } \Omega, \tag{2.3.1b}$$

$$\mathbf{u}(t) = \mathbf{g}_D(t) \qquad \text{on } \Gamma_D, \tag{2.3.1c}$$

$$\boldsymbol{\sigma}(t)\mathbf{n} = \mathbf{g}_N(t) \qquad \text{on } \Gamma_N. \tag{2.3.1d}$$

$$\mathbf{u}(0) = \mathbf{u}_0 \qquad \text{in } \Omega, \tag{2.3.1e}$$

$$\dot{\mathbf{u}}(0) = \mathbf{v}_0 \qquad \text{in } \Omega, \tag{2.3.1f}$$

for $\mathbf{u}_0 \in H^1(\Omega; \mathbb{R}^d), \mathbf{v}_0 \in L^2(\Omega; \mathbb{R}^d)$, where

$$\begin{aligned} \mathbf{f} &: [0, \infty) \to L^2(\Omega; \mathbb{R}^d), \\ \mathbf{g}_D &: [0, \infty) \to H^{1/2}(\Gamma_D; \mathbb{R}^d), \\ \text{and } \mathbf{g}_N &: [0, \infty) \to L^2(\Gamma_N; \mathbb{R}^d). \end{aligned}$$

2.4 Quasi-static linear elasticity

The quasi-static model is found by dropping the momentum term $\rho\ddot{\mathbf{u}}$ in (2.3.1):

$$\mathcal{A}\boldsymbol{\sigma} - \boldsymbol{\varepsilon}(\mathbf{u}) = \mathbf{0} \qquad \text{in } \Omega, \tag{2.4.1a}$$

$$-\mathrm{div}\ \boldsymbol{\sigma} = \mathbf{f} \qquad \text{in } \Omega, \tag{2.4.1b}$$

$$\mathbf{u} = \mathbf{g}_D \qquad \text{on } \Gamma_D, \tag{2.4.1c}$$

$$\boldsymbol{\sigma}\,\mathbf{n} = \mathbf{g}_N \qquad \text{on } \Gamma_N. \tag{2.4.1d}$$

It is an elliptic problem that we will not be dealing with in this thesis.

2.5 Time-harmonic linear elasticity

In Chapter 3, we will restrict ourselves to the time-harmonic case, namely looking for $\widehat{\mathbf{u}} \in H^1(\Omega; \mathbb{C}^d)$ and $\widehat{\boldsymbol{\sigma}} \in H(\Omega, \mathrm{div}; \mathbb{C}^{d\times d}_{\mathrm{sym}})$ such that

$$\mathcal{A}\widehat{\boldsymbol{\sigma}} - \boldsymbol{\varepsilon}(\widehat{\mathbf{u}}) = \mathbf{0} \qquad \text{in } \Omega, \tag{2.5.1a}$$

$$-\mathrm{div}\, \widehat{\boldsymbol{\sigma}} - \rho\, \kappa^2 \widehat{\mathbf{u}} = \widehat{\mathbf{f}} \qquad \text{in } \Omega, \tag{2.5.1b}$$

$$\widehat{\mathbf{u}} = \widehat{\mathbf{g}}_D \qquad \text{on } \Gamma_D, \tag{2.5.1c}$$

$$\widehat{\boldsymbol{\sigma}}\, \mathbf{n} = \widehat{\mathbf{g}}_N \qquad \text{on } \Gamma_N, \tag{2.5.1d}$$

where the parameter κ is the angular frequency of the solution $\widehat{\mathbf{u}}$.

We will assume that κ^2 is not an eigenvalue for the associated Navier-Lamé operator $\mathbf{u} \mapsto -\rho^{-1}\mathrm{div}\,(\mathcal{C}\boldsymbol{\varepsilon}(\mathbf{u}))$ with homogenous boundary conditions and forcing data, i.e., we assume that the only solution of (2.5.1) with zero right-hand side is the trivial solution.

Following [24], we will work on a first order (in space and frequency) reformulation of (2.5.1). We introduce the new unknown and data

$$\boldsymbol{\sigma} := \frac{\imath}{\kappa}\widehat{\boldsymbol{\sigma}} = \frac{\imath}{\kappa}\mathcal{C}\boldsymbol{\varepsilon}(\widehat{\mathbf{u}}), \qquad \mathbf{f} := \frac{\imath}{\kappa}\widehat{\mathbf{f}}, \qquad \mathbf{g}_N := \frac{\imath}{\kappa}\widehat{\mathbf{g}}_N, \qquad \mathbf{u} := \widehat{\mathbf{u}},$$

and write (2.5.1) as the equivalent first order system

$$\imath\kappa\mathcal{A}\boldsymbol{\sigma} + \boldsymbol{\varepsilon}(\mathbf{u}) = \mathbf{0} \qquad \text{in } \Omega, \tag{2.5.2a}$$

$$\mathrm{div}\, \boldsymbol{\sigma} + \imath\kappa\, \rho\, \mathbf{u} = \mathbf{f} \qquad \text{in } \Omega, \tag{2.5.2b}$$

$$\mathbf{u} = \mathbf{g}_D \qquad \text{on } \Gamma_D, \tag{2.5.2c}$$

$$\boldsymbol{\sigma}\mathbf{n} = \mathbf{g}_N \qquad \text{on } \Gamma_N. \tag{2.5.2d}$$

Note that for the frequency domain (time-harmonic) equations the physical magnitudes will have a hat, while the computational ones will not.

2.6 Laplace domain formulation

Let us now consider the Laplace transforms of the quantities in (2.3.1),

$$\begin{aligned}
\mathbf{f}(t) &\longmapsto \int_0^\infty \mathbf{f} e^{-st} dt =: \mathbf{G}_F(s) \equiv \mathcal{L}(\mathbf{f}(t)),\\
\mathbf{g}_D(t) &\longmapsto \int_0^\infty \mathbf{g}_D e^{-st} dt =: \mathbf{G}_D(s) \equiv \mathcal{L}(\mathbf{g}_D(t)),\\
\mathbf{g}_N(t) &\longmapsto \int_0^\infty \mathbf{g}_N e^{-st} dt =: \mathbf{G}_N(s) \equiv \mathcal{L}(\mathbf{g}_N(t)),\\
\mathbf{u}(t) &\longmapsto \int_0^\infty \mathbf{u} e^{-st} dt =: \mathbf{U}(s) \equiv \mathcal{L}(\mathbf{u}(t)),\\
\boldsymbol{\sigma}(t) &\longmapsto \int_0^\infty \boldsymbol{\sigma} e^{-st} dt =: \boldsymbol{\Sigma}(s) \equiv \mathcal{L}(\boldsymbol{\sigma}(t)).
\end{aligned}$$

Taking the Laplace transform of (2.3.1), and assuming $\mathbf{u}(0) = \dot{\mathbf{u}}(0) = \mathbf{0}$, we have

$$\mathcal{A}\boldsymbol{\Sigma} - \boldsymbol{\varepsilon}(\mathbf{U}) = \mathbf{0} \qquad \text{in } \Omega, \tag{2.6.2a}$$

$$-\text{div}\, \boldsymbol{\Sigma} + \rho\, s^2 \mathbf{U} = \mathbf{G}_F \qquad \text{in } \Omega, \tag{2.6.2b}$$

$$\mathbf{U} = \mathbf{G}_D \qquad \text{on } \Gamma_D, \tag{2.6.2c}$$

$$\boldsymbol{\Sigma}\mathbf{n} = \mathbf{G}_N \qquad \text{on } \Gamma_N. \tag{2.6.2d}$$

These equations will be considered for $s \in \mathbb{C}^+ := \{s \in \mathbb{C} : \text{Re}\, s > 0\}$, so they will not display resonance (eigenvalue) phenomena. We will use these Laplace domain (or resolvent) equations for the CQ treatment of the transient problem.

2.7 Convolution Quadrature

We turn our attention now to a particular time-discretization method called CQ (convolution quadrature) developed by Christian Lubich [34] in the late 1980's for discretizing convolutions of causal (vanishing on the negative real line) distributions. Suppose we have two Banach spaces X and Y, and two functions

$$g : [0, \infty) \to X \qquad \text{and} \qquad f : [0, \infty) \to B(X, Y),$$

and we want a numerical solution to

$$u(t) = f * g(t) := \int_0^\infty f(t - s) g(s) ds : [0, \infty) \to Y. \tag{2.7.1}$$

For a uniform timestep grid with timestep δ_t,

$$t_n = n\delta_t, \text{ for } n = 0, \dots, N,$$

and sampled data

$$g_n := g(t_n),$$

we want approximations

$$u_n \approx u(t_n).$$

A Laplace transform of (2.7.1) yields

$$U(s) = F(s)G(s). \tag{2.7.2}$$

We consider $\delta : U \subset \mathbb{C} \to \mathbb{C}$ (here U is a neighborhood of the origin), depending on some multistep time-stepping method (δ is the characteristic function of the multistep method). In particular, we will consider

$$\delta(s) = \begin{cases} 1 - s & \text{Backward Euler,} \\ \frac{3}{2} - 2s + \frac{1}{2}s^2 & \text{BDF2,} \\ 2\frac{1-s}{1+s} & \text{Trapezoidal Rule.} \end{cases}$$

In practice we will only use the trapezoidal rule for numerical tests. We then consider

$$F_\kappa(\zeta) = F\left(\frac{1}{\kappa}\delta(\zeta)\right) = \sum_{n=0}^{\infty} \omega_n^F(\kappa)\zeta^n, \tag{2.7.3}$$

and the discrete counterpart to (2.7.2) written in terms of the ζ-transform (we use the same symbol for the time-discretized unknown). Note that $\omega_n^F(\kappa) \in B(X, Y)$ are the Taylor coefficients of $F_\kappa(\zeta)$, and

$$U(\zeta) = \sum_{n=0}^{\infty} u_n\zeta^n \quad \text{and} \quad G(\zeta) = \sum_{n=0}^{\infty} g_n\zeta^n,$$

so

$$U(\zeta) = F_\kappa(\zeta)G(\zeta).$$

Then

$$U(\zeta) = \sum_{n=0}^{\infty} u_n \zeta^n = \left(\sum_{n=0}^{\infty} \omega_n^F(\kappa)\zeta^n\right)\left(\sum_{n=0}^{\infty} g_n \zeta^n\right)$$
$$= \sum_{n=0}^{\infty}\sum_{m=0}^{n} \omega_{n-m}^F(\kappa)\zeta^{n-m} g_m \zeta^m$$
$$= \sum_{n=0}^{\infty}\left(\sum_{m=0}^{n} \omega_{n-m}^F(\kappa) g_m\right)\zeta^n.$$

Pairing up values of n, we have

$$u_n = \sum_{m=0}^{n} \omega_{n-m}^F(\kappa) g_m.$$

Notice that we have the time-sampled data g_m (taken directly from g) in discrete convolution with the Taylor coefficients of F_κ, which are derived from F, the Laplace domain solver.

To calculate $\omega_n^F(\kappa) \in B(X,Y)$, we take a contour integral around a circle C_R of radius R around the origin, and then approximate the integral with a trapezoidal sum of $N+1$ terms:

$$\omega_n^F(\kappa) = \frac{1}{2\pi\imath}\oint_{C_R} \xi^{n-1} F\left(\frac{1}{\kappa}\delta(\xi)\right) d\xi$$
$$= R^{-n}\int_0^1 e^{2\pi n\imath\theta} F\left(\frac{1}{\kappa}\delta\left(Re^{\imath\pi\theta}\right)\right) d\theta$$
$$\approx \frac{R^{-n}}{N+1}\sum_{\ell=0}^{N} e^{\frac{2\pi\imath n\ell}{N+1}} F\left(\frac{1}{\kappa}\delta\left(Re^{\frac{-2\pi\imath\ell}{N+1}}\right)\right).$$

Setting $\xi_{N+1} := e^{\frac{2\pi\imath}{N+1}}$ and $\widehat{F}_\ell(\kappa) := F\left(\frac{1}{\kappa}\delta\left(Re^{\frac{-2\pi\imath\ell}{N+1}}\right)\right) = F\left(\frac{1}{\kappa}\delta\left(R\xi_{N+1}^{-\ell}\right)\right)$,

$$u_n = \sum_{m=0}^{N} \omega_{n-m}^F(\kappa) g_m \approx \sum_{m=0}^{N}\left(\frac{R^{-(n-m)}}{N+1}\sum_{\ell=0}^{N} e^{\frac{2\pi\imath(n-m)\ell}{N+1}}\widehat{F}_\ell(\kappa)\right) g_m$$
$$= \sum_{m=0}^{N}\left(\frac{R^{(m-n)}}{N+1}\sum_{\ell=0}^{N}\xi_{N+1}^{(n-m)\ell}\widehat{F}_\ell(\kappa)\right) g_m,$$
$$= \sum_{\ell=0}^{N}\sum_{m=0}^{N}\frac{R^{-n}R^m}{N+1}\xi_{N+1}^{n\ell}\xi_{N+1}^{-m\ell}\widehat{F}_\ell(\kappa) g_m$$
$$= \sum_{\ell=0}^{N}\frac{1}{N+1}\xi_{N+1}^{n\ell}R^{-n}\widehat{F}_\ell(\kappa)\left(\sum_{m=0}^{N}\xi_{N+1}^{-m\ell}R^m g_m\right).$$

More work on convolution quadrature for BEM/FEM problems can be found in [25] and [46].

2.8 CQ and elasticity

Regarding the practical implementation of CQ for elasticity, we use a black box method that can be found in [3]. We take the spaces,

$$\mathbb{X} = L^2(\Omega;\mathbb{C}^d) \times H^{1/2}(\Gamma_D;\mathbb{C}^d) \times L^2(\Gamma_N;\mathbb{C}^d) \quad \text{and} \quad \mathbb{Y} = H^1(\Omega;\mathbb{C}^d) \times H(\mathrm{div},\Omega;\mathbb{C}^{d\times d}_{\mathrm{sym}})$$

and a bounded linear function $\mathbf{F}(s) : \mathbb{X} \to \mathbb{Y}$ that takes the Laplace transforms of our data

$$(\mathbf{G}_F, \mathbf{G}_D, \mathbf{G}_N) \in \mathbb{X},$$

and outputs $(\mathbf{U}(s), \mathbf{\Sigma}(s)) \in \mathbb{Y}$, with $\mathbf{U}(s), \mathbf{\Sigma}(s)$ solving equations (2.6.2).

Our goal is to produce $U = [U_n]_{n=0}^N$ where $U_n = [\mathbf{u}_n.\boldsymbol{\sigma}_n] \approx [\mathbf{u}(t_n), \boldsymbol{\sigma}(t_n)]$. We begin by sampling the time-domain data

$$\mathbf{d}_n = [\mathbf{f}(t_n), \mathbf{g}_D(t_n), \mathbf{g}_N(t_n)] \text{ for } n = 0, \ldots, N$$

and considering the Taylor expansion of

$$\mathbf{F}_\kappa(\zeta) := \mathbf{F}\left(\frac{1}{\kappa}\delta(\zeta)\right) = \sum_{n=0}^{\infty} \boldsymbol{\omega}_n^{\mathbf{F}}(\kappa)\zeta^n.$$

The CQ approximation of (2.3.1) with vanishing initial conditions is then given by the discrete convolution

$$U_n = \sum_{m=0}^{N} \boldsymbol{\omega}_{n-m}^{\mathbf{F}}(\kappa)\mathbf{d}_m.$$

These convolutions will be computed with the parallelizable all-timesteps-at-once method explained in Section 2.7. As is made clear in [25], this requires about $N/2$ solves of the Laplace domain equations for different values of s.

Chapter 3

HDG FOR THE TIME-HARMONIC PROBLEM

This chapter proposes and analyzes an HDG method with strongly symmetric stresses for the time-harmonic elastic wave equations. The chapter is contained in the paper *HDG Methods for Elastodynamics* [26] co-authored with D. Prada and F.-J. Sayas.

3.1 Introduction

We are concerned with numerical methods for the evolution of elastic waves on general (non-homogeneous anisotropic) linearly elastic solids. It is well known that elastodynamics, in the time and frequency domains, has multiple applications in the fields of geophysics, material science, structural engineering, oil exploration, aerospace, etc. This chapter is a first contribution on the use of the Hybridizable Discontinuous Galerkin (HDG) method to the three-dimensional linear elastic and poroelastic wave equations in the time-harmonic regime.

Mathematical literature contains a plethora of numerical methods for dealing with the elastic wave equation, each with its own virtue and applications: spectral elements [14], particle-based methods such as the Hamiltonian Particle method (HPM) [48], as well as the more finite element styled Continuous Galerkin (CG) methods [28] and Discontinuous Galerkin (DG) methods [39]. CG is well-known for its accuracy and reliability with smoother data and simpler meshes. The DG framework is praised for its capacity to handle all sorts of complicated meshes and discontinuous data, but also disdained for the large number of degrees of freedom required to make a calculation when compared to CG.

Certain DG methods, however, including the ones we shall explore here, have the key property of being *hybridizable*, i.e., the global system can be recast in terms of (statically condensed onto) a single "hybrid" variable defined on the skeleton formed by the union of the boundaries of the elements. These form a family of methods that are naturally called the Hybridizable Discontinuous Galerkin (HDG) methods [9]. The main idea is that unknowns are solved elementwise, in parallel, in terms of the hybrid variable. This creates a global linear system for only the hybrid variable, which is inverted, after which the unknowns are recovered locally, again in parallel. This is similar to the hybridized implementation of mixed methods such as the Raviart-Thomas elements (see [9], [37] and [45] for more on this), except that the HDG method uses a stabilization function instead of a stable mixed finite element pair. In certain cases, namely for polynomial expansions above approximately degree 4 [10], the hybrid space is smaller than that of the displacement/stress spaces, and this computational advantage over traditional CG methods has resulted in renewed interest in HDG.

The HDG methodology was successfully applied to time-harmonic acoustic waves by Roland Griesmaier and Peter Monk [24]. Their analysis involves first rephrasing the classical system as first order in frequency before moving to the weak formulation. Testing the equations with the projected errors leads to a Gårding-type identity, and, combined with the dual equations to the classical system, the projected errors of both amplitude and its gradient can be bounded. This last bound requires a rather involved bootstrapping argument which is indispensable within our argument here.

Hybridizable DG methods have lately enjoyed further exposure in time-domain wave problems. For example, Cockburn and Quenneville-Bélair's work on HDG for the acoustic wave equation [11] provides much of the framework for the insights on the time-domain elastic problem in the next chapter of this work. Nguyen, Peraire, and Cockburn implement an implicit HDG numerical scheme for both time-dependent acoustic and elastic equations [39], and more recently, Stanglmeier, Nguyen, Peraire, and Cockburn explore an explicit HDG scheme for the acoustic case [47].

The vector field formulation of elasticity introduces several distinct complications in both the analysis and the implementation of HDG. Cockburn, Soon, and Stolarski give a numerical implementation of HDG for planar elasticity, along with a proof of existence and uniqueness of a solution to their particular HDG formulation [13]. Fu, Cockburn, and Stolarski go on to analyze the convergence of this last method, which uses degree k polynomial bases for displacement, stress, and hybrid spaces. They prove convergence at an order of $k+1$ for displacement and $k+1/2$ for the stress [17], which is suboptimal; this has prompted the exploration of optimally convergent HDG methods.

One issue is that the tailored HDG projections often used in the analysis may not play well with the symmetry of the approximate stress tensor. Another is that using bases of the same polynomial degree for displacement, stress, and hybrid spaces leads to a suboptimal method. One method for addressing both of these issues is to introduce special divergence-free symmetric "bubble matrices" as in [8], providing an extra control on the stress-associated approximation space. This yields a weakly-enforced symmetry of the approximate stress as well as optimal convergence of a postprocessed solution.

Another approach entirely is that of Weifeng Qiu, Jiguang Shen, and Ke Shi for the steady-state elasticity problem [41]. The special tailored HDG projections are left behind for simpler L^2 projections, and the displacement-associated approximation space is expanded by one polynomial degree (hence the "+" in "HDG+"). While this does then require some extra terms to be bounded in the analysis, the net result is shown to achieve optimal convergence directly. An important feature of this approach is the strong symmetry of the approximate stress. See the introduction of [41] for more on this. Expanding the polynomial degree of the primal unknown by one is an idea that can be traced back to Lehrenfeld and Schöberl [31], but Qiu, Shen and Shi compensate by adjusting the order of the primal unknown piece of the stabilization function to $O(h^{-1})$ as well as a projection operator from primal approximation space onto hybrid space.

Our choice of polynomial approximating spaces and projections is that of Qiu, Shen, and Shi [41] in order to be able to work on the most general polyhedral mesh possible. However, the frequency-domain problem, unlike the steady-state problem, is not coercive, so we wind up with a Gårding-type identity similar to that of Griesmaier and Monk's [24], after following their example and first phrasing the classical system as first order in both frequency and space. The two analytical recipes from [41] and [24] are here carefully blended to approach the time-harmonic elasticity case, which has implications on the choice of numerical flux and its dependence on the wavenumber.

The following treatment of HDG+ for time-harmonic elasticity, however, comes with its own complications, not only with regard to the hybridization of the DG scheme, but also in consideration of the dependence on wavenumber. We have also developed a simplified system for dealing with the double-bootstrapping process, which is now even messier considering the use of L^2 projections rather than tailored HDG projections. By varying the numerical flux, we wind up with several different HDG+ methods for the time-harmonic linear elastic problem. We proceed to show how some of these methods can be used to produce semi-discretizations in the time domain and that one of them is actually conservative.

What follows is a rigorous treatment of the error analysis and well-posedness of HDG+ methodology as applied to the problem of three-dimensional time-harmonic elasticity on a polyhedron with mixed boundary conditions and strong symmetric stresses. We explore how this analysis can shape the stability mechanism for a method of numerically integrating the time-dependent system, in particular for the 2nd-order-in-frequency case. Numerical experiments are carried out to demonstrate convergence of both the first-order method and a second-order variant. We then compare, using various polynomial degrees and tetrahedrizations, the sizes of the global linear systems involved in HDG+ and classical Lagrange element CG, demonstrating an advantage of HDG+ at large polynomial degrees.

3.2 HDG+ discretization

We now introduce the HDG+ discretization of (2.5.2), the first-order-in-space-and-frequency reformulation of the frequency-domain system of elasticity:

$$\imath\kappa\mathcal{A}\boldsymbol{\sigma} + \boldsymbol{\varepsilon}(\mathbf{u}) = \mathbf{0} \qquad \text{in } \Omega, \tag{3.2.1a}$$

$$\operatorname{div} \boldsymbol{\sigma} + \imath\kappa\,\rho\,\mathbf{u} = \mathbf{f} \qquad \text{in } \Omega, \tag{3.2.1b}$$

$$\mathbf{u} = \mathbf{g}_D \qquad \text{on } \Gamma_D, \tag{3.2.1c}$$

$$\boldsymbol{\sigma}\mathbf{n} = \mathbf{g}_N \qquad \text{on } \Gamma_N. \tag{3.2.1d}$$

Since the method we use is Qiu, Shen, and Shi's [41], we will not repeat the derivation. We start with a shape-regular conforming tetrahedrization $\mathcal{T}_h$ of the domain Ω. The set of all faces of elements of $\mathcal{T}_h$ is denoted $\mathcal{E}_h$, and we will sometimes understand that $\mathcal{E}_h$ is the geometric skeleton of the triangulation, i.e., the union of all the faces of all elements. The method involves three discrete spaces

$$\mathbb{V}_h \;:=\; \{\boldsymbol{\xi} : \Omega \to \mathbb{C}^{3\times 3}_{\text{sym}} \,:\, \boldsymbol{\xi}|_K \in \mathcal{P}_k(K;\mathbb{C}^{3\times 3}_{\text{sym}}) \quad \forall K \in \mathcal{T}_h\}, \tag{3.2.2a}$$

$$\mathbf{W}_h \;:=\; \{\mathbf{u} : \Omega \to \mathbb{C}^3 \,:\, \mathbf{u}|_K \in \mathcal{P}_{k+1}(K;\mathbb{C}^3) \quad \forall K \in \mathcal{T}_h\}, \tag{3.2.2b}$$

$$\mathbf{M}_h \;:=\; \{\boldsymbol{\mu} : \mathcal{E}_h \to \mathbb{C}^3 \,:\, \boldsymbol{\mu}|_F \in \mathcal{P}_k(F;\mathbb{C}^3) \quad \forall F \in \mathcal{E}_h\}. \tag{3.2.2c}$$

In (3.2.2), $\mathcal{P}_r(K;S)$ is the set of polynomials of total degree up to r defined on K and with values in $S \in \{\mathbb{C}^{3\times 3}_{\text{sym}}, \mathbb{C}^3\}$, while $\mathcal{P}_k(F;\mathbb{C}^3)$ are vector valued polynomials on the tangential coordinates defined on the face F and of degree not greater than k. We will also use the orthogonal projector

$$\mathbf{P}_M : \prod_{K\in\mathcal{T}_h} L^2(\partial K) \longrightarrow \prod_{K\in\mathcal{T}_h}\prod_{F\in\mathcal{E}(K)} \mathcal{P}_k(F;\mathbb{C}^3), \tag{3.2.3}$$

where $\mathcal{E}(K)$ is the set of faces of ∂K. Note that $\mathbf{M}_h$ can be identified with the subspace of the set of the right-hand side of (3.2.3) consisting of functions that are single-valued on internal faces.

Stabilization is carried out through a function $\boldsymbol{\tau}$ defined as follows: for each element $K \in \mathcal{T}_h$, a function $\boldsymbol{\tau}_K : \partial K \to \mathbb{R}^{3\times 3}_{\text{sym}}$ satisfying (a) $\boldsymbol{\tau}_K|_F$ is constant on each

$F \in \mathcal{E}(K)$ for a given tetrahedrization $\mathcal{T}_h$; (b) there exist two positive constants C_1 and C_2 such that

$$C_1 h_K^{-1} \|\boldsymbol{\mu}\|_{\partial K}^2 \le \langle \boldsymbol{\tau}_K \boldsymbol{\mu}, \overline{\boldsymbol{\mu}} \rangle_{\partial K} \le C_2 h_K^{-1} \|\boldsymbol{\mu}\|_{\partial K}^2 \quad \forall \boldsymbol{\mu} \in \mathbf{L}^2(\partial K), \quad \forall K \in \mathcal{T}_h, \tag{3.2.4}$$

where h_K is the diameter of K. The symbol $\boldsymbol{\tau}$ will be used to denote the function defined on the set of boundaries of all elements as above, understanding that $\boldsymbol{\tau}$ can be double-valued on interior faces. The numerical fluxes follow the pattern of HDG methods: the one corresponding to the displacement will be an unknown $\widehat{\mathbf{u}}_h \in \mathbf{M}_h$, while the one related to the (normal) stress is given elementwise with a formula in terms of all the unknowns

$$\widehat{\boldsymbol{\sigma}}_h \mathbf{n} := \boldsymbol{\sigma}_h \mathbf{n} + \boldsymbol{\tau}_K (\mathbf{P}_M \mathbf{u}_h - \widehat{\mathbf{u}}_h) \, : \, \partial K \to \mathbb{C}^3. \tag{3.2.5}$$

Here the unit normal vector field $\mathbf{n} : \partial K \to \mathbb{R}^3$ points to the exterior of K. At this time, we can write the HDG discrete equations for (2.5.2). We look for $(\boldsymbol{\sigma}_h, \mathbf{u}_h, \widehat{\mathbf{u}}_h) \in \mathbb{V}_h \times \mathbf{W}_h \times \mathbf{M}_h$ satisfying

$$\imath\kappa(\mathcal{A}\boldsymbol{\sigma}_h, \boldsymbol{\xi})_{\mathcal{T}_h} - (\mathbf{u}_h, \operatorname{div} \boldsymbol{\xi})_{\mathcal{T}_h} + \langle \widehat{\mathbf{u}}_h, \boldsymbol{\xi}\mathbf{n} \rangle_{\partial \mathcal{T}_h} = 0 \qquad \forall \boldsymbol{\xi} \in \mathbb{V}_h, \tag{3.2.6a}$$

$$-(\boldsymbol{\sigma}_h, \nabla \mathbf{w})_{\mathcal{T}_h} + \langle \widehat{\boldsymbol{\sigma}}_h \mathbf{n}, \mathbf{w} \rangle_{\partial \mathcal{T}_h} + \imath\kappa(\rho\, \mathbf{u}_h, \mathbf{w})_{\mathcal{T}_h} = (\mathbf{f}, \mathbf{w})_{\mathcal{T}_h} \qquad \forall \mathbf{w} \in \mathbf{W}_h, \tag{3.2.6b}$$

$$\langle \widehat{\boldsymbol{\sigma}}_h \mathbf{n}, \boldsymbol{\mu} \rangle_{\partial \mathcal{T}_h \setminus \Gamma_D} = \langle \mathbf{g}_N, \boldsymbol{\mu} \rangle_{\Gamma_N} \qquad \forall \boldsymbol{\mu} \in \mathbf{M}_h, \tag{3.2.6c}$$

$$\langle \widehat{\mathbf{u}}_h, \boldsymbol{\mu} \rangle_{\Gamma_D} = \langle \mathbf{g}_D, \boldsymbol{\mu} \rangle_{\Gamma_D} \qquad \forall \boldsymbol{\mu} \in \mathbf{M}_h, \tag{3.2.6d}$$

with (3.2.5) as the definition of $\widehat{\boldsymbol{\sigma}}_h \mathbf{n}$ and brackets defined as follows:

$$(\mathbf{u}, \mathbf{v})_{\mathcal{T}_h} := \sum_{K \in \mathcal{T}_h} (\mathbf{u}, \mathbf{v})_K, \qquad \langle \mathbf{u}, \mathbf{v} \rangle_{\partial \mathcal{T}_h} := \sum_{K \in \mathcal{T}_h} \langle \mathbf{u}, \mathbf{v} \rangle_{\partial K} := \sum_{K \in \mathcal{T}_h} \int_{\partial K} \mathbf{u} \cdot \mathbf{v},$$

and

$$\langle \mathbf{u}, \mathbf{v} \rangle_{\partial \mathcal{T}_h \setminus \Gamma_D} := \sum_{K \in \mathcal{T}_h} \langle \mathbf{u}, \mathbf{v} \rangle_{\partial K \setminus \Gamma_D}.$$

Equations (3.2.6c) and (3.2.6d) can be added together as a single equation tested against $\mathbf{M}_h$, which shows that (3.2.6) is a square system of linear equations. The discrete momentum equation (3.2.6b) can be equivalently written as

$$(\operatorname{div} \boldsymbol{\sigma}_h, \mathbf{w})_{\mathcal{T}_h} + \langle \boldsymbol{\tau}(\mathbf{P}_M \mathbf{u}_h - \widehat{\mathbf{u}}_h), \mathbf{P}_M \mathbf{w} \rangle_{\partial \mathcal{T}_h} + \imath\kappa(\rho\, \mathbf{u}_h, \mathbf{w})_{\mathcal{T}_h} = (\mathbf{f}, \mathbf{w})_{\mathcal{T}_h} \quad \forall \mathbf{w} \in \mathbf{W}_h. \tag{3.2.7}$$

We note that the degree of the polynomial space used for $\mathbf{u}_h$ is one higher than the one used for the other unknowns and the fact that $\mathbf{P}_M$ has been introduced in the definition of the flux (3.2.5) so that $\widehat{\boldsymbol{\sigma}}_h\mathbf{n} \in \prod_{F\in\mathcal{E}(K)} \mathcal{P}_k(F;\mathbb{C}^3)$.

3.3 Main results

Regularity assumptions. From now on we will assume that ρ and the coefficients of $\mathcal{C}$ are in $W^{1,\infty}(\mathcal{T}_h)$. Let us now consider the coercive problem

$$\nabla\cdot(\mathcal{C}\boldsymbol{\varepsilon}(\mathbf{w})) - \rho\,\mathbf{w} = \mathbf{r} \qquad \text{in } \Omega, \tag{3.3.1a}$$

$$\mathbf{w} = \mathbf{0} \qquad \text{on } \Gamma_D, \tag{3.3.1b}$$

$$(\mathcal{C}\boldsymbol{\varepsilon}(\mathbf{w}))\,\mathbf{n} = \mathbf{0} \qquad \text{on } \Gamma_N. \tag{3.3.1c}$$

We will also assume that the solution of (3.3.1) for arbitrary $\mathbf{r} \in L^2(\Omega;\mathbb{R}^3)$ is in $H^2(\Omega;\mathbb{R}^3)$ and that there exists a constant $C > 0$ such that

$$\|\mathbf{w}\|_{2,\Omega} \le C\|\mathbf{r}\|_{\Omega}. \tag{3.3.2}$$

For the time-harmonic problem, we will denote by $C_\kappa > 0$ the constant such that the solution of

$$\nabla\cdot(\mathcal{C}\boldsymbol{\varepsilon}(\mathbf{w})) + \kappa^2\rho\,\mathbf{w} = \mathbf{r} \qquad \text{in } \Omega, \tag{3.3.3a}$$

$$\mathbf{w} = \mathbf{0} \qquad \text{on } \Gamma_D, \tag{3.3.3b}$$

$$(\mathcal{C}\boldsymbol{\varepsilon}(\mathbf{w}))\,\mathbf{n} = \mathbf{0} \qquad \text{on } \Gamma_N. \tag{3.3.3c}$$

can be bounded by

$$\|\mathbf{w}\|_{1,\Omega} \le C_\kappa\|\mathbf{r}\|_{\Omega}. \tag{3.3.4}$$

Note that we have assumed the unique solvability of (3.3.3).

Error quantities. The error analysis will be carried out by comparing numerical solutions and orthogonal projections. Let $\Pi_V : L^2(\Omega;\mathbb{C}^{3\times 3}_{\mathrm{sym}}) \to \mathbb{V}_h$ and $\Pi_W : L^2(\Omega;\mathbb{C}^3) \to \mathbf{W}_h$ be the orthogonal projections onto the discrete spaces. Consider the errors

$$e_h^\sigma := \Pi_V\boldsymbol{\sigma} - \boldsymbol{\sigma}_h, \qquad \mathbf{e}_h^u := \Pi_W\mathbf{u} - \mathbf{u}_h, \qquad \widehat{\mathbf{e}}_h^u := \mathbf{P}_M\mathbf{u} - \widehat{\mathbf{u}}_h,$$

and the best approximation errors

$$\varepsilon_h^\sigma := \Pi_V \boldsymbol{\sigma} - \boldsymbol{\sigma}, \qquad \boldsymbol{\varepsilon}_h^u := \Pi_W \mathbf{u} - \mathbf{u}.$$

For convenience, we introduce the skeleton norm

$$\|\boldsymbol{\mu}\|_\tau := \langle \boldsymbol{\tau}\boldsymbol{\mu}, \overline{\boldsymbol{\mu}}\rangle_{\partial\mathcal{T}_h}^{1/2}.$$

For the error analysis we will allow constants to depend on the density ρ and on the coefficients of $\mathcal{A}$. While the influence of these physical coefficients in the inequalities can be tracked with careful arguments, the results seem to be too involved to obtain precise conclusions on how h and κ interact with them. However, we will pay attention to the maximum spectral value of the inverse compliance tensor, i.e., to the positive bounded function such that for almost every $\mathbf{x} \in \Omega$

$$(\mathcal{A}(\mathbf{x})\boldsymbol{\xi}) : \boldsymbol{\xi} \le c_{\mathcal{A}}(\mathbf{x})\, \boldsymbol{\xi} : \boldsymbol{\xi} \qquad \forall \boldsymbol{\xi} \in \mathbb{R}^{3\times 3}_{\mathrm{sym}}. \tag{3.3.5}$$

Theorem 3.3.1. *There exist $C_1, C_2 > 0$, dependent only on the shape-regularity of $\mathcal{T}_h$, the density ρ and the coefficients of the inverse compliance tensor $\mathcal{A}$ such that if $h(1+\kappa)^{3/2}(1+\kappa C_\kappa + C_\kappa)$ is small enough, then the errors can be bounded by*

$$\|e_h^\sigma\|_{\mathcal{A}} + \kappa^{-1/2}\|\mathbf{P}_M \mathbf{e}_h^u - \widehat{\mathbf{e}}_h^u\|_\tau \le C_1(1+\kappa^{-1/2})\big(h^t|\boldsymbol{\sigma}|_{t,\Omega} + h^{s-1}|\mathbf{u}|_{s,\Omega}\big)$$

and

$$\|\mathbf{e}_h^u\|_\Omega \le C_2(1+\kappa C_\kappa)\kappa^{-1/2}(1+\kappa)^2\big(h^{t+1}|\boldsymbol{\sigma}|_{t,\Omega} + h^s|\mathbf{u}|_{s,\Omega}\big),$$

if $k \ge 1$, $\mathbf{u} \in H^s(\Omega;\mathbb{C}^3)$ with $1 \le s \le k+2$, and $\boldsymbol{\sigma} \in H^t(\Omega;\mathbb{C}^{3\times 3})$ with $1 \le t \le k+1$.

Optimal error estimates are

$$\|\boldsymbol{\sigma} - \boldsymbol{\sigma}_h\|_\Omega = \mathcal{O}(h^{k+1}), \qquad \|\mathbf{u} - \mathbf{u}_h\|_\Omega = \mathcal{O}(h^{k+2}).$$

With some additional scaling inequalities, keeping in mind that $\boldsymbol{\tau}$ scales like h_K^{-1} elementwise, it is possible to show that

$$\|\mathbf{u} - \widehat{\mathbf{u}}_h\|_\tau = \mathcal{O}(h^{k+1}).$$

The estimates of Theorem 3.3.1 can also be written in terms of the original physical variables. If we denote $\widetilde{\boldsymbol{\sigma}}_h := -\imath\kappa\boldsymbol{\sigma}_h$, then

$$\|\Pi_V\widetilde{\boldsymbol{\sigma}} - \widetilde{\boldsymbol{\sigma}}_h\|_\Omega + \kappa^{1/2}\|\mathbf{P}_M\mathbf{e}_h^u - \widehat{\mathbf{e}}_h^u\|_\tau \le C_1(1+\kappa^{-1/2})\big(h^t|\widetilde{\boldsymbol{\sigma}}|_{t,\Omega} + h^{s-1}\kappa|\mathbf{u}|_{s,\Omega}\big),$$
$$\|\mathbf{e}_h^u\|_\Omega \le C_2(1+\kappa C_\kappa)\kappa^{-3/2}(1+\kappa)^2\big(h^{t+1}|\widetilde{\boldsymbol{\sigma}}|_{t,\Omega} + h^s\kappa|\mathbf{u}|_{s,\Omega}\big).$$

Unique solvability. Theorem 3.3.1 can be used to prove existence and uniqueness of solution of (3.2.6) for h small enough (depending on the wave number κ). The argument is as follows. Consider the system (3.2.6) with homogenous data: $\mathbf{f} = \mathbf{0}$, $\mathbf{g}_N = \mathbf{0}$, and $\mathbf{g}_D = \mathbf{0}$. Let $(\boldsymbol{\sigma}_h, \mathbf{u}_h, \widehat{\mathbf{u}}_h)$ be any solution of this homogenous set of linear equations. Theorem 3.3.1 applied to this solution and the exact zero solution shows that $(\boldsymbol{\sigma}_h, \mathbf{u}_h, \widehat{\mathbf{u}}_h)$ has to vanish. Therefore, the linear system (3.2.6) (with as many equations as unknowns) is uniquely solvable for any right-hand side. The logic of the use of Theorem 3.3.1 is slightly roundabout: it assumes the existence of a discrete solution, which we know to happen at least for the homogenous case, and then it uses the error estimates to show that the system is actually uniquely solvable.

3.4 Local solvability and energy identity

Lemma 3.4.1. *There exists $C > 0$, depending only on the shape regularity of the grid, such that*

$$\|\mathbf{v}\|_K \le Ch_K\|\boldsymbol{\varepsilon}(\mathbf{v})\|_K$$

for all $\mathbf{v} \in H^1(K;\mathbb{C}^3)$ satisfying

$$\langle \mathbf{v}, \boldsymbol{\mu}\rangle_{\partial K} = 0 \qquad \forall \boldsymbol{\mu} \in \prod_{F\in\mathcal{E}(K)} \mathcal{P}_0(F;\mathbb{C}^3). \tag{3.4.1}$$

Proof. A scaling argument, using only that $\int_{\partial K}\mathbf{v} = \mathbf{0}$ and a Poincaré inequality on the reference element prove that

$$\|\mathbf{v}\|_K \le Ch_K\|\nabla\mathbf{v}\|_K.$$

On the other hand, by a straightforward extension of [41, Lemma 4.1] to our complex-valued fields, we have the local Korn inequality

$$\inf_{\boldsymbol{\xi}\in\mathbb{C}^{3\times 3}_{\mathrm{skw}}} \|\nabla \mathbf{v} + \boldsymbol{\xi}\|_K \le C\|\boldsymbol{\varepsilon}(\mathbf{v})\|_K \quad \forall \mathbf{v} \in H^1(K;\mathbb{C}^3). \tag{3.4.2}$$

The constant in (3.4.2) depends only on the shape-regularity constant of the mesh. Finally, if $\boldsymbol{\xi} \in \mathbb{C}^{3\times 3}$, then

$$(\nabla \mathbf{v}, \boldsymbol{\xi})_K = \langle \mathbf{v}, \boldsymbol{\xi}\mathbf{n}\rangle_{\partial K} = 0,$$

since $\mathbf{v}$ satisfies (3.4.1). Therefore

$$\inf_{\boldsymbol{\xi}\in\mathbb{C}^{3\times 3}_{\mathrm{skw}}} \|\nabla \mathbf{v} + \boldsymbol{\xi}\|_K = \|\nabla \mathbf{v}\|_K$$

and the proof is finished. □

The following result shows that the local equations associated to (3.2.6a)-(3.2.6b) are uniquely solvable, i.e., given the data functions and $\widehat{\mathbf{u}}_h$, we can compute $\boldsymbol{\sigma}_h$ and $\mathbf{u}_h$ element by element. This is the key ingredient to show that the HDG method (3.2.6) is actually hybridizable, that is, it can be recast as a linear system where $\widehat{\mathbf{u}}_h \in \mathbf{M}_h$ is the only variable. To simplify the proof, we introduce the weighted norms

$$\|\boldsymbol{\xi}\|^2_{\mathcal{A},K} := (\mathcal{A}\boldsymbol{\xi}, \overline{\boldsymbol{\xi}})_K, \qquad \|\mathbf{v}\|^2_{\rho,K} := (\rho\,\mathbf{v}, \overline{\mathbf{v}})_K.$$

Proposition 3.4.2 (Local solvers)**.** *If $C > 0$ is the constant of Lemma 3.4.1 and*

$$\kappa\, h_K < \frac{1}{C\,\|c_{\mathcal{A}}\|^{1/2}_{L^\infty(K)}\|\rho\|^{1/2}_{L^\infty(K)}}, \tag{3.4.3}$$

then the local solver associated to the element $K \in \mathcal{T}_h$ is well defined. In other words, if $(\boldsymbol{\sigma}, \mathbf{u}) \in \mathcal{P}_k(K;\mathbb{C}^{3\times 3}_{\mathrm{sym}}) \times \mathcal{P}_{k+1}(K;\mathbb{C}^3)$ satisfies

$$\imath\kappa(\mathcal{A}\boldsymbol{\sigma}, \boldsymbol{\xi})_K - (\mathbf{u}, \nabla\cdot\boldsymbol{\xi})_K = 0 \qquad \forall \boldsymbol{\xi} \in \mathcal{P}_k(K;\mathbb{C}^{3\times 3}_{\mathrm{sym}}), \tag{3.4.4a}$$

$$(\nabla\cdot\boldsymbol{\sigma}, \mathbf{w})_K + \langle \boldsymbol{\tau}\mathbf{P}_M\mathbf{u}, \mathbf{w}\rangle_{\partial K} + \imath\kappa(\rho\mathbf{u}, \mathbf{w})_K = 0 \qquad \forall \mathbf{w} \in \mathcal{P}_{k+1}(K;\mathbb{C}^3), \tag{3.4.4b}$$

then $(\boldsymbol{\sigma}, \mathbf{u}) = (\mathbf{0}, \mathbf{0})$.

Proof. Note that we only need to prove that $\mathbf{u} = \mathbf{0}$. Testing (3.4.4a) with $\overline{\boldsymbol{\sigma}}$, conjugating (3.4.4b) and testing it with $\overline{\mathbf{u}}$, and adding the result of these two equations, it follows that

$$\imath\kappa \left(\|\boldsymbol{\sigma}\|^2_{\mathcal{A},K} - \|\mathbf{u}\|^2_{\rho,K} \right) + \langle \boldsymbol{\tau} \mathbf{P}_M \overline{\mathbf{u}}, \mathbf{P}_M \mathbf{u} \rangle_{\partial K} = 0.$$

By (3.2.4) it follows that $\mathbf{P}_M \mathbf{u} = \mathbf{0}$ and $\|\boldsymbol{\sigma}\|_{\mathcal{A},K} = \|\mathbf{u}\|_{\rho,K}$. Going back to (3.4.4a), integrating by parts, and using that $\mathbf{P}_M \mathbf{u} = \mathbf{0}$, it follows that

$$\imath\kappa(\mathcal{A}\boldsymbol{\sigma}, \boldsymbol{\xi})_K + (\nabla \mathbf{u}, \boldsymbol{\xi})_K = 0 \quad \forall \boldsymbol{\xi} \in \mathcal{P}_k(K; \mathbb{C}^{3\times 3}_{\mathrm{sym}}). \tag{3.4.5}$$

Testing (3.4.5) with $\boldsymbol{\xi} = \boldsymbol{\varepsilon}(\overline{\mathbf{u}})$, it follows that

$$\|\boldsymbol{\varepsilon}(\mathbf{u})\|^2_K = (\nabla \mathbf{u}, \boldsymbol{\varepsilon}(\overline{\mathbf{u}}))_K = \kappa |(\mathcal{A}\boldsymbol{\sigma}, \boldsymbol{\varepsilon}(\overline{\mathbf{u}}))_K| \leq \kappa \|c_{\mathcal{A}}\|^{1/2}_{L^\infty(K)} \|\boldsymbol{\sigma}\|_{\mathcal{A},K} \|\boldsymbol{\varepsilon}(\mathbf{u})\|_K,$$

where we have used (3.3.5). Note that $\mathbf{u}$ satisfies (3.4.1), given the fact that $\mathbf{P}_M \mathbf{u} = \mathbf{0}$. Therefore, by Lemma 3.4.1, if $\boldsymbol{\varepsilon}(\mathbf{u}) = \mathbf{0}$, then $\mathbf{u} = \mathbf{0}$ and the proof is finished. Otherwise $\mathbf{u} \neq \mathbf{0}$ and, by Lemma 3.4.1 and the equality $\|\boldsymbol{\sigma}\|_{\mathcal{A},K} = \|\mathbf{u}\|_{\rho,K}$, we can bound

$$\begin{aligned} \|\mathbf{u}\|_K &\leq C h_K \|\boldsymbol{\varepsilon}(\mathbf{u})\|_K \leq C\kappa\, h_K \|c_{\mathcal{A}}\|^{1/2}_{L^\infty(K)} \|\boldsymbol{\sigma}\|_{\mathcal{A},K} = C\kappa\, h_K \|c_{\mathcal{A}}\|^{1/2}_{L^\infty(K)} \|\mathbf{u}\|_{\rho,K} \\ &\leq C\kappa\, h_K \|c_{\mathcal{A}}\|^{1/2}_{L^\infty(K)} \|\rho\|^{1/2}_{L^\infty(K)} \|\mathbf{u}\|_K \end{aligned}$$

and we arrive at a contradiction if the conditions for proposition (3.4.2) hold. $\square$

Proposition 3.4.3. *The following discrete Gårding inequality holds:*

$$\begin{aligned} &\imath\kappa(\|e^\sigma_h\|^2_{\mathcal{A}} - \|\mathbf{e}^u_h\|^2_\rho) + \|\mathbf{P}_M \mathbf{e}^u_h - \widehat{\mathbf{e}}^u_h\|^2_\tau \\ &\quad = \imath\kappa \left((\mathcal{A}\varepsilon^\sigma_h, \overline{e^\sigma_h})_{\mathcal{T}_h} - (\rho \overline{\boldsymbol{\varepsilon}^u_h}, \mathbf{e}^u_h)_{\mathcal{T}_h} \right) + \langle \overline{\varepsilon^\sigma_h} \mathbf{n}, \mathbf{e}^u_h - \widehat{\mathbf{e}}^u_h \rangle_{\partial \mathcal{T}_h} + \langle \boldsymbol{\tau}\, \overline{\boldsymbol{\varepsilon}^u_h}, \mathbf{P}_M \mathbf{e}^u_h - \widehat{\mathbf{e}}^u_h \rangle_{\partial \mathcal{T}_h}. \end{aligned}$$

Proof. Substituting $(\Pi_V \boldsymbol{\sigma}, \Pi_W \mathbf{u}, \mathbf{P}_M \mathbf{u})$, where $(\boldsymbol{\sigma}, \mathbf{u})$ is the exact solution of (2.5.2) in the left-hand side of discrete equations, and subtracting the actual discrete equations

(3.2.6) (with (3.2.6b) better written in the form (3.2.7)), it is simple to prove that the errors $(e_h^\sigma, \mathbf{e}_h^u, \widehat{\mathbf{e}}_h^u) \in \mathbb{V}_h \times \mathbf{W}_h \times \mathbf{M}_h$ satisfy

$$\imath\kappa(\mathcal{A}e_h^\sigma, \boldsymbol{\xi})_{\mathcal{T}_h} - (\mathbf{e}_h^u, \nabla\cdot\boldsymbol{\xi})_{\mathcal{T}_h} + \langle \widehat{\mathbf{e}}_h^u, \boldsymbol{\xi}\mathbf{n}\rangle_{\partial\mathcal{T}_h} = \imath\kappa(\mathcal{A}\varepsilon_h^\sigma, \boldsymbol{\xi})_{\mathcal{T}_h}, \tag{3.4.6a}$$

$$\begin{aligned}(\nabla\cdot e_h^\sigma, \mathbf{w})_{\mathcal{T}_h} &+ \imath\kappa(\rho\mathbf{e}_h^u, \mathbf{w})_{\mathcal{T}_h} \\ +\langle\boldsymbol{\tau}(\mathbf{P}_M\mathbf{e}_h^u - \widehat{\mathbf{e}}_h^u), \mathbf{P}_M\mathbf{w}\rangle_{\partial\mathcal{T}_h} &= \imath\kappa(\rho\boldsymbol{\varepsilon}_h^u, \mathbf{w})_{\mathcal{T}_h} \\ &\quad + \langle\varepsilon_h^\sigma\mathbf{n}, \mathbf{w}\rangle_{\partial\mathcal{T}_h} + \langle\boldsymbol{\tau}\boldsymbol{\varepsilon}_h^u, \mathbf{P}_M\mathbf{w}\rangle_{\partial\mathcal{T}_h},\end{aligned} \tag{3.4.6b}$$

$$\langle e_h^\sigma\mathbf{n} + \boldsymbol{\tau}(\mathbf{P}_M\mathbf{e}_h^u - \widehat{\mathbf{e}}_h^u), \boldsymbol{\mu}\rangle_{\partial\mathcal{T}_h\setminus\Gamma_D} = \langle\varepsilon_h^\sigma\mathbf{n}, \boldsymbol{\mu}\rangle_{\partial\mathcal{T}_h\setminus\Gamma_D} + \langle\boldsymbol{\tau}\mathbf{P}_M\boldsymbol{\varepsilon}_h^u, \boldsymbol{\mu}\rangle_{\partial\mathcal{T}_h\setminus\Gamma_D} \tag{3.4.6c}$$

$$\langle\widehat{\mathbf{e}}_h^u, \boldsymbol{\mu}\rangle_{\Gamma_D} = 0, \tag{3.4.6d}$$

for all $(\boldsymbol{\xi}, \mathbf{w}, \boldsymbol{\mu}) \in \mathbb{V}_h \times \mathbf{W}_h \times \mathbf{M}_h$. Clearly (3.4.6d) is equivalent to $\widehat{\mathbf{e}}_h^u = \mathbf{0}$ on Γ_D. We now (i) test (3.4.6a) with $\boldsymbol{\xi} = \overline{e_h^\sigma}$, (ii) conjugate (3.4.6b) and test the result with $\mathbf{w} = \overline{\mathbf{e}_h^u}$, (iii) conjugate (3.4.6c) and test the result with $\boldsymbol{\mu} = -\overline{\widehat{\mathbf{e}}_h^u}$. The results of these three steps are added and reorganized ((3.4.6d) is used for this) to prove the proposition. □

We next bound the last two terms in the right-hand side of the identity in Proposition 3.4.3. From this moment on, we will frequently use, without additional warning, approximation properties of the L^2 projections onto the space of piecewise polynomial functions.

Proposition 3.4.4. *If $k \geq 1$,*

$$\begin{aligned}\left|\langle\overline{\varepsilon_h^\sigma}\mathbf{n}, \mathbf{e}_h^u - \widehat{\mathbf{e}}_h^u\rangle_{\partial\mathcal{T}_h} + \langle\boldsymbol{\tau}\,\overline{\boldsymbol{\varepsilon}_h^u}, \mathbf{P}_M\mathbf{e}_h^u - \widehat{\mathbf{e}}_h^u\rangle_{\partial\mathcal{T}_h}\right| &\leq C_1\left(h^t|\boldsymbol{\sigma}|_{t,\Omega} + h^{s-1}|\mathbf{u}|_{s,\Omega}\right)\|\mathbf{P}_M\mathbf{e}_h^u - \widehat{\mathbf{e}}_h^u\|_\tau \\ &\quad + C_2\kappa h^t|\boldsymbol{\sigma}|_{t,\Omega}\left(h^t|\boldsymbol{\sigma}|_{t,\Omega} + \|e_h^\sigma\|_{\mathcal{A}}\right),\end{aligned}$$

if $\boldsymbol{\sigma} \in H^t(\Omega; \mathbb{C}^{3\times 3})$ for $1 \leq t \leq k+1$ and $\mathbf{u} \in \mathbf{H}^s(\Omega; \mathbb{C}^3)$ for $1 \leq s \leq k+2$.

Proof. Following [41, Lemma 4.3], it is possible to show that

$$\left|\langle\overline{\varepsilon_h^\sigma}\mathbf{n}, \mathbf{e}_h^u - \widehat{\mathbf{e}}_h^u\rangle_{\partial\mathcal{T}_h}\right| \leq Ch^t|\boldsymbol{\sigma}|_{t,\Omega}\left(\|\mathbf{P}_M\mathbf{e}_h^u - \widehat{\mathbf{e}}_h^u\|_\tau + \|\boldsymbol{\varepsilon}(\mathbf{e}_h^u)\|_{\mathcal{T}_h}\right) \tag{3.4.7a}$$

$$\left|\langle\boldsymbol{\tau}\,\overline{\boldsymbol{\varepsilon}_h^u}, \mathbf{P}_M\mathbf{e}_h^u - \widehat{\mathbf{e}}_h^u\rangle_{\partial\mathcal{T}_h}\right| \leq Ch^{s-1}|\mathbf{u}|_{s,\Omega}\|\mathbf{P}_M\mathbf{e}_h^u - \widehat{\mathbf{e}}_h^u\|_\tau. \tag{3.4.7b}$$

We recall that the argument leading to the proof of (3.4.7b) needs the traces of rigid motions to be in $\mathbf{M}_h$, which is where the additional hypothesis $k \geq 1$ is used.

We next test the first error equation (3.4.6a) with $\boldsymbol{\xi} = \boldsymbol{\varepsilon}(\overline{\mathbf{e}_h^u})$ restricted to K to obtain

$$\|\boldsymbol{\varepsilon}(\mathbf{e}_h^u)\|_K^2 = (\nabla \mathbf{e}_h^u, \boldsymbol{\varepsilon}(\overline{\mathbf{e}_h^u}))_K = \imath\kappa(\mathcal{A}(\varepsilon_h^\sigma - e_h^\sigma), \boldsymbol{\varepsilon}(\overline{\mathbf{e}_h^u}))_K + \langle \mathbf{P}_M \mathbf{e}_h^u - \widehat{\mathbf{e}}_h^u, \boldsymbol{\varepsilon}(\overline{\mathbf{e}_h^u})\mathbf{n}\rangle_{\partial K}. \quad (3.4.8)$$

The scaling hypothesis on $\boldsymbol{\tau}$ given in (3.2.4) and a scaling argument using the fact that $\boldsymbol{\varepsilon}(\mathbf{e}_h^u)$ is a polynomial on K show then

$$\begin{aligned}
\left|\langle \mathbf{P}_M \mathbf{e}_h^u - \widehat{\mathbf{e}}_h^u, \boldsymbol{\varepsilon}(\overline{\mathbf{e}_h^u})\mathbf{n}\rangle_{\partial K}\right| &\leq \|\mathbf{P}_M \mathbf{e}_h^u - \widehat{\mathbf{e}}_h^u\|_{\partial K} \|\boldsymbol{\varepsilon}(\mathbf{e}_h^u)\|_{\partial K} \\
&\leq C\|\boldsymbol{\tau}_K^{1/2}(\mathbf{P}_M \mathbf{e}_h^u - \widehat{\mathbf{e}}_h^u)\|_{\partial K} h_K^{1/2} \|\boldsymbol{\varepsilon}(\mathbf{e}_h^u)\|_{\partial K} \\
&\leq C'\|\boldsymbol{\tau}_K^{1/2}(\mathbf{P}_M \mathbf{e}_h^u - \widehat{\mathbf{e}}_h^u)\|_{\partial K} \|\boldsymbol{\varepsilon}(\mathbf{e}_h^u)\|_K.
\end{aligned}$$

Substituting these bounds in the right-hand side of (3.4.8), and adding over all elements, using (3.3.5) (the spectral bounds on the inverse compliance tensor) it follows that

$$\|\boldsymbol{\varepsilon}(\mathbf{e}_h^u)\|_{\mathcal{T}_h} \leq C\kappa\left(\|\varepsilon_h^\sigma\|_{\mathcal{A}} + \|e_h^\sigma\|_{\mathcal{A}}\right) + C\|\mathbf{P}_M \mathbf{e}_h^u - \widehat{\mathbf{e}}_h^u\|_\tau. \quad (3.4.9)$$

Plugging (3.4.9) in (3.4.7), the proposition is proved. □

3.5 Dual problem and bootstrapping process

We consider the adjoint system to (3.2.1):

$$-\imath\kappa\mathcal{A}\boldsymbol{\psi} - \boldsymbol{\varepsilon}(\boldsymbol{\phi}) = \mathbf{0} \qquad \text{in } \Omega, \quad (3.5.1a)$$

$$-\nabla\cdot\boldsymbol{\psi} - \imath\kappa\,\rho\,\boldsymbol{\phi} = \mathbf{e}_h^u \qquad \text{in } \Omega, \quad (3.5.1b)$$

$$\boldsymbol{\phi} = \mathbf{0} \qquad \text{on } \Gamma_D, \quad (3.5.1c)$$

$$\boldsymbol{\psi}\mathbf{n} = \mathbf{0} \qquad \text{on } \Gamma_N. \quad (3.5.1d)$$

This problem is uniquely solvable if (3.3.3), or equivalently, (2.5.1), is. If we assume regularity for the coercive problem (3.3.1), expressed in the bound (3.3.2), and assume the local smoothness of the coefficients given at the beginning of Section 3.3, then it is easy to see that $\boldsymbol{\phi} \in H^2(\Omega;\mathbb{C}^3)$ and $\boldsymbol{\psi} \in H^1(\Omega;\mathbb{C}^{3\times 3})$.

Lemma 3.5.1. *We can bound*

$$\|\boldsymbol{\phi}\|_{1,\Omega} + \|\rho\boldsymbol{\phi}\|_{1,\mathcal{T}_h} + \|\mathcal{A}\boldsymbol{\psi}\|_{1,\Omega} + \|\boldsymbol{\psi}\|_{1,\mathcal{T}_h} + \kappa^{-1}\|\boldsymbol{\phi}\|_{2,\Omega} \leq D_\kappa \|\mathbf{e}_h^u\|_\Omega, \tag{3.5.2}$$

where $D_\kappa := C\,(\kappa^2 C_\kappa + \kappa C_\kappa + C_\kappa + 1)$, C_κ *being the constant in* (3.3.4) *and* C *being allowed to depend on the regularity constant* (3.3.2) *as well as on the physical coefficients. Here the norm* $\|\cdot\|_{1,\mathcal{T}_h}$ *is the natural norm of the broken Sobolev space* $\prod_{K\in\mathcal{T}_h} H^1(K)$.

Remark 3.5.2. *We note that, while the regularity requirement can be somewhat relaxed, the analysis in this paper (see also [41] and [24]) needs a certain amount of regularity for the solution of the dual problem (which can be translated to regularity of the solution of* (3.3.1)*) due to the need of having square integrable normal traces of* $\boldsymbol{\psi}$ *on the faces of the elements.*

Proof. First, we begin by bounding $\|\boldsymbol{\phi}\|1,\Omega$ in terms of κ and $\mathbf{e}_h^u$. Using the bound from (3.3.4), and plugging in $\mathbf{w} = \imath\kappa\mathbf{e}_h^u$ we see that

$$\operatorname{div}\,(\mathcal{C}\varepsilon(\boldsymbol{\phi})) + \kappa^2\rho\boldsymbol{\phi} = \imath\kappa\mathbf{e}_h^u \tag{3.5.3}$$

implies a bound

$$\|\boldsymbol{\phi}\|_{1,\Omega} \leq C_\kappa \kappa \|\mathbf{e}_h^u\|_\Omega \tag{3.5.4}$$

and that, assuming the broken norm $\|\cdot\|_{1,\mathcal{T}_h} \leq E\|\cdot\|_{1,\Omega}$ where C is allowed to depend on the elliptic regularity coefficient as well as the coefficients of $\mathcal{A}$ and ρ,

$$\|\rho\boldsymbol{\phi}\|_{1,\mathcal{T}_h} \leq C C_\kappa \kappa \|\mathbf{e}_h^u\|_\Omega \tag{3.5.5}$$

Next we bound $\mathcal{A}\boldsymbol{\psi}$ and $\boldsymbol{\psi}$ in terms of $\boldsymbol{\phi}$ and κ. Consider that through (3.5.1) we know that

$$\|\imath\kappa\mathcal{A}\boldsymbol{\psi}\|_{1,\Omega} = \|\boldsymbol{\varepsilon}(\boldsymbol{\phi})\|_{1,\Omega}$$

and therefore

$$\|\mathcal{A}\boldsymbol{\psi}\|_{1,\Omega} = \frac{1}{\kappa}\|\boldsymbol{\varepsilon}(\boldsymbol{\phi})\|_{1,\Omega} \leq \frac{1}{\kappa}\|\boldsymbol{\phi}\|_{2,\Omega}. \tag{3.5.6}$$

and we also have

$$\|\boldsymbol{\psi}\|_{1,\mathcal{T}_h} \leq \frac{C}{\kappa}\|\boldsymbol{\phi}\|_{2,\Omega} \tag{3.5.7}$$

We note now that we can rewrite the elliptic regularity requirement (3.3.2) as

$$\|\mathbf{w}\|_{2,\Omega} \leq C\|\mathbf{r}\|_\Omega = C\|\text{div }(\mathcal{C}\varepsilon(\mathbf{w})) - \rho\mathbf{w}\|_\Omega \qquad \forall \mathbf{w} \in H_0^2(\Omega;\mathbb{C}^3) \tag{3.5.8}$$

where $H_0^2(\Omega;\mathbb{C}^3)$ is the space of functions from Ω to $\mathbb{C}^3$ which are twice differentiable and have homogenous boundary conditions, whether on Γ_D or Γ_N where applicable. Since $\boldsymbol{\phi} \in H_0^2(\Omega;\mathbb{C}^3)$, considering (3.5.5), we have

$$\begin{aligned}
\|\boldsymbol{\phi}\|_{2,\Omega} &\leq C(\|\text{div }\mathcal{C}\varepsilon(\boldsymbol{\phi}) - \rho\boldsymbol{\phi}\|_{\mathcal{T}_h}) \\
&\leq C(\|\text{div }\mathcal{C}\varepsilon(\boldsymbol{\phi})\|_\Omega + \|\rho\boldsymbol{\phi}\|_{\mathcal{T}_h}) \\
&= C(\|\kappa^2\rho\boldsymbol{\phi} - \imath\kappa\mathbf{e}_h^u\|_\Omega + \|\rho\boldsymbol{\phi}\|_{\mathcal{T}_h}) \\
&\leq C(\kappa^2\|\rho\phi\|_{\mathcal{T}_h} + \kappa\|\mathbf{e}_h^u\|_\Omega + \|\rho\phi\|_{\mathcal{T}_h}) \\
&\leq C(C_\kappa\kappa^3 + \kappa + C_\kappa\kappa)\|\mathbf{e}_h^u\|_\Omega
\end{aligned}$$

and therefore we may write

$$\frac{1}{\kappa}\|\boldsymbol{\phi}\|_{2,\Omega} \leq C(C_\kappa\kappa^2 + C_\kappa + 1)\|\mathbf{e}_h^u\|_\Omega \tag{3.5.9}$$

and therefore

$$\|\boldsymbol{\phi}\|_{1,\Omega} + \|\rho\boldsymbol{\phi}\|_{1,\mathcal{T}_h} + \|\mathcal{A}\boldsymbol{\psi}\|_{1,\Omega} + \|\boldsymbol{\psi}\|_{1,\mathcal{T}_h} + \kappa^{-1}\|\boldsymbol{\phi}\|_{2,\Omega} \leq D_\kappa\|\mathbf{e}_h^u\|_\Omega, \tag{3.5.10}$$

which was the statement of the lemma. □

Proposition 3.5.3 (Duality identity)**.**

$$\begin{aligned}
\|\mathbf{e}_h^u\|_\Omega^2 \quad = \quad & \imath\kappa\left((\mathcal{A}e_h^\sigma, \overline{\boldsymbol{\psi}} - \Pi_V\overline{\boldsymbol{\psi}})_{\mathcal{T}_h} + (\mathcal{A}\varepsilon_h^\sigma, \Pi_V\overline{\boldsymbol{\psi}})_{\mathcal{T}_h}\right) \\
& +\imath\kappa\left((\rho\,\mathbf{e}_h^u, \overline{\boldsymbol{\phi}} - \Pi_W\overline{\boldsymbol{\phi}})_{\mathcal{T}_h} + (\rho\,\boldsymbol{\varepsilon}_h^u, \Pi_W\overline{\boldsymbol{\phi}})_{\mathcal{T}_h}\right) \\
& +\langle\mathbf{e}_h^u - \widehat{\mathbf{e}}_h^u, (\overline{\boldsymbol{\psi}} - \Pi_V\overline{\boldsymbol{\psi}})\mathbf{n}\rangle_{\partial\mathcal{T}_h} \\
& +\langle\boldsymbol{\tau}(\mathbf{P}_M\mathbf{e}_h^u - \widehat{\mathbf{e}}_h^u) - \boldsymbol{\tau}\mathbf{P}_M\boldsymbol{\varepsilon}_h^u, \overline{\boldsymbol{\phi}} - \Pi_W\overline{\boldsymbol{\phi}}\rangle_{\partial\mathcal{T}_h} + \langle\varepsilon_h^\sigma\mathbf{n}, \Pi_W\overline{\boldsymbol{\phi}} - \mathbf{P}_M\overline{\boldsymbol{\phi}}\rangle_{\partial\mathcal{T}_h}.
\end{aligned}$$

Proof. The proof is similar to duality arguments in [41] (and related references). We give here a very systematic approach to help understand the logic of the argument. We first conjugate equations (3.5.1) and then test them with the discrete errors $(e_h^\sigma, \mathbf{e}_h^u, \widehat{\mathbf{e}}_h^u)$:

$$\imath\kappa(\mathcal{A}e_h^\sigma, \overline{\boldsymbol{\psi}})_{\mathcal{T}_h} + (\nabla\cdot e_h^\sigma, \Pi_W\overline{\boldsymbol{\phi}})_{\mathcal{T}_h} - \langle e_h^\sigma\mathbf{n}, \overline{\boldsymbol{\phi}}\rangle_{\partial\mathcal{T}_h} = 0, \tag{3.5.11a}$$

$$-(\mathbf{e}_h^u, \nabla\cdot\Pi_V\overline{\boldsymbol{\psi}})_{\mathcal{T}_h} + \langle\mathbf{e}_h^u, (\Pi_V\overline{\boldsymbol{\psi}} - \overline{\boldsymbol{\psi}})\mathbf{n}\rangle_{\partial\mathcal{T}_h} + \imath\kappa(\rho\,\mathbf{e}_h^u, \overline{\boldsymbol{\phi}})_{\mathcal{T}_h} = \|\mathbf{e}_h^u\|_\Omega^2, \tag{3.5.11b}$$

$$\langle\widehat{\mathbf{e}}_h^u, \overline{\boldsymbol{\psi}}\mathbf{n}\rangle_{\partial\mathcal{T}_h} = 0. \tag{3.5.11c}$$

Note that to reach (3.5.11a) and (3.5.11b) we need to integrate by parts and introduce projections wherever possible. Also, (3.5.11c) reflects the fact that $\boldsymbol{\psi}$ does not jump across interelement faces as well as the equality $\widehat{\mathbf{e}}_h^u = \mathbf{0}$ on Γ_D. The second ingredient for the proof is the set of error equations (3.4.6) tested with $(\Pi_V\overline{\boldsymbol{\psi}}, \Pi_W\overline{\boldsymbol{\phi}}, \mathbf{P}_M\overline{\boldsymbol{\phi}})$, to yield

$$\imath\kappa(\mathcal{A}e_h^\sigma, \overline{\boldsymbol{\psi}})_{\mathcal{T}_h} - (\mathbf{e}_h^u, \nabla\cdot\Pi_V\overline{\boldsymbol{\psi}})_{\mathcal{T}_h} + \langle\widehat{\mathbf{e}}_h^u, \overline{\boldsymbol{\psi}}\mathbf{n}\rangle_{\partial\mathcal{T}_h} = \ell_1(\boldsymbol{\psi}), \tag{3.5.12a}$$

$$(\nabla\cdot e_h^\sigma, \Pi_W\overline{\boldsymbol{\phi}})_{\mathcal{T}_h} + \imath\kappa(\rho\mathbf{e}_h^u, \overline{\boldsymbol{\phi}})_{\mathcal{T}_h} = \ell_2(\boldsymbol{\phi}), \tag{3.5.12b}$$

$$-\langle e_h^\sigma\mathbf{n}, \overline{\boldsymbol{\phi}}\rangle_{\partial\mathcal{T}_h} = \ell_3(\boldsymbol{\phi}), \tag{3.5.12c}$$

where

$$\begin{aligned}
\ell_1(\boldsymbol{\psi}) &:= \imath\kappa\left((\mathcal{A}e_h^\sigma, \overline{\boldsymbol{\psi}} - \Pi_V\overline{\boldsymbol{\psi}})_{\mathcal{T}_h} + (\mathcal{A}\varepsilon_h^\sigma, \Pi_V\overline{\boldsymbol{\psi}})_{\mathcal{T}_h}\right) + \langle\widehat{\mathbf{e}}_h^u, (\overline{\boldsymbol{\psi}} - \Pi_V\overline{\boldsymbol{\psi}})\mathbf{n}\rangle_{\partial\mathcal{T}_h},\\
\ell_2(\boldsymbol{\phi}) &:= \imath\kappa\left((\rho\mathbf{e}_h^u, \overline{\boldsymbol{\phi}} - \Pi_W\overline{\boldsymbol{\phi}})_{\mathcal{T}_h} + (\rho\boldsymbol{\varepsilon}_h^u, \Pi_W\overline{\boldsymbol{\phi}})_{\mathcal{T}_h}\right)\\
&\quad + \langle\varepsilon_h^\sigma\mathbf{n}, \Pi_W\overline{\boldsymbol{\phi}}\rangle_{\partial\mathcal{T}_h} + \langle\boldsymbol{\tau}\mathbf{P}_M\boldsymbol{\varepsilon}_h^u, \Pi_W\overline{\boldsymbol{\phi}}\rangle_{\partial\mathcal{T}_h} - \langle\boldsymbol{\tau}(\mathbf{P}_M\mathbf{e}_h^u - \widehat{\mathbf{e}}_h^u), \Pi_W\overline{\boldsymbol{\phi}}\rangle_{\partial\mathcal{T}_h}\\
\ell_3(\boldsymbol{\phi}) &:= -\langle\varepsilon_h^\sigma\mathbf{n}, \mathbf{P}_M\overline{\boldsymbol{\phi}}\rangle_{\partial\mathcal{T}_h} - \langle\boldsymbol{\tau}\mathbf{P}_M\boldsymbol{\varepsilon}_h^u, \overline{\boldsymbol{\phi}}\rangle_{\partial\mathcal{T}_h} + \langle\boldsymbol{\tau}(\mathbf{P}_M\mathbf{e}_h^u - \widehat{\mathbf{e}}_h^u), \overline{\boldsymbol{\phi}}\rangle_{\partial\mathcal{T}_h}.
\end{aligned}$$

Note that in (3.5.12) we have kept in the left-hand side of the error equations only those terms that appear in the left-hand side of (3.5.11). We have also eliminated some redundant projections and applied that $\boldsymbol{\phi} = \mathbf{0}$ on Γ_D. The proof of the result is now straightforward: add equations (3.5.11) and substitute equations (3.5.12) in the result. $\square$

The next step in the proof of the error estimates is a bound for $\|\mathbf{e}_h^u\|_\Omega$ obtained by carefully working on the right-hand side of the duality identity in Proposition 3.5.3. To alleviate the proof from an excess of constants, we will use the convention that $a \lesssim b$, whenever there exists a positive constant C independent of h and κ such that $a \leq C\, b$.

Proposition 3.5.4. *If $h\kappa D_\kappa$ is small enough, if $\boldsymbol{\sigma} \in H^t(\Omega;\mathbb{C}^{3\times 3})$ for $1 \leq t \leq k+1$, and if $\mathbf{u} \in H^s(\Omega;\mathbb{C}^3)$ for $1 \leq s \leq k+2$, then*

$$\|\mathbf{e}_h^u\|_\Omega \lesssim h(\kappa+1)D_\kappa \left(\|e_h^\sigma\|_{\mathcal{A}} + \|\mathbf{P}_M\mathbf{e}_h^u - \widehat{\mathbf{e}}_h^u\|_\tau + h^t|\boldsymbol{\sigma}|_{t,\Omega} + h^{s-1}|\mathbf{u}|_{s,\Omega}\right).$$

Proof. As already mentioned, we first estimate the right-hand side of the equality in Proposition 3.5.3. Let $[f]_h$ be the best $L^2(\Omega)$ projection of f on the space of piecewise constant functions, i.e., $[f]_h = \frac{1}{|K|}\int_K f$ in K for every K.

Notice that

$$(\mathcal{A}e_h^\sigma, \overline{\boldsymbol{\psi}} - \Pi_V\overline{\boldsymbol{\psi}})_{\mathcal{T}_h} + (\mathcal{A}\varepsilon_h^\sigma, \Pi_V\overline{\boldsymbol{\psi}})_{\mathcal{T}_h} = (\mathcal{A}(\boldsymbol{\sigma}-\boldsymbol{\sigma}_h), \overline{\boldsymbol{\psi}} - \Pi_V\overline{\boldsymbol{\psi}})_{\mathcal{T}_h} + (\varepsilon_h^\sigma, \mathcal{A}\overline{\boldsymbol{\psi}} - [\mathcal{A}\overline{\boldsymbol{\psi}}]_h)_{\mathcal{T}_h},$$

and then we can bound

$$|(\mathcal{A}e_h^\sigma, \overline{\boldsymbol{\psi}} - \Pi_V\overline{\boldsymbol{\psi}})_{\mathcal{T}_h} + (\mathcal{A}\varepsilon_h^\sigma, \Pi_V\overline{\boldsymbol{\psi}})_{\mathcal{T}_h}| \lesssim h\|\boldsymbol{\sigma}-\boldsymbol{\sigma}_h\|_{\mathcal{A}}|\boldsymbol{\psi}|_{1,\mathcal{T}_h} + h\|\varepsilon_h^\sigma\|_\Omega|\mathcal{A}\boldsymbol{\psi}|_{1,\Omega}. \quad (3.5.13)$$

Similarly, the equality

$$(\rho\, \mathbf{e}_h^u, \overline{\boldsymbol{\phi}} - \Pi_W\overline{\boldsymbol{\phi}})_{\mathcal{T}_h} + (\rho\, \boldsymbol{\varepsilon}_h^u, \Pi_W\overline{\boldsymbol{\phi}})_{\mathcal{T}_h} = (\rho(\mathbf{u}-\mathbf{u}_h), \overline{\boldsymbol{\phi}} - \Pi_W\overline{\boldsymbol{\phi}})_{\mathcal{T}_h} + (\boldsymbol{\varepsilon}_h^u, \rho\overline{\boldsymbol{\phi}} - [\rho\overline{\boldsymbol{\phi}}]_h)_{\mathcal{T}_h}$$

can be used to estimate

$$|(\rho\, \mathbf{e}_h^u, \overline{\boldsymbol{\phi}} - \Pi_W\overline{\boldsymbol{\phi}})_{\mathcal{T}_h} + (\rho\, \boldsymbol{\varepsilon}_h^u, \Pi_W\overline{\boldsymbol{\phi}})_{\mathcal{T}_h}| \lesssim h\|\mathbf{u}-\mathbf{u}_h\|_\Omega|\boldsymbol{\phi}|_{1,\Omega} + h\|\boldsymbol{\varepsilon}_h^u\|_\Omega|\rho\,\boldsymbol{\phi}|_{1,\mathcal{T}_h} \quad (3.5.14)$$

Using (3.4.7a) with $\boldsymbol{\psi}$ in place of $\boldsymbol{\sigma}$ and $t=1$ and (3.4.9), we can estimate

$$|\langle \mathbf{e}_h^u - \widehat{\mathbf{e}}_h^u, (\overline{\boldsymbol{\psi}} - \Pi_V\overline{\boldsymbol{\psi}})\mathbf{n}\rangle_{\partial\mathcal{T}_h}| \lesssim h\left(\|\varepsilon_h^\sigma\|_{\mathcal{A}} + \|e_h^\sigma\|_{\mathcal{A}} + \|\mathbf{P}_M\mathbf{e}_h^u - \widehat{\mathbf{e}}_h^u\|_\tau\right)|\boldsymbol{\psi}|_{1,\mathcal{T}_h}. \quad (3.5.15)$$

Using (3.4.7b) with $\boldsymbol{\phi}$ in place of $\mathbf{u}$ and $s=2$, we bound

$$|\langle \boldsymbol{\tau}(\mathbf{P}_M\mathbf{e}_h^u - \widehat{\mathbf{e}}_h^u), \overline{\boldsymbol{\phi}} - \Pi_W\overline{\boldsymbol{\phi}}\rangle_{\partial\mathcal{T}_h}| \lesssim h\|\mathbf{P}_M\mathbf{e}_h^u - \widehat{\mathbf{e}}_h^u\|_\tau|\boldsymbol{\phi}|_{2,\Omega}. \quad (3.5.16)$$

With a scaling argument and the bound (3.2.4) (stating the size of the stabilization parameter), we can bound on every K

$$
\begin{aligned}
|\langle \boldsymbol{\tau} \mathbf{P}_M(\mathbf{u}-\Pi_W\mathbf{u}), \overline{\boldsymbol{\phi}}-\Pi_W\overline{\boldsymbol{\phi}}\rangle_{\partial K}| &\lesssim h_K^{-1}\|\mathbf{u}-\Pi_W\mathbf{u}\|_{\partial K}\|\boldsymbol{\phi}-\Pi_W\boldsymbol{\phi}\|_{\partial K}\\
&\lesssim h_K^s|\mathbf{u}|_{s,K}|\boldsymbol{\phi}|_{2,K}
\end{aligned}
$$

and therefore

$$
|\langle \boldsymbol{\tau} \mathbf{P}_M \boldsymbol{\varepsilon}_h^u, \overline{\boldsymbol{\phi}}-\Pi_W\overline{\boldsymbol{\phi}}\rangle_{\partial \mathcal{T}_h}| \lesssim h^s|\mathbf{u}|_{s,\Omega}|\boldsymbol{\phi}|_{2,\Omega}. \tag{3.5.17}
$$

Similarly

$$
|\langle \varepsilon_h^\sigma \mathbf{n}, \mathbf{P}_M\overline{\boldsymbol{\phi}}-\Pi_W\overline{\boldsymbol{\phi}}\rangle_{\partial \mathcal{T}_h}| \lesssim h^{t+1}|\boldsymbol{\sigma}|_{t,\Omega}|\boldsymbol{\phi}|_{2,\Omega}. \tag{3.5.18}
$$

Collecting the estimates (3.5.13)-(3.5.18) to bound the right-hand side of the identity in Proposition 3.5.3, and using the regularity bound (3.3.2), we can bound

$$
\begin{aligned}
\|\mathbf{e}_h^u\|_\Omega^2 \lesssim{}& h\kappa D_\kappa \|\mathbf{e}_h^u\|_\Omega \left(\|\mathbf{e}_h^u\|_\Omega + \|e_h^\sigma\|_{\mathcal{A}} + \|\mathbf{P}_M\mathbf{e}_h^u - \widehat{\mathbf{e}}_h^u\|_\tau\right)\\
&+ h(1+\kappa)D_\kappa\left(h^t|\boldsymbol{\sigma}|_{t,\Omega} + h^{s-1}|\mathbf{u}|_{s,\Omega}\right)
\end{aligned}
$$

The proposition is now a simple consequence of the latter inequality. □

The proof of Theorem 3.3.1 follows from the energy identity (Proposition 3.4.3) and the estimates of Propositions 3.4.4 and 3.5.4 by a careful bootstrapping process.

Proof of Theorem 3.3.1. To simplify the algebra involved in this final step, let us give symbols for the quantities we want to bound

$$
\Sigma := \|e_h^\sigma\|_{\mathcal{A}}, \qquad \mathrm{T} := \kappa^{-1/2}\|\mathbf{P}_M\mathbf{e}_h^u - \widehat{\mathbf{e}}_h^u\|_\tau, \qquad \mathrm{U} := \|\mathbf{e}_h^u\|_\Omega,
$$

and for the approximation terms

$$
\Sigma_h := h^t|\boldsymbol{\sigma}|_{t,\Omega}, \qquad \mathrm{U}_h := h^{s-1}|\mathbf{u}|_{s,\Omega}.
$$

With this shorthand, Propositions 3.4.3 and 3.4.4 yield

$$
|\Sigma^2 - \imath \mathrm{T}^2| \lesssim \Sigma\,\Sigma_h + \mathrm{U}\,\mathrm{U}_h + \kappa^{-1/2}(\Sigma_h+\mathrm{U}_h)\mathrm{T} + \Sigma_h^2 + \mathrm{U}^2. \tag{3.5.19}
$$

If $\alpha := h(1+\kappa)(\kappa + \kappa C_\kappa + \kappa^2 C_\kappa + C_\kappa) = D_\kappa h(1+\kappa)$, Proposition 3.5.4 can then be rephrased as

$$\mathrm{U} \lesssim \alpha(\Sigma + \Sigma_h + \mathrm{U}_h + \kappa^{1/2}\mathrm{T}). \tag{3.5.20}$$

Substituting (3.5.20) in the right-hand side of (3.5.19), and reordering terms, we have

$$\begin{aligned} \Sigma^2 + \mathrm{T}^2 \quad &\lesssim \quad \alpha^2\Sigma^2 + \Sigma(\Sigma_h + \alpha\mathrm{U}_h) \\ &\quad +\alpha^2\kappa\mathrm{T}^2 + \mathrm{T}(\kappa^{-1/2}\mathrm{U}_h + \alpha\kappa^{1/2}\mathrm{U}_h + \kappa^{-1/2}\Sigma_h) \\ &\quad +(1+\alpha^2)\Sigma_h^2 + (\alpha+\alpha^2)\mathrm{U}_h^2. \end{aligned} \tag{3.5.21}$$

Let now C be the constant that is hidden in the symbol $\lesssim$, and let us assume that

$$C\alpha^2 \le \tfrac{1}{4} \qquad \text{and} \qquad C\alpha^2\kappa \le \tfrac{1}{4}. \tag{3.5.22}$$

We now use Young's inequality $ab \le \frac{1}{4}a^2 + b^2$ in (3.5.21) to get

$$\begin{aligned} \Sigma^2 + \mathrm{T}^2 \quad &\le \quad \tfrac{1}{2}\Sigma^2 + \tfrac{1}{2}\mathrm{T}^2 \\ &\quad +C^2(\Sigma_h + \alpha\mathrm{U}_h)^2 + C^2(\kappa^{-1/2}\mathrm{U}_h + \alpha\kappa^{1/2}\mathrm{U}_h + \kappa^{-1/2}\Sigma_h)^2 \\ &\quad +C(1+\alpha^2)\Sigma_h^2 + C(\alpha+\alpha^2)\mathrm{U}_h^2. \end{aligned}$$

We can now simplify this expression using (3.5.22) to obtain $\Sigma^2 + \mathrm{T}^2 \lesssim (1+\kappa^{-1})(\Sigma_h^2 + \mathrm{U}_h^2)$, or equivalently

$$\Sigma + \mathrm{T} \lesssim (1+\kappa^{-1/2})(\Sigma_h + \mathrm{U}_h). \tag{3.5.23}$$

Using (3.5.23) in (3.5.20), we can finally prove that

$$\mathrm{U} \lesssim \alpha(1 + \kappa^{1/2} + \kappa^{-1/2})(\Sigma_h + \mathrm{U}_h). \tag{3.5.24}$$

This finishes the proof. $\square$

3.6 Variants and insights

Matrix form. We first give a matrix representation of the method of Section 3.3. Equations (3.2.6c) and (3.2.6d) suggest the following orthogonal decomposition $\mathbf{M}_h = \mathbf{M}_h^{nD} \oplus \mathbf{M}_h^D$, where $\mathbf{M}_h^{nD} = \{\boldsymbol{\mu} : \boldsymbol{\mu}|_{\Gamma_D} = 0\} \equiv \{\boldsymbol{\mu}|_{\partial\mathcal{T}_h\setminus\Gamma_D} : \boldsymbol{\mu} \in \mathbf{M}_h\}$. We now take real-valued bases for the spaces $\mathbb{V}_h$, $\mathbf{W}_h$, $\mathbf{M}_h^{nD}$, and $\mathbf{M}_h^{D}$ and identify the unknowns $\boldsymbol{\sigma}_h \in \mathbb{V}_h$, $\mathbf{u}_h \in \mathbf{W}_h$, $\widehat{\mathbf{u}}_h|_{\partial\mathcal{T}_h\setminus\Gamma_D} \in \mathbf{M}_h^{nD}$, and $\widehat{\mathbf{u}}_h|_{\Gamma_D} \in \mathbf{M}_h^{D}$, with respective complex column vectors $\underline{\sigma}$, $\underline{u}$, $\underline{\widehat{u}}^{nD}$, and $\underline{\widehat{u}}^{D}$. We then consider *real matrices* associated to the following *bilinear forms* that are understood as functionals acting on the unknowns:

$$
\begin{array}{rcl}
(\mathcal{A}\boldsymbol{\sigma}_h, \boldsymbol{\xi})_{\mathcal{T}_h} & \boldsymbol{\xi} \in \mathbb{V}_h & \mathrm{A}\underline{\sigma}, \\
(\nabla\cdot\boldsymbol{\sigma}_h, \mathbf{w})_{\mathcal{T}_h} & \mathbf{w} \in \mathbf{W}_h & \mathrm{D}\underline{\sigma}, \\
\langle \boldsymbol{\sigma}_h \mathbf{n}, \boldsymbol{\mu}\rangle_{\partial\mathcal{T}_h\setminus\Gamma_D} & \boldsymbol{\mu} \in \mathrm{M}_h^{nD} & \mathrm{N}\underline{\sigma}, \\
\langle \boldsymbol{\sigma}_h \mathbf{n}, \boldsymbol{\mu}\rangle_{\Gamma_D} & \boldsymbol{\mu} \in \mathrm{M}_h^{D} & \mathrm{N}_D\underline{\sigma}, \\
(\rho\mathbf{u}_h, \mathbf{w})_{\mathcal{T}_h} & \mathbf{w} \in \mathbf{W}_h & \mathrm{M}\underline{u}, \\
\langle \boldsymbol{\tau}\mathbf{P}_M\mathbf{u}_h, \mathbf{P}_M\mathbf{w}\rangle_{\mathcal{T}_h} & \mathbf{w} \in \mathbf{W}_h & \mathrm{T}_{11}\underline{u}, \\
\langle \boldsymbol{\tau}\widehat{\mathbf{u}}_h, \mathbf{w}_h\rangle_{\partial\mathcal{T}_h\setminus\Gamma_D} & \mathbf{w} \in \mathbf{W}_h & \mathrm{T}_{12}\underline{u}^{nD}, \\
\langle \boldsymbol{\tau}\widehat{\mathbf{u}}_h, \mathbf{w}_h\rangle_{\Gamma_D} & \mathbf{w} \in \mathbf{W}_h & \mathrm{T}_{D}\underline{u}^{D}, \\
\langle \boldsymbol{\tau}\widehat{\mathbf{u}}_h, \boldsymbol{\mu}\rangle_{\partial\mathcal{T}_h\setminus\Gamma_D} & \boldsymbol{\mu} \in \mathrm{M}_h^{nD} & \mathrm{T}_{22}\underline{u}^{nD}, \\
\langle \widehat{\mathbf{u}}_h, \boldsymbol{\mu}\rangle_{\Gamma_D} & \boldsymbol{\mu} \in \mathrm{M}_h^{D} & \mathrm{M}_D\underline{\widehat{u}}^{D}.
\end{array}
$$

Note that the matrices A, M, and T_{22} are symmetric and positive definite, while T_{11} is symmetric and positive semidefinite. The method given by equations (3.2.6) is then equivalent to the linear system

$$
\begin{bmatrix}
\imath\kappa\mathrm{A} & -\mathrm{D}^\top & \mathrm{N}^\top & \mathrm{N}_D^\top \\
\mathrm{D} & \imath\kappa\mathrm{M}+\mathrm{T}_{11} & -\mathrm{T}_{12} & -\mathrm{T}_D \\
-\mathrm{N} & -\mathrm{T}_{12}^\top & \mathrm{T}_{22} & \mathrm{O} \\
\mathrm{O} & \mathrm{O} & \mathrm{O} & \mathrm{M}_D
\end{bmatrix}
\begin{bmatrix}
\underline{\sigma} \\ \underline{u} \\ \underline{\widehat{u}}^{nD} \\ \underline{\widehat{u}}^{D}
\end{bmatrix}
=
\begin{bmatrix}
\underline{0} \\ \underline{f} \\ -\underline{g}_N \\ \underline{g}_D
\end{bmatrix}, \tag{3.6.1}
$$

where the definition of the vectors $\underline{f}$, $\underline{g}_N$ and $\underline{g}_D$ is self-evident. Equations (3.6.1) are equivalent to the following system

$$
\begin{bmatrix}
\mathrm{A} & \mathrm{D}^\top & -\mathrm{N}^\top & -\mathrm{N}_D^\top \\
-\mathrm{D} & -\kappa^2\mathrm{M}-\imath\kappa\mathrm{T}_{11} & \imath\kappa\mathrm{T}_{12} & \imath\kappa\mathrm{T}_D \\
\mathrm{N} & -\imath\kappa\mathrm{T}_{12}^\top & \imath\kappa\mathrm{T}_{22} & \mathrm{O} \\
\mathrm{O} & \mathrm{O} & \mathrm{O} & \mathrm{M}_D
\end{bmatrix}
\begin{bmatrix}
\underline{\widetilde{\sigma}} \\ \underline{u} \\ \underline{\widehat{u}}^{nD} \\ \underline{\widehat{u}}^{D}
\end{bmatrix}
=
\begin{bmatrix}
\underline{0} \\ \underline{\widetilde{f}} \\ \underline{\widetilde{g}}_N \\ \underline{g}_D
\end{bmatrix}, \tag{3.6.2}
$$

where $\underline{\widetilde{\sigma}} = -\imath\kappa\underline{\sigma}$, $\underline{\widetilde{f}} = -\imath\kappa\underline{f}$, and $\underline{\widetilde{g}}_N = -\imath\kappa\underline{g}_N$. This change of variables in the first unknown and in the right-hand side reverts the system to the original physical variables (the ones with a tilde in Section 2.2) so that the equations are second-order-in-frequency. It is clear how the stabilization terms are the only complex-valued ones in the system.

Hybridization. The four matrices in the upper left 2×2 block of the matrix of (3.6.1) are elementwise block diagonal. The hybridization process consists of solving the system

$$\left(\begin{bmatrix} \mathrm{N} & \mathrm{T}_{12}^\top \end{bmatrix} \mathrm{C}^{-1} \begin{bmatrix} \mathrm{N}^\top \\ -\mathrm{T}_{12} \end{bmatrix} + \mathrm{T}_{22} \right) \underline{\widehat{u}}^{nD} = -\,\underline{g}_N + \begin{bmatrix} \mathrm{N} & \mathrm{T}_{12}^\top \end{bmatrix} \mathrm{C}^{-1} \begin{bmatrix} \underline{0} \\ \underline{f} \end{bmatrix}$$
$$- \begin{bmatrix} \mathrm{N} & \mathrm{T}_{12}^\top \end{bmatrix} \mathrm{C}^{-1} \begin{bmatrix} \mathrm{N}_D^\top \\ -\mathrm{T}_D \end{bmatrix} \mathrm{M}_D^{-1} \underline{g}_D,$$

where the invertibility of

$$\mathrm{C} := \begin{bmatrix} \imath\kappa\mathrm{A} & -\mathrm{D}^\top \\ \mathrm{D} & \imath\kappa\mathrm{M} + \mathrm{T}_{11} \end{bmatrix}$$

was the object of Proposition 3.4.2.

Variant # 1: time reversal. While we are not making any claims about the behavior of the method for high frequency problems, we have kept κ visible everywhere. We next explore some variants of the method that can be obtained by changing to second-order-in-frequency form and exploring different choices of the stabilization parameter. The energy identity of Proposition 3.4.3 is the trigger for the analysis of the method. It is there clear that the sign of the boundary term is not relevant and a method based on the numerical flux

$$\widehat{\boldsymbol{\sigma}}_h\mathbf{n} := \boldsymbol{\sigma}_h\mathbf{n} - \boldsymbol{\tau}_K(\mathbf{P}_M\mathbf{u}_h - \widehat{\mathbf{u}}_h) \,:\, \partial K \to \mathbb{C}^3$$

has the same convergence properties as the method presented in Section 2.2. As we will see later in this section, this method corresponds to time reversal.

Variant # 2: κ-scaled stabilization. The factor $\kappa^{-1/2}$ in the error estimate of Theorem 3.3.1 suggests the following variant of the numerical method: we still use equations (3.2.6) by changing the definition of the numerical flux to be

$$\widehat{\boldsymbol{\sigma}}_h\mathbf{n} := \boldsymbol{\sigma}_h\mathbf{n} + \kappa\boldsymbol{\tau}_K(\mathbf{P}_M\mathbf{u}_h - \widehat{\mathbf{u}}_h) \,:\, \partial K \to \mathbb{C}^3. \tag{3.6.3}$$

(Note that, as shown in [23] for the acoustic wave equation, making the stabilization parameter depend on κ is a must when we want to deal with complex frequencies. This dependence has also some desirable properties.) The proof of Theorem 3.3.1 can be easily adapted to deal with the method whose stabilization term is given by (3.6.3). The error estimate is given in the following theorem.

Theorem 3.6.1. *There exist $C_1, C_2 > 0$, dependent only on the shape-regularity of $\mathcal{T}_h$, the density ρ and the coefficients of the inverse compliance tensor $\mathcal{A}$ such that if $h(1+\kappa)^{3/2}(1+\kappa C_\kappa)$ is small enough, then the errors can be bounded by*

$$\|e_h^\sigma\|_{\mathcal{A}} + \|\mathbf{P}_M\mathbf{e}_h^u - \widehat{\mathbf{e}}_h^u\|_\tau \le C_1\big((1+\kappa^{-1})h^t|\boldsymbol{\sigma}|_{t,\Omega} + h^{s-1}|\mathbf{u}|_{s,\Omega}\big)$$

and

$$\|\mathbf{e}_h^u\|_\Omega \le C_2(1+\kappa C_\kappa)(1+\kappa)\big((\kappa+\kappa^{-1})h^{t+1}|\boldsymbol{\sigma}|_{t,\Omega} + h^s(1+\kappa)|\mathbf{u}|_{s,\Omega}\big),$$

if $k \ge 1$, $\mathbf{u} \in H^s(\Omega;\mathbb{C}^3)$ with $1 \le s \le k+2$, and $\boldsymbol{\sigma} \in H^t(\Omega;\mathbb{C}^{3\times 3})$ with $1 \le t \le k+1$.

Second-order-in-frequency formulations. Since all methods presented above are based in a first-order-in-frequency formulation, defining $\boldsymbol{\sigma} := (\imath/\kappa)\widetilde{\boldsymbol{\sigma}}$, where $\widetilde{\boldsymbol{\sigma}}$ is the physical stress for the displacement field $\mathbf{u}$. Consider now the following family of HDG schemes based on a second-order-in-frequency formulation: the spaces are unchanged and α_κ is a fixed parameter that is allowed to depend on the frequency:

$$(\mathcal{A}\widetilde{\boldsymbol{\sigma}}_h, \boldsymbol{\xi})_{\mathcal{T}_h} + (\mathbf{u}_h, \nabla\cdot\boldsymbol{\xi})_{\mathcal{T}_h} - \langle\widehat{\mathbf{u}}_h, \boldsymbol{\xi}\mathbf{n}\rangle_{\partial\mathcal{T}_h} = 0 \qquad \forall\boldsymbol{\xi} \in \mathbb{V}_h, \tag{3.6.4a}$$

$$(\widetilde{\boldsymbol{\sigma}}_h, \nabla\mathbf{w})_{\mathcal{T}_h} - \langle\widehat{\boldsymbol{\sigma}}_h\mathbf{n}, \mathbf{w}\rangle_{\boldsymbol{\tau}} - \kappa^2(\rho\,\mathbf{u}_h, \mathbf{w})_{\mathcal{T}_h} = -(\widetilde{\mathbf{f}}, \mathbf{w})_{\mathcal{T}_h} \qquad \forall\mathbf{w} \in \mathbf{W}_h, \tag{3.6.4b}$$

$$\langle\widehat{\boldsymbol{\sigma}}_h\mathbf{n}, \boldsymbol{\mu}\rangle_{\partial\mathcal{T}_h\setminus\Gamma_D} = \langle\widetilde{\mathbf{g}}_N, \boldsymbol{\mu}\rangle_{\Gamma_N} \qquad \forall\boldsymbol{\mu} \in \mathbf{M}_h, \tag{3.6.4c}$$

$$\langle\widehat{\mathbf{u}}_h, \boldsymbol{\mu}\rangle_{\Gamma_D} = \langle\mathbf{g}_D, \boldsymbol{\mu}\rangle_{\Gamma_D} \qquad \forall\boldsymbol{\mu} \in \mathbf{M}_h, \tag{3.6.4d}$$

where

$$\widehat{\boldsymbol{\sigma}}_h \mathbf{n} := \widetilde{\boldsymbol{\sigma}}_h \mathbf{n} - \alpha_\kappa \boldsymbol{\tau}(\mathbf{P}_M \mathbf{u}_h - \widehat{\mathbf{u}}_h). \tag{3.6.4e}$$

Note that the equations are written in terms of the original data in (2.5.1). The choice $\alpha_\kappa = 1$ is the direct application of the method in [41] to the equation $\nabla \cdot \widetilde{\boldsymbol{\sigma}} + \kappa^2 \rho \mathbf{u} = \widetilde{\mathbf{f}}$. This choice of the parameter α_κ yields a method that transitions smoothly (analytically) to the zero-frequency limit. Methods based on the first-order-in-frequency formulation can be rewritten in the form (3.6.4) with the relation $\widetilde{\boldsymbol{\sigma}}_h = -\imath\kappa\boldsymbol{\sigma}_h$ and the parameter $\alpha_\kappa := \imath\kappa$ (for the method of Section 3.3, $\alpha_\kappa := -\imath\kappa$ (time reversed method) or $\alpha_\kappa = \imath\kappa^2$ (for the method with the flux defined in (3.6.3).

Variant # 3: conservative method. The error estimate for the method in (3.6.4) with the choice $\alpha_\kappa = 1$ is given in the next theorem. Not surprisingly the estimates hold as $\kappa \to 0$, since we end up with a smooth perturbation of the discretization of the steady-state equations. Note that when $\kappa \to 0$ and we are not dealing with the pure Neumann problem, the quantity C_κ converges to a finite value. Later in this section we will see that this choice corresponds to a conservative method in the time domain.

Theorem 3.6.2. *There exist $D_1, D_2 > 0$, dependent only on the shape-regularity of $\mathcal{T}_h$, the density ρ and the coefficients of the inverse compliance tensor $\mathcal{A}$ such that if $h(1+\kappa)E_\kappa$ is small enough, then the errors can be bounded by*

$$\|\Pi_V \widetilde{\boldsymbol{\sigma}} - \widetilde{\boldsymbol{\sigma}}_h\|_{\mathcal{A}} + \|\mathbf{P}_M \mathbf{e}_h^u - \widehat{\mathbf{e}}_h^u\|_\tau \le D_1\big(h^t |\widetilde{\boldsymbol{\sigma}}|_{t,\Omega} + (1+\kappa) h^{s-1} |\mathbf{u}|_{s,\Omega}\big)$$

and

$$\|\mathbf{e}_h^u\|_\Omega \le D_2 E_\kappa (1+\kappa)\big(h^{t+1} |\widetilde{\boldsymbol{\sigma}}|_{t,\Omega} + h^s (1+\kappa) |\mathbf{u}|_{s,\Omega}\big),$$

if $k \ge 1$, $\mathbf{u} \in H^s(\Omega; \mathbb{C}^3)$ with $1 \le s \le k+2$, and $\widetilde{\boldsymbol{\sigma}} \in H^t(\Omega; \mathbb{C}^{3\times 3})$ with $1 \le t \le k+1$. Here $E_\kappa \le C(1 + \kappa C_\kappa + C_\kappa + \kappa C_\kappa^{1/2})$.

Proof. See Section 3.8. □

3.7 Numerical experiments

For the following experiments, consider the unit cube $\Omega = [0, 1]^3$. We imbue the domain with Lamé parameters $\lambda(\mathbf{x})$ and $\mu(\mathbf{x})$ as well as mass density $\rho(\mathbf{x})$ given, respectively, by

$$\lambda = 2 + 0.2x^2 + 0.3y^2 + 0.04z^2 \qquad \mu = 3 + 0.5y^2 + 0.03z^2 \qquad \rho = 1 + x^2$$

and then subject Ω to a time-invariant displacement vector field of

$$\mathbf{u}(x, y, z) = \begin{bmatrix} \cos(\pi x)\sin(\pi x)\cos(\pi z) \\ 5x^2yz + 4xy^z + 3xyz^2 + 17 \\ \cos(2x)\cos(3y)\cos(z) \end{bmatrix}$$

attached to a fixed wavenumber $\kappa = 1$.

Dirichlet conditions ($\mathbf{u}$ itself) are applied to the top and bottom faces of the cube, which are those that, undisturbed, lie on the planes $z = 1$ and $z = 0$, respectively. The side faces (those parallel to the xz and yz planes) are subject to Neumann conditions consistent with $\mathbf{u}$. The forcing function, which is either $\mathbf{f}$ or $\widetilde{\mathbf{f}}$, depending on the method variant, is adjusted accordingly to match the exact solution.

Each trial consists of dividing each edge of Ω into $n = 1, 2, 3, \ldots, 7$ segments, yielding n^3 subcubes; each subcube is then split into six elements (three different pairs of respectively isometrically reflected tetrahedra), and so we have seven tetrahedrizations $\{\mathcal{T}_h{}^n\}_{n=1}^7$ of Ω, each with $6n^3$ elements, respectively.

We program the first-order method that we have analyzed in full as well as the second-order variant corresponding to the conservative method in MATLAB. Here we use Dubiner bases of Jacobi polynomials in three dimensions for $\mathbb{V}_h$ and $\mathbf{W}_h$ and two dimensions for $\mathbf{M}_h$. Note that the Dubiner basis is hierarchical, hence the basis needs only to be evaluated once at each point to be tested at degree $k+1$ for $\mathbf{W}_h$, then truncated to a basis of degree k for $\mathbb{V}_h$. In all cases $\tau = n\mathrm{I}_{3\times 3}$

Functions are tested via a Stroud quadrature rule, using the function `ccdqf.m` by John Burkhardt (open source) in order to generate Gauss-Jacobi quadrature rules in the interval $[-1, 1]$, and then applying this twice on a transformation from the reference face to the square $[-1, 1]^2$. The code is built from the work of Fu, Gatica, and Sayas [18] for working with HDG in three dimensions, and adjusted to match the dimensions of the time-harmonic elasticity problem.

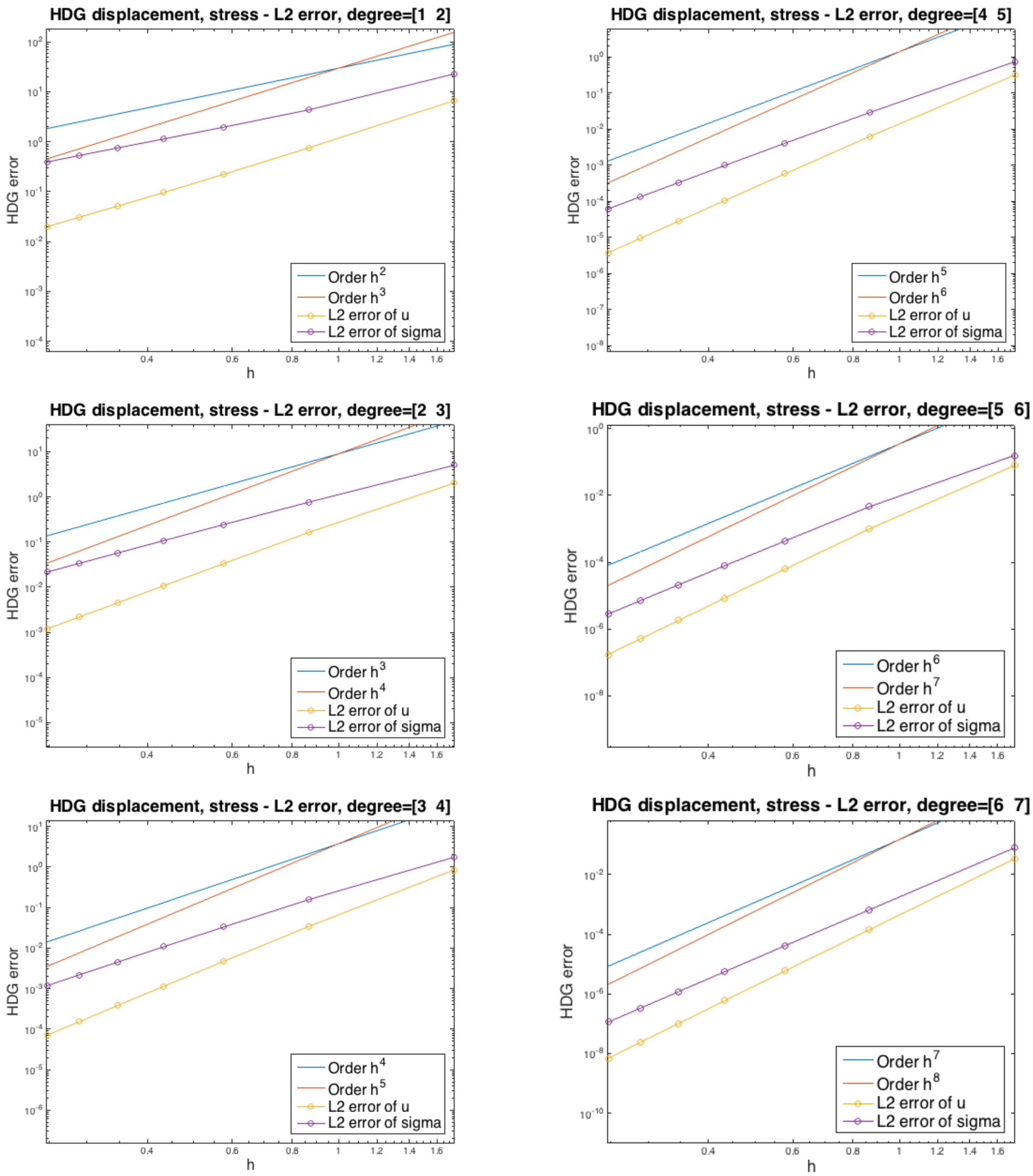

Figure 3.1: First-order-in-frequency method. Mixed boundary conditions. $\kappa = 1$. Expected order of convergence: $\mathcal{O}(h^{k+2})$ for $\mathbf{u}$ and $\mathcal{O}(h^{k+1})$ for $\boldsymbol{\sigma}$. ($k = 1$ top-left, $k = 2$ top-right, $k = 3$ mid-left, $k = 4$ mid-right, $k = 5$ bottom left, $k = 6$ bottom right)

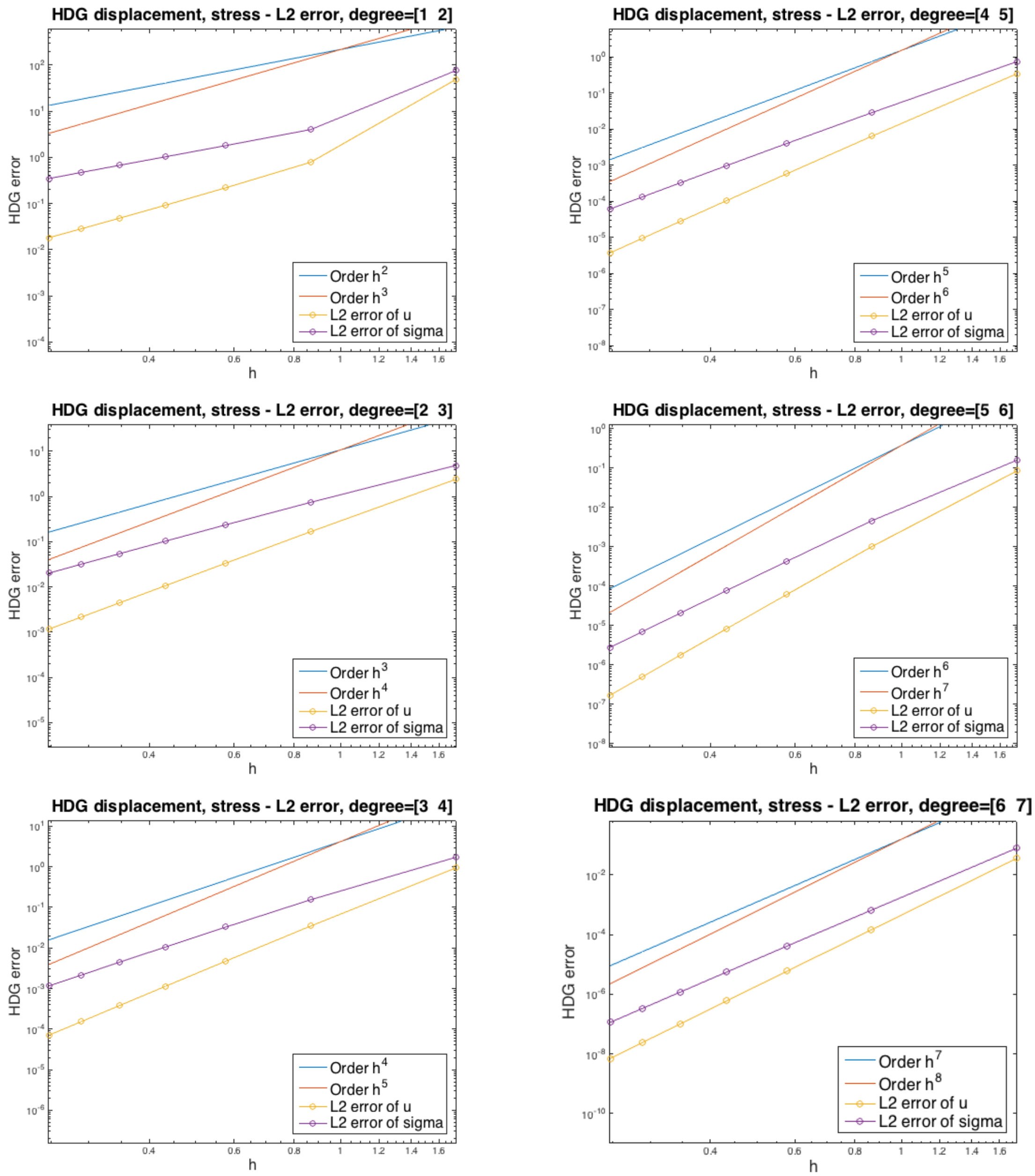

Figure 3.2: Second-order-in-frequency method. Mixed boundary conditions. $\kappa = 1$. Expected order of convergence: $\mathcal{O}(h^{k+2})$ for $\mathbf{u}$ and $\mathcal{O}(h^{k+1})$ for $\boldsymbol{\sigma}$.($k = 1$ top-left, $k = 2$ top-right, $k = 3$ mid-left, $k = 4$ mid-right, $k = 5$ bottom-left, $k = 6$ bottom-right

Comparison of the dimensions of the global solution spaces. We now compare the dimension of the Lagrange element displacement approximation space for a CG trial to that of the hybrid $\mathbf{M}_h$ in the HDG framework at different polynomial degrees. Note that this dimension corresponds to the size of the global linear system that must be inverted in order to achieve optimal ($\mathcal{O}(h^{k+2})$) convergence of $\|\mathbf{u}-\mathbf{u}_h\|_{L^2(\Omega)}$. Note also that all variants of the HDG method use precisely the same space $\mathbf{M}_h$ (whether over the complex or real fields), whose elementwise polynomials have maximum degree one less than that of those of the displacement space.

We observe that for this particular family of seven tetrahedrizations of the unit cube, it is when $k \geq 6$ that the global HDG system is smaller than that of the corresponding CG system. The reason behind this is clear: Lagrange element CG methods require much higher numbers of internal (volume) nodes, which increase at $O\left(\binom{k+3}{3}N_{\text{elt}}\right)$. The hybridization of the HDG system transfers global information onto only the skeleton $\mathcal{E}_h$; the number of degrees of freedom corresponding to $\mathbf{M}_h$ only grows at $O\left(\binom{k+2}{2}N_{\text{elt}}\right)$. Thus, as the polynomial degree k increases, the HDG method tends to have a smaller global system than that of the corresponding CG system. For more on this, see [10].

Dim(FEM_h)	Dim($\mathbf{M}_h$)	Dim(FEM_h)	Dim($\mathbf{M}_h$)	Dim(FEM_h)	Dim($\mathbf{M}_h$)	Dim(FEM_h)	Dim($\mathbf{M}_h$)
($k = 1$)	($k = 0$)	($k = 4$)	($k = 3$)	($k = 7$)	($k = 6$)	($k = 10$)	($k = 9$)
24	54	375	540	1536	1512	3993	2970
81	360	2187	3600	10125	10080	27783	19800
192	1134	6591	11340	31944	31752	89373	62370
375	2592	14739	25920	73167	72576	206763	142560
648	4950	27783	49500	139968	138600	397953	272250
1029	8424	46875	84240	238521	235872	680943	463320
1536	13230	73167	132300	375000	370440	1073733	727650

Dim(FEM_h)	Dim($\mathbf{M}_h$)	Dim(FEM_h)	Dim($\mathbf{M}_h$)	Dim(FEM_h)	Dim($\mathbf{M}_h$)	Dim(FEM_h)	Dim($\mathbf{M}_h$)
($k = 2$)	($k = 1$)	($k = 5$)	($k = 4$)	($k = 8$)	($k = 7$)	($k = 11$)	($k = 10$)
81	162	648	810	2187	1944	5184	3564
375	1080	3993	5400	14739	12960	36501	23760
1029	3402	12288	17010	46875	40824	117912	74844
2187	7776	27783	38880	107811	93312	273375	171072
3993	14850	52728	74250	206763	178200	526848	326700
6591	25272	89373	126360	352947	303264	902289	555984
10125	39690	139968	198450	555579	476280	1423656	873180

Dim(FEM_h)	Dim($\mathbf{M}_h$)	Dim(FEM_h)	Dim($\mathbf{M}_h$)	Dim(FEM_h)	Dim($\mathbf{M}_h$)	Dim(FEM_h)	Dim($\mathbf{M}_h$)
($k = 3$)	($k = 2$)	($k = 6$)	($k = 5$)	($k = 9$)	($k = 8$)	($k = 12$)	($k = 11$)
192	324	1029	1134	3000	2430	6591	4212
1029	2160	6591	7560	20577	16200	46875	28080
3000	6804	20577	23814	65856	51030	151959	88452
6591	15552	46875	54432	151959	116640	352947	202176
12288	29700	89373	103950	292008	222750	680943	386100
20577	50544	151959	176904	499125	379080	1167051	657072
31944	79380	238521	277830	786432	595350	1842375	1031940

Table 3.1: Comparison of dimensions of global solution spaces

3.8 Some additional proof

Sketch of the proof of Theorem 3.6.2. The first order in space, second order in frequency system is

$$\begin{aligned} \mathcal{A}\widetilde{\boldsymbol{\sigma}} - \boldsymbol{\varepsilon}(\mathbf{u}) &= \mathbf{0} && \text{in } \Omega,\\ \mathrm{div}\, \widetilde{\boldsymbol{\sigma}} + \kappa^2 \rho\, \mathbf{u} &= \widetilde{\mathbf{f}} && \text{in } \Omega,\\ \mathbf{u} &= \mathbf{g}_D && \text{on } \Gamma_D,\\ \widetilde{\boldsymbol{\sigma}}\mathbf{n} &= \widetilde{\mathbf{g}}_N && \text{on } \Gamma_N. \end{aligned}$$

From this moment on, we will drop all tildes in the formulas. It has to be understood though that the stress that we are computing with this method is the physical stress and not the one scaled by $\imath/\kappa$. The error equations are

$$(\mathcal{A}e_h^\sigma, \boldsymbol{\xi})_{\mathcal{T}_h} + (\mathbf{e}_h^u, \mathrm{div}\, \boldsymbol{\xi})_{\mathcal{T}_h} - \langle \widehat{\mathbf{e}}_h^u, \boldsymbol{\xi}\mathbf{n}\rangle_{\partial\mathcal{T}_h} = (\mathcal{A}\varepsilon_h^\sigma, \boldsymbol{\xi})_{\mathcal{T}_h}, \tag{3.8.2a}$$

$$\begin{aligned} -(\mathrm{div}\; e_h^\sigma, \mathbf{w})_{\mathcal{T}_h} - \kappa^2(\rho\mathbf{e}_h^u, \mathbf{w})_{\mathcal{T}_h} &\\ +\langle \boldsymbol{\tau}(\mathbf{P}_M\mathbf{e}_h^u - \widehat{\mathbf{e}}_h^u), \mathbf{P}_M\mathbf{w}\rangle_{\partial\mathcal{T}_h} &= -\kappa^2(\rho\boldsymbol{\varepsilon}_h^u, \mathbf{w})_{\mathcal{T}_h} \\ &\quad - \langle \varepsilon_h^\sigma\mathbf{n}, \mathbf{w}\rangle_{\partial\mathcal{T}_h} + \langle \boldsymbol{\tau}\boldsymbol{\varepsilon}_h^u, \mathbf{P}_M\mathbf{w}\rangle_{\partial\mathcal{T}_h}, \end{aligned} \tag{3.8.2b}$$

$$\langle e_h^\sigma\mathbf{n} - \boldsymbol{\tau}(\mathbf{P}_M\mathbf{e}_h^u - \widehat{\mathbf{e}}_h^u), \boldsymbol{\mu}\rangle_{\partial\mathcal{T}_h\setminus\Gamma_D} = \langle \varepsilon_h^\sigma\mathbf{n}, \boldsymbol{\mu}\rangle_{\partial\mathcal{T}_h\setminus\Gamma_D} - \langle \boldsymbol{\tau}\mathbf{P}_M\boldsymbol{\varepsilon}_h^u, \boldsymbol{\mu}\rangle_{\partial\mathcal{T}_h\setminus\Gamma_D} \tag{3.8.2c}$$

$$\langle \widehat{\mathbf{e}}_h^u, \boldsymbol{\mu}\rangle_{\Gamma_D} = 0, \tag{3.8.2d}$$

and a simple argument shows the new energy identity

$$\begin{aligned} &\|e_h^\sigma\|_{\mathcal{A}}^2 - \kappa^2\|\mathbf{e}_h^u\|_\rho^2 + \|\mathbf{P}_M\mathbf{e}_h^u - \widehat{\mathbf{e}}_h^u\|_\tau^2 \\ &= (\mathcal{A}\varepsilon_h^\sigma, \overline{e_h^\sigma})_{\mathcal{T}_h} - \kappa^2(\rho\overline{\boldsymbol{\varepsilon}_h^u}, \mathbf{e}_h^u)_{\mathcal{T}_h} - \langle \overline{\varepsilon_h^\sigma}\mathbf{n}, \mathbf{e}_h^u - \widehat{\mathbf{e}}_h^u\rangle_{\partial\mathcal{T}_h} + \langle \boldsymbol{\tau}\, \overline{\boldsymbol{\varepsilon}_h^u}, \mathbf{P}_M\mathbf{e}_h^u - \widehat{\mathbf{e}}_h^u\rangle_{\partial\mathcal{T}_h}. \end{aligned} \tag{3.8.3}$$

The adjoint problem has to be written as

$$\mathcal{A}\boldsymbol{\psi} + \boldsymbol{\varepsilon}(\boldsymbol{\phi}) = \mathbf{0} \qquad \text{in } \Omega, \tag{3.8.4a}$$

$$-\nabla\cdot\boldsymbol{\psi} + \kappa^2\rho\,\boldsymbol{\phi} = -\mathbf{e}_h^u \qquad \text{in } \Omega, \tag{3.8.4b}$$

$$\boldsymbol{\phi} = \mathbf{0} \qquad \text{on } \Gamma_D, \tag{3.8.4c}$$

$$\boldsymbol{\psi}\mathbf{n} = \mathbf{0} \qquad \text{on } \Gamma_N, \tag{3.8.4d}$$

where the negative sign in the right hand side is added for convenience. With the usual regularity hypotheses, the scaled regularity inequalities for the solution of this problem are:

$$\kappa(\|\boldsymbol{\phi}\|_{1,\Omega} + \|\rho\boldsymbol{\phi}\|_{1,\mathcal{T}_h}) + \|\mathcal{A}\boldsymbol{\psi}\|_{1,\Omega} + \|\boldsymbol{\psi}\|_{1,\mathcal{T}_h} + \|\boldsymbol{\phi}\|_{2,\Omega} \leq E_\kappa \|\mathbf{e}_h^u\|_\Omega,$$

with E_κ bounded as in the statement of the theorem. The proof of this inequality is very similar to the proof of (3.5.1) above. After integration by parts and introduction of projections it can be shown that the solution of (3.8.4) satisfies the following identities

$$(\mathcal{A}e_h^\sigma, \overline{\boldsymbol{\psi}})_{\mathcal{T}_h} - (\text{div } e_h^\sigma, \Pi_W \overline{\boldsymbol{\phi}})_{\mathcal{T}_h} + \langle e_h^\sigma \mathbf{n}, \overline{\boldsymbol{\phi}} \rangle_{\partial\mathcal{T}_h} = 0, \tag{3.8.5a}$$

$$(\mathbf{e}_h^u, \nabla \cdot \Pi_V \overline{\boldsymbol{\psi}})_{\mathcal{T}_h} + \langle \mathbf{e}_h^u, (\Pi_V \overline{\boldsymbol{\psi}} - \overline{\boldsymbol{\psi}})\mathbf{n} \rangle_{\partial\mathcal{T}_h} - \kappa^2 (\rho\, \mathbf{e}_h^u, \overline{\boldsymbol{\phi}})_{\mathcal{T}_h} = \|\mathbf{e}_h^u\|_\Omega^2, \tag{3.8.5b}$$

$$\langle \widehat{\mathbf{e}}_h^u, \overline{\boldsymbol{\psi}}\mathbf{n} \rangle_{\partial\mathcal{T}_h} = 0. \tag{3.8.5c}$$

Testing the error equations (3.8.2) with the conjugates of the projections of the adjoint problem and rearranging terms, we prove

$$(\mathcal{A}e_h^\sigma, \overline{\boldsymbol{\psi}})_{\mathcal{T}_h} + (\mathbf{e}_h^u, \nabla \cdot \Pi_V \overline{\boldsymbol{\psi}})_{\mathcal{T}_h} - \langle \widehat{\mathbf{e}}_h^u, \overline{\boldsymbol{\psi}}\mathbf{n} \rangle_{\partial\mathcal{T}_h} = \ell_1(\boldsymbol{\psi}), \tag{3.8.6a}$$

$$-(\text{div } e_h^\sigma, \Pi_W \overline{\boldsymbol{\phi}})_{\mathcal{T}_h} - \kappa^2 (\rho \mathbf{e}_h^u, \overline{\boldsymbol{\phi}})_{\mathcal{T}_h} = \ell_2(\boldsymbol{\phi}), \tag{3.8.6b}$$

$$\langle e_h^\sigma \mathbf{n}, \overline{\boldsymbol{\phi}} \rangle_{\partial\mathcal{T}_h} = \ell_3(\boldsymbol{\phi}), \tag{3.8.6c}$$

where

$$\begin{aligned}
\ell_1(\boldsymbol{\psi}) \;&:=\; (\mathcal{A}e_h^\sigma, \overline{\boldsymbol{\psi}} - \Pi_V \overline{\boldsymbol{\psi}})_{\mathcal{T}_h} + (\mathcal{A}\varepsilon_h^\sigma, \Pi_V \overline{\boldsymbol{\psi}})_{\mathcal{T}_h} - \langle \widehat{\mathbf{e}}_h^u, (\overline{\boldsymbol{\psi}} - \Pi_V \overline{\boldsymbol{\psi}})\mathbf{n} \rangle_{\partial\mathcal{T}_h}, \\
\ell_2(\boldsymbol{\phi}) \;&:=\; -\kappa^2 \left((\rho \mathbf{e}_h^u, \overline{\boldsymbol{\phi}} - \Pi_W \overline{\boldsymbol{\phi}})_{\mathcal{T}_h} + (\rho \boldsymbol{\varepsilon}_h^u, \Pi_W \overline{\boldsymbol{\phi}})_{\mathcal{T}_h} \right) \\
&\quad - \langle \varepsilon_h^\sigma \mathbf{n}, \Pi_W \overline{\boldsymbol{\phi}} \rangle_{\partial\mathcal{T}_h} + \langle \boldsymbol{\tau} \mathbf{P}_M \boldsymbol{\varepsilon}_h^u, \Pi_W \overline{\boldsymbol{\phi}} \rangle_{\partial\mathcal{T}_h} - \langle \boldsymbol{\tau}(\mathbf{P}_M \mathbf{e}_h^u - \widehat{\mathbf{e}}_h^u), \Pi_W \overline{\boldsymbol{\phi}} \rangle_{\partial\mathcal{T}_h} \\
\ell_3(\boldsymbol{\phi}) \;&:=\; \langle \varepsilon_h^\sigma \mathbf{n}, \mathbf{P}_M \overline{\boldsymbol{\phi}} \rangle_{\partial\mathcal{T}_h} - \langle \boldsymbol{\tau} \mathbf{P}_M \boldsymbol{\varepsilon}_h^u, \overline{\boldsymbol{\phi}} \rangle_{\partial\mathcal{T}_h} + \langle \boldsymbol{\tau}(\mathbf{P}_M \mathbf{e}_h^u - \widehat{\mathbf{e}}_h^u), \overline{\boldsymbol{\phi}} \rangle_{\partial\mathcal{T}_h}.
\end{aligned}$$

The sum of equations (3.8.5) can then be compared with the sum of equations (3.8.6) to prove the duality identity:

$$\begin{aligned}\|\mathbf{e}_h^u\|_\Omega^2 &= ((\mathcal{A}e_h^\sigma, \overline{\boldsymbol{\psi}} - \Pi_V\overline{\boldsymbol{\psi}})_{\mathcal{T}_h} + (\mathcal{A}\varepsilon_h^\sigma, \Pi_V\overline{\boldsymbol{\psi}})_{\mathcal{T}_h} \\ &\quad -\kappa^2\left((\rho\,\mathbf{e}_h^u, \overline{\boldsymbol{\phi}} - \Pi_W\overline{\boldsymbol{\phi}})_{\mathcal{T}_h} + (\rho\,\boldsymbol{\varepsilon}_h^u, \Pi_W\overline{\boldsymbol{\phi}})_{\mathcal{T}_h}\right) \\ &\quad +\langle \mathbf{e}_h^u - \widehat{\mathbf{e}}_h^u, (\overline{\boldsymbol{\psi}} - \Pi_V\overline{\boldsymbol{\psi}})\mathbf{n}\rangle_{\partial\mathcal{T}_h} \\ &\quad +\langle \boldsymbol{\tau}(\mathbf{P}_M\mathbf{e}_h^u - \widehat{\mathbf{e}}_h^u) - \boldsymbol{\tau}\mathbf{P}_M\boldsymbol{\varepsilon}_h^u, \overline{\boldsymbol{\phi}} - \Pi_W\overline{\boldsymbol{\phi}}\rangle_{\partial\mathcal{T}_h} - \langle \varepsilon_h^\sigma\mathbf{n}, \Pi_W\overline{\boldsymbol{\phi}} - \mathbf{P}_M\overline{\boldsymbol{\phi}}\rangle_{\partial\mathcal{T}_h}.\end{aligned} \tag{3.8.7}$$

What is left now is the proof of bounds for the right-hand sides of (3.8.3) and (3.8.7). This process requires just going carefully over the proofs of Proposition (3.4.4) and (3.5.4). Nothing essential is changed. We can write the results with our shorthand notation for errors $\Sigma := \|e_h^\sigma\|_{\mathcal{A}}$, $\mathrm{T} := \|\mathbf{P}_M\mathbf{e}_h^u - \widehat{\mathbf{e}}_h^u\|_\tau$, $\mathrm{U} := \|\mathbf{e}_h^u\|_\Omega$, and approximation terms $\Sigma_h := h^t|\boldsymbol{\sigma}|_{t,\Omega}$, $\mathrm{U}_h := h^{s-1}|\mathbf{u}|_{s,\Omega}$. The bounds we obtain are:

$$\begin{aligned}\Sigma^2 + \mathrm{T}^2 &\lesssim \Sigma\,\Sigma_h + \kappa^2\mathrm{U}\,\mathrm{U}_h + (\Sigma_h + \mathrm{U}_h)\mathrm{T} + \Sigma_h^2 + \kappa^2\mathrm{U}^2, \\ \mathrm{U} &\lesssim \alpha^2(\Sigma + \Sigma_h + \mathrm{U}_h + \mathrm{T}),\end{aligned}$$

where $\alpha := E_\kappa h(1+\kappa)$. The condition that allows us to bootstrap is $C(\alpha\kappa)^2 \le 1/4$, where C is a constant related to the constants hidden in the symbols $\lesssim$ above. After simplification, we prove

$$\Sigma + \mathrm{T} \lesssim \Sigma_h + (1+\kappa)\mathrm{U}_h \qquad \mathrm{U} \lesssim \alpha(\Sigma_h + (1+\kappa)\mathrm{U}_h),$$

which is the statement of the theorem. $\square$

Chapter 4

HDG+ AND EXTENDED HDG+ FOR TRANSIENT LINEAR ELASTICITY

We now prepare and numerically test an HDG discretization in time (and an extended version thereof) for the transient elastic wave equation. The analysis of this method is being done by Shukai Du and F.-J. Sayas [16], so we do not go too deeply into it. We write the equations, and then the HDG+ semidiscretized equations, provide numerical evidence of convergence to the exact weak solution, and then do the same for the extended version. We will use the trapezoid rule in the time variable, implemented through a convolution quadrature strategy.

4.1 Transient Waves

Let us now write some HDG+ semidiscrete methods for the transient elastic wave equation. The data functions are $\mathbf{f} : [0,\infty) \to L^2(\Omega;\mathbb{R}^3)$, $\mathbf{g}_D : [0,\infty) \to H^{1/2}(\Gamma_D;\mathbb{R}^3)$, and $\mathbf{g}_N : [0,\infty) \to L^2(\Gamma_N;\mathbb{R}^3)$. We are looking for $\mathbf{u} : [0,\infty) \to H^1(\Omega;\mathbb{R}^3)$ and $\boldsymbol{\sigma} : [0,\infty) \to H(\mathrm{div},\Omega;\mathbb{R}^{3\times 3}_{\mathrm{sym}})$ satisfying

$$\mathcal{A}\boldsymbol{\sigma}(t) - \boldsymbol{\varepsilon}(\mathbf{u})(t) = \mathbf{0} \qquad \text{in } \Omega, \quad \forall t \geq 0, \tag{4.1.1a}$$

$$-\mathrm{div}\, \boldsymbol{\sigma}(t) + \rho\, \ddot{\mathbf{u}}(t) = \mathbf{f}(t) \qquad \text{in } \Omega, \quad \forall t \geq 0, \tag{4.1.1b}$$

$$\mathbf{u}(t) = \mathbf{g}_D(t) \qquad \text{on } \Gamma_D, \quad \forall t \geq 0, \tag{4.1.1c}$$

$$\boldsymbol{\sigma}(t)\, \mathbf{n} = \mathbf{g}_N(t) \qquad \text{on } \Gamma_N, \quad \forall t \geq 0, \tag{4.1.1d}$$

and initial conditions $\mathbf{u}(0) = \mathbf{u}_0$, $\dot{\mathbf{u}}(0) = \mathbf{v}_0$.

The HDG+ semidiscretization uses three spaces

$$\mathbb{V}_h := \{\boldsymbol{\xi} : \Omega \to \mathbb{R}^{3\times 3}_{\mathrm{sym}} : \boldsymbol{\xi}|_K \in \mathcal{P}_k(K; \mathbb{R}^{3\times 3}_{\mathrm{sym}}) \quad \forall K \in \mathcal{T}_h\}, \tag{4.1.2a}$$

$$\mathbf{W}_h := \{\mathbf{u} : \Omega \to \mathbb{R}^3 : \mathbf{u}|_K \in \mathcal{P}_{k+1}(K; \mathbb{R}^3) \quad \forall K \in \mathcal{T}_h\}, \tag{4.1.2b}$$

$$\mathbf{M}_h := \{\boldsymbol{\mu} : \mathcal{E}_h \to \mathbb{R}^3 : \boldsymbol{\mu}|_F \in \mathcal{P}_k(F; \mathbb{R}^3) \quad \forall K \in \mathcal{E}_h\}, \tag{4.1.2c}$$

for some polynomial degree k. A priori all the methods can be written for $k = 0$, but the convergence theory [16] only works for $k \geq 1$. We will show that the method does not converge for $k = 0$. We look for

$$\boldsymbol{\sigma}_h : [0, \infty) \to \mathbb{V}_h, \ \mathbf{u}_h : [0, \infty) \to \mathbf{W}_h, \ \text{and } \widehat{\mathbf{u}}_h : [0, \infty) \to \mathbf{M}_h,$$

satisfying

$$(\mathcal{A}\boldsymbol{\sigma}_h(t), \boldsymbol{\xi})_{\mathcal{T}_h} + (\mathbf{u}_h(t), \nabla \cdot \boldsymbol{\xi})_{\mathcal{T}_h} - \langle \widehat{\mathbf{u}}_h(t), \boldsymbol{\xi}\mathbf{n}\rangle_{\partial\mathcal{T}_h} = 0, \tag{4.1.3a}$$

$$(\boldsymbol{\sigma}_h(t), \nabla \mathbf{w})_{\mathcal{T}_h} - \langle \widehat{\boldsymbol{\sigma}}_h(t)\mathbf{n}, \mathbf{w}\rangle_{\partial\mathcal{T}_h} + (\rho\, \ddot{\mathbf{u}}_h(t), \mathbf{w})_{\mathcal{T}_h} = (\mathbf{f}(t), \mathbf{w})_{\mathcal{T}_h}, \tag{4.1.3b}$$

$$\langle \widehat{\boldsymbol{\sigma}}_h(t)\mathbf{n}, \boldsymbol{\mu}\rangle_{\partial\mathcal{T}_h \setminus \Gamma_D} = \langle \mathbf{g}_N(t), \boldsymbol{\mu}\rangle_{\Gamma_N}, \tag{4.1.3c}$$

$$\langle \widehat{\mathbf{u}}_h(t), \boldsymbol{\mu}\rangle_{\Gamma_D} = \langle \mathbf{g}_D(t), \boldsymbol{\mu}\rangle_{\Gamma_D}, \tag{4.1.3d}$$

for all $(\boldsymbol{\xi}, \mathbf{w}, \boldsymbol{\mu}) \in \mathbb{V}_h \times \mathbf{W}_h \times \mathbf{M}_h$ and $t \geq 0$. The numerical flux $\widehat{\boldsymbol{\sigma}}_h$ can be defined in different ways which influence the choice of initial conditions. If we take the inverse Fourier transform of equations (3.6.4) with $\alpha_\kappa = \pm\imath\kappa$, we obtain the following proposals for the numerical flux

$$\widehat{\boldsymbol{\sigma}}_h(t)\mathbf{n} := \boldsymbol{\sigma}_h(t)\mathbf{n} \pm \boldsymbol{\tau}(\mathbf{P}_M \dot{\mathbf{u}}_h(t) - \dot{\widehat{\mathbf{u}}}_h(t)). \tag{4.1.4}$$

Note the positive sign corresponds to the method of Section 3.3 while the negative sign is the one obtained by time reversal. (It is clear from this why the sign change in the parameter α_κ corresponded to time reversal.) For equations (3.6.4) with $\alpha_\kappa = 1$ we obtain the flux

$$\widehat{\boldsymbol{\sigma}}_h(t)\mathbf{n} := \boldsymbol{\sigma}_h(t)\mathbf{n} - \boldsymbol{\tau}(\mathbf{P}_M \mathbf{u}_h(t) - \widehat{\mathbf{u}}_h(t)), \tag{4.1.5}$$

which is the method used by Qiu, Shi, and Shen [41] for quasi-static elasticity.

The following result shows that the method with flux given by (4.1.4) with positive sign accumulates energy over time, the method with flux (4.1.4) with negative sign is dissipative, and the method with flux (4.1.5) is conservative. The build-up or dissipation of energy happens at the interfaces, while the conservative method needs to add a potential energy term in the interfaces.

Proposition 4.1.1. *Assume that the problem is unforced (*$\mathbf{f} = \mathbf{0}$ *and* $\mathbf{g}_N = \mathbf{0}$*) and the Dirichlet boundary conditions are static (*$\dot{\mathbf{g}}_D = \mathbf{0}$*). Then the solution to the HDG-semidiscrete equations (4.1.3) with flux defined by (4.1.4) satisfies*

$$\frac{\mathrm{d}}{\mathrm{d}t}\left(\frac{1}{2}\|\boldsymbol{\sigma}_h(t)\|^2_{\mathcal{A}} + \frac{1}{2}\|\dot{\mathbf{u}}_h(t)\|^2_\rho\right) = \pm\|\mathbf{P}_M\dot{\mathbf{u}}_h(t) - \dot{\widehat{\mathbf{u}}}_h(t)\|^2_\tau \qquad \forall t \geq 0.$$

The solution to the HDG equations (4.1.3) with flux defined by (4.1.5) satisfy

$$\frac{\mathrm{d}}{\mathrm{d}t}\left(\frac{1}{2}\|\boldsymbol{\sigma}_h(t)\|^2_{\mathcal{A}} + \frac{1}{2}\|\dot{\mathbf{u}}_h(t)\|^2_\rho + \frac{1}{2}\|\mathbf{P}_M\mathbf{u}_h(t) - \widehat{\mathbf{u}}_h(t)\|^2_\tau\right) = 0 \qquad \forall t \geq 0.$$

Proof. It follows from a simple argument: (a) differentiate (4.1.3a) and test with $\boldsymbol{\sigma}_h(t)$, (b) test (4.1.3b) with $\dot{\mathbf{u}}_h(t)$, (c) test (4.1.3c) with $\dot{\widehat{\mathbf{u}}}_h(t)$; finally add the result of (a)-(c) using the fact that $\widehat{\mathbf{u}}_h(t)$ is constant in time on the Dirichlet faces. □

Therefore, only the HDG semidiscretization with the flux given by (4.1.5) conserves energy. This is the one that we will use for all the numerical experiments.

4.2 Numerical Experiments

We take the unit cube $\Omega = [0,1]^3$ as our domain. After subdividing Ω into $N \times N \times N$ cubes and each of those cubes into 6 tetrahedra, we have a tetrahedrization $\mathcal{T}_h$ of Ω with $6N^3$ elements. For mixed boundary conditions, we take the sides of the cube parallel to the yz plane to be Dirichlet and the rest of the faces Neumann. We take a variable mass density and Lamé parameters,

$$\rho = 1 + x^2 + y^2 + z^2, \quad \lambda = 1 + 0.5(x^2 + y^2 + z^2), \quad \mu = 8 + 0.5(x^3 + y^2 + z^2).$$

We use as an exact solution the displacement field

$$\mathbf{u}(t) = \sin^4 t \begin{pmatrix} \cos(\pi x)\sin(\pi y)\cos(\pi z) \\ 5x^2yz + 4xy^2z + 3xyz^2 + 17 \\ \cos(2x)\cos(3y)\cos(z) \end{pmatrix} \qquad \text{for } t \geq 0,$$

with a corresponding forcing function

$$\mathbf{f}(t) = -\text{div }(\lambda \nabla \mathbf{u}(t) + 2\mu\epsilon(\mathbf{u}(t))) + \rho\ddot{\mathbf{u}}(t).$$

For the j^{th} refinement we will identify $h_j = 1/j$ with the maximum length of an edge of a tetrahedron, since they are asymptotically equivalent. Our spatial discretization is given by the discrete equations,

$$(\mathcal{A}\boldsymbol{\sigma}_h(t), \boldsymbol{\xi})_{\mathcal{T}_h} + (\mathbf{u}_h(t), \nabla\cdot\boldsymbol{\xi})_{\mathcal{T}_h} - \langle \widehat{\mathbf{u}}_h(t), \boldsymbol{\xi}\mathbf{n}\rangle_{\partial\mathcal{T}_h} = 0,$$

$$-(\text{div }\boldsymbol{\sigma}_h(t), \nabla\mathbf{w})_{\mathcal{T}_h} + \langle \boldsymbol{\tau}(\mathbf{P}_M\mathbf{u}_h - \widehat{\mathbf{u}}_h), \mathbf{w}\rangle_{\partial\mathcal{T}_h} + (\rho\ddot{\mathbf{u}}_h(t), \mathbf{w})_{\partial\mathcal{T}_h} = (\mathbf{f}(t), \mathbf{w})_{\mathcal{T}_h},$$

along with boundary and interelement balancing equations,

$$\langle \boldsymbol{\sigma}_h(t)\mathbf{n} - \tau(\mathbf{P}_M\mathbf{u}_h(t) - \widehat{\mathbf{u}}_h(t)), \boldsymbol{\mu}\rangle_{\partial\mathcal{T}_h\setminus\Gamma_D} = \langle \mathbf{g}_N(t), \boldsymbol{\mu}\rangle_{\Gamma_N},$$

$$\langle \widehat{\mathbf{u}}_h(t), \boldsymbol{\mu}\rangle_{\Gamma_D} = \langle \mathbf{g}_D(t), \boldsymbol{\mu}\rangle_{\Gamma_D}.$$

Note that the negative sign we use in the numerical flux still corresponds to the conservative case.

We use the convolution quadrature based on the trapezoid rule for the time discretization. The HDG implementation is built from the work of Fu, Gatica, and Sayas, HDG Tools for MATLAB [18], for working with HDG in three dimensions, and from the work of Hassell and Sayas [25] on convolution quadrature in MATLAB.

We will take a fixed value of $c_t = 100$ and the final time $T = 5$. We use a timestep

$$\delta_t = \left\lceil \frac{T}{c_t} h_j^{\frac{k+2}{2}} \right\rceil.$$

We do this type of refinement in time because if we want to see the maximum convergence of $O(h_j^{k+2})$ knowing that the trapezoid rule gives $O(\delta_t^2)$,

$$O(h_j^{k+2}) = h_j^{k+2} + \delta_t^2,$$

we naturally set the timestep $\delta_t \approx \frac{T}{c_t}\sqrt{h_j^{k+2}}$.

In the tables below we compare h_j (with $j = 1, \ldots, N_{\text{ref}}$ and N_{ref} being the maximum refinement level) to the relative errors

$$e_{\mathbf{u}}^j = \frac{\|\mathbf{u}(T) - \mathbf{u}_h^j(T)\|_\Omega}{\|\mathbf{u}(T)\|_\Omega}, \qquad e_{\boldsymbol{\sigma}}^j = \frac{\|\boldsymbol{\sigma}(T) - \boldsymbol{\sigma}_h^j(T)\|_\Omega}{\|\boldsymbol{\sigma}(T)\|_\Omega},$$

where $\mathbf{u}_h^j(T)$ and $\boldsymbol{\sigma}_h^j(T)$ are the computed solutions from the j^{th} refinement. In the pictures below we compare $\log h_j$ to

$$\ell_{\mathbf{u}}^j = \log e_{\mathbf{u}}^j \qquad \text{and} \qquad \ell_{\boldsymbol{\sigma}}^j = \log e_{\sigma}^j,$$

to observe the orders of convergence for Dirichlet, Neumann, and mixed boundary conditions at polynomial degrees $k \in \{1, 2, 3, 4\}$, respectively. We also compute

$$L_{\mathbf{u}}^j = \frac{\ell_{\mathbf{u}}^j - \ell_{\mathbf{u}}^{j-1}}{\log h_j - \log h_{j-1}} \text{ for } j = 2, \ldots, N$$

and

$$L_{\boldsymbol{\sigma}}^j = \frac{\ell_{\boldsymbol{\sigma}}^j - \ell_{\boldsymbol{\sigma}}^{j-1}}{\log h_j - \log h_{j-1}} \text{ for } j = 1, \ldots, N$$

in the tables below to approximate the order of convergence.

We see that we achieve the optimal order ($\mathcal{O}(h_j^{k+2})$ for $e_{\mathbf{u}}^j$ and $\mathcal{O}(h_j^{k+1})$ for $e_{\boldsymbol{\sigma}}^j$).

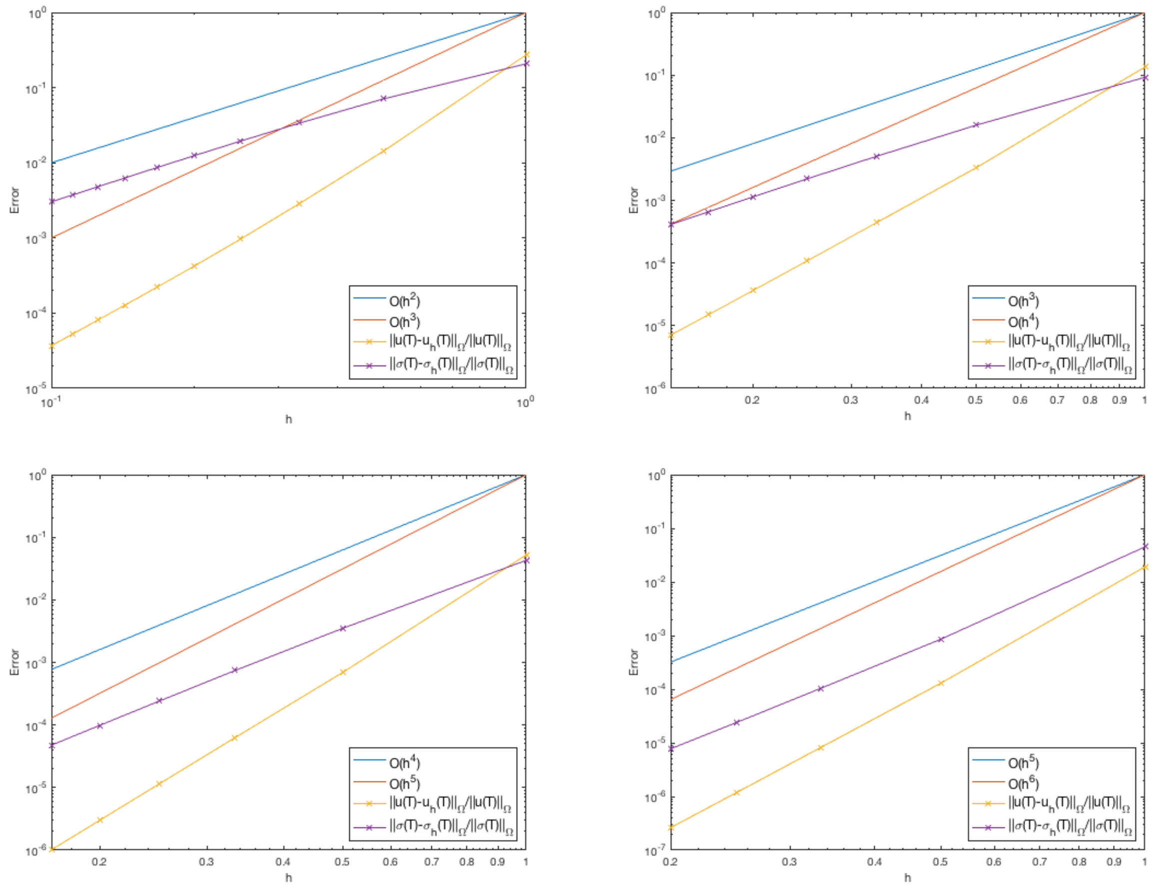

Figure 4.1: Dirichlet conditions, Time-Dependent Case: Expected order of convergence: $\mathcal{O}(h^{k+2})$ for $\mathbf{u}_h$ and $\mathcal{O}(h^{k+1})$ for $\boldsymbol{\sigma}_h$ (top-left $k = 1$, top-right $k = 2$, bottom-left $k = 3$, bottom-right $k = 4$)

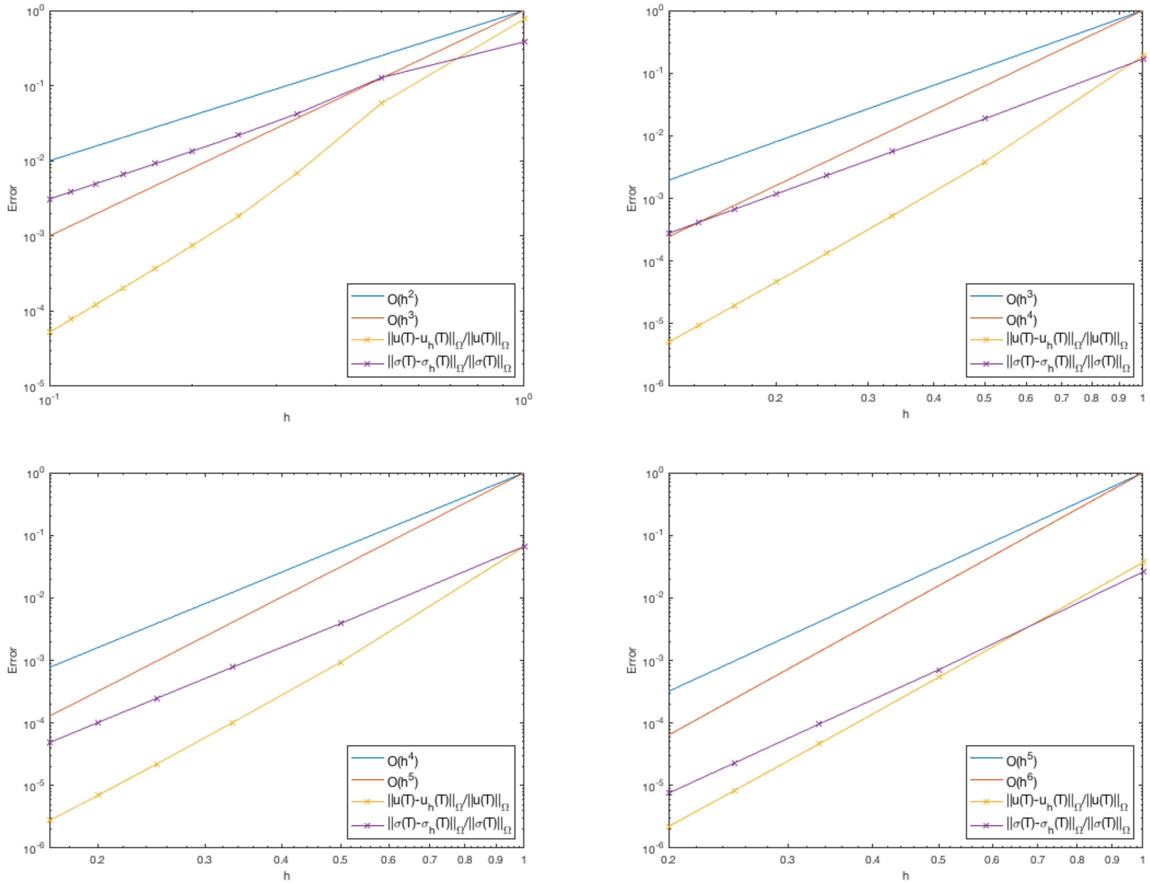

Figure 4.2: Neumann conditions, Time-Dependent Case: Expected order of convergence: $\mathcal{O}(h^{k+2})$ for $\mathbf{u}_h$ and $\mathcal{O}(h^{k+1})$ for $\boldsymbol{\sigma}_h$ (top-left $k = 1$, top-right $k = 2$,, bottom-left $k = 3$, bottom-right $k = 4$)

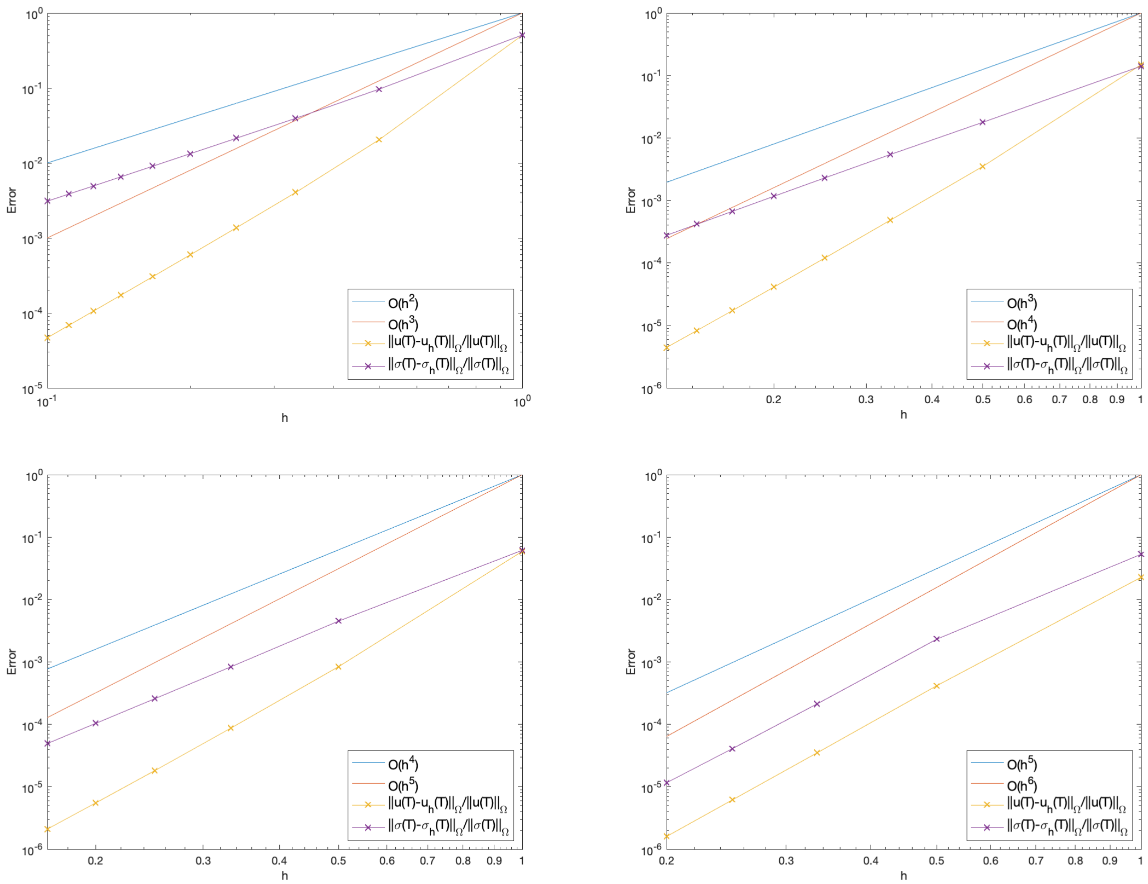

Figure 4.3: Mixed conditions, Time-Dependent Case: Expected order of convergence: $\mathcal{O}(h^{k+2})$ for $\mathbf{u}_h$ and $\mathcal{O}(h^{k+1})$ for $\boldsymbol{\sigma}_h$ (top-left $k = 1$, top-right $k = 2$, bottom-left $k = 3$, bottom-right $k = 4$)

h_j	$e_{\mathbf{u}}^j$	$e_{\boldsymbol{\sigma}}^j$	$L_{\mathbf{u}}^j$	$L_{\boldsymbol{\sigma}}^j$
h_1	2.73e-01	2.08e-01		
h_2	1.42e-02	7.07e-02	4.26	1.56
h_3	2.88e-03	3.38e-02	3.94	1.82
h_4	9.62e-04	1.94e-02	3.81	1.93
h_5	4.23e-04	1.25e-02	3.68	1.99
h_6	2.20e-04	8.61e-03	3.58	2.02
h_7	1.28e-04	6.29e-03	3.53	2.04
h_8	8.02e-05	4.78e-03	3.5	2.05
h_9	5.32e-05	3.75e-03	3.48	2.06
h_{10}	3.69e-05	3.02e-03	3.48	2.06

Table 4.1: Time-Dependent Elasticity: Dirichlet Conditions at $k = 1$

h_j	$e_{\mathbf{u}}^j$	$e_{\boldsymbol{\sigma}}^j$	$L_{\mathbf{u}}^j$	$L_{\boldsymbol{\sigma}}^j$
h_1	1.35e-01	9.23e-02		
h_2	3.30e-03	1.58e-02	5.35	2.54
h_3	4.46e-04	5.09e-03	4.94	2.8
h_4	1.08e-04	2.20e-03	4.94	2.91
h_5	3.61e-05	1.13e-03	4.9	2.97
h_6	1.49e-05	6.55e-04	4.87	3.01
h_7	7.05e-06	4.11e-04	4.84	3.03

Table 4.2: Time-Dependent Elasticity: Dirichlet Conditions at $k = 2$

h_j	$e_{\mathbf{u}}^j$	$e_{\boldsymbol{\sigma}}^j$	$L_{\mathbf{u}}^j$	$L_{\boldsymbol{\sigma}}^j$
h_1	5.22e-02	4.28e-02		
h_2	6.88e-04	3.50e-03	6.24	3.61
h_3	6.28e-05	7.42e-04	5.9	3.82
h_4	1.13e-05	2.39e-04	5.95	3.93
h_5	3.00e-06	9.86e-05	5.96	3.98
h_6	1.01e-06	4.76e-05	5.97	4.0

Table 4.3: Time-Dependent Elasticity: Dirichlet Conditions at $k = 3$

h_j	$e_{\mathbf{u}}^j$	$e_{\boldsymbol{\sigma}}^j$	$L_{\mathbf{u}}^j$	$L_{\boldsymbol{\sigma}}^j$
h_1	1.92e-02	4.51e-02		
h_2	1.29e-04	8.54e-04	7.22	5.72
h_3	8.27e-06	1.05e-04	6.78	5.18
h_4	1.18e-06	2.39e-05	6.77	5.14
h_5	2.62e-07	7.73e-06	6.74	5.05

Table 4.4: Time-Dependent Elasticity: Dirichlet Conditions at $k = 4$

h_j	$e^j_{\mathbf{u}}$	$e^j_{\boldsymbol{\sigma}}$	$L^j_{\mathbf{u}}$	$L^j_{\boldsymbol{\sigma}}$
h_1	7.68e-01	3.83e-01		
h_2	5.81e-02	1.28e-01	3.72	1.59
h_3	6.95e-03	4.26e-02	5.24	2.7
h_4	1.82e-03	2.18e-02	4.66	2.32
h_5	7.47e-04	1.35e-02	3.99	2.17
h_6	3.67e-04	9.11e-03	3.9	2.14
h_7	2.03e-04	6.56e-03	3.85	2.12
h_8	1.22e-04	4.95e-03	3.83	2.11
h_9	7.77e-05	3.87e-03	3.81	2.1
h_{10}	5.21e-05	3.10e-03	3.79	2.09

Table 4.5: Time-Dependent Elasticity: Neumann Conditions at $k = 1$

h_j	$e^j_{\mathbf{u}}$	$e^j_{\boldsymbol{\sigma}}$	$L^j_{\mathbf{u}}$	$L^j_{\boldsymbol{\sigma}}$
h_1	1.89e-01	1.68e-01		
h_2	3.82e-03	1.86e-02	5.63	3.17
h_3	5.29e-04	5.57e-03	4.88	2.98
h_4	1.33e-04	2.32e-03	4.8	3.05
h_5	4.60e-05	1.17e-03	4.76	3.07
h_6	1.94e-05	6.68e-04	4.73	3.07
h_7	9.42e-06	4.16e-04	4.69	3.07
h_8	5.06e-06	2.76e-04	4.65	3.06

Table 4.6: Time-Dependent Elasticity: Neumann Conditions at $k = 2$

h_j	$e_{\mathbf{u}}^j$	$e_{\boldsymbol{\sigma}}^j$	$L_{\mathbf{u}}^j$	$L_{\boldsymbol{\sigma}}^j$
h_1	6.60e-02	6.64e-02		
h_2	9.34e-04	3.88e-03	6.14	4.1
h_3	1.03e-04	7.85e-04	5.45	3.94
h_4	2.22e-05	2.48e-04	5.32	4.0
h_5	6.94e-06	1.01e-04	5.21	4.02
h_6	2.75e-06	4.85e-05	5.07	4.04

Table 4.7: Time-Dependent Elasticity: Neumann Conditions at $k = 3$

h_j	$e_{\mathbf{u}}^j$	$e_{\boldsymbol{\sigma}}^j$	$L_{\mathbf{u}}^j$	$L_{\boldsymbol{\sigma}}^j$
h_1	3.69e-02	2.60e-02		
h_2	5.37e-04	7.08e-04	6.1	5.2
h_3	4.65e-05	9.62e-05	6.03	4.92
h_4	8.31e-06	2.29e-05	5.99	4.98
h_5	2.22e-06	7.55e-06	5.92	4.98

Table 4.8: Time-Dependent Elasticity: Neumann Conditions at $k = 4$

h_j	$e^j_{\mathbf{u}}$	$e^j_{\boldsymbol{\sigma}}$	$L^j_{\mathbf{u}}$	$L^j_{\boldsymbol{\sigma}}$
h_1	5.04e-01	5.08e-01		
h_2	2.05e-02	9.66e-02	4.62	2.4
h_3	4.04e-03	3.94e-02	4.01	2.21
h_4	1.37e-03	2.14e-02	3.76	2.13
h_5	5.96e-04	1.33e-02	3.72	2.12
h_6	3.04e-04	9.04e-03	3.69	2.11
h_7	1.72e-04	6.53e-03	3.68	2.11
h_8	1.06e-04	4.94e-03	3.67	2.1
h_9	6.86e-05	3.86e-03	3.66	2.1
h_{10}	4.67e-05	3.09e-03	3.65	2.09

Table 4.9: Time-Dependent Elasticity: Mixed Conditions at $k = 1$

h_j	$e^j_{\mathbf{u}}$	$e^j_{\boldsymbol{\sigma}}$	$L^j_{\mathbf{u}}$	$L^j_{\boldsymbol{\sigma}}$
h_1	1.48e-01	1.41e-01		
h_2	3.51e-03	1.78e-02	5.4	2.98
h_3	4.83e-04	5.43e-03	4.89	2.93
h_4	1.19e-04	2.29e-03	4.85	3.0
h_5	4.09e-05	1.16e-03	4.8	3.04
h_6	1.72e-05	6.67e-04	4.76	3.05
h_7	8.30e-06	4.16e-04	4.73	3.06
h_8	4.44e-06	2.76e-04	4.69	3.06

Table 4.10: Time-Dependent Elasticity: Mixed Conditions at $k = 2$

h_j	$e^j_{\mathbf{u}}$	$e^j_{\boldsymbol{\sigma}}$	$L^j_{\mathbf{u}}$	$L^j_{\boldsymbol{\sigma}}$
h_1	5.91e-02	6.15e-02		
h_2	8.40e-04	4.51e-03	6.14	3.77
h_3	8.74e-05	8.38e-04	5.58	4.15
h_4	1.82e-05	2.58e-04	5.46	4.1
h_5	5.51e-06	1.04e-04	5.35	4.08
h_6	2.10e-06	4.93e-05	5.29	4.08

Table 4.11: Time-Dependent Elasticity: Mixed Conditions at $k = 3$

h_j	$e^j_{\mathbf{u}}$	$e^j_{\boldsymbol{\sigma}}$	$L^j_{\mathbf{u}}$	$L^j_{\boldsymbol{\sigma}}$
h_1	2.27e-02	5.30e-02		
h_2	4.16e-04	2.31e-03	5.77	4.52
h_3	3.50e-05	2.13e-04	6.1	5.88
h_4	6.15e-06	4.08e-05	6.05	5.75
h_5	1.60e-06	1.16e-05	6.04	5.64

Table 4.12: Time-Dependent Elasticity: Mixed Conditions at $k = 4$

We can generate a wave by "lifting" one side of the box $[0,1] \times [0,4] \times [0,1]$ with the Dirichlet condition $\mathbf{u}(\mathbf{x},t)|_{\Gamma_D} = (0,0,\sin^4 t)$ for $0 \le t \le \pi$ and 0 for $t \ge \pi$, and the rest $\boldsymbol{\sigma}\mathbf{n} = 0$ on Γ_N. Areas under high stress are plotted lighter.

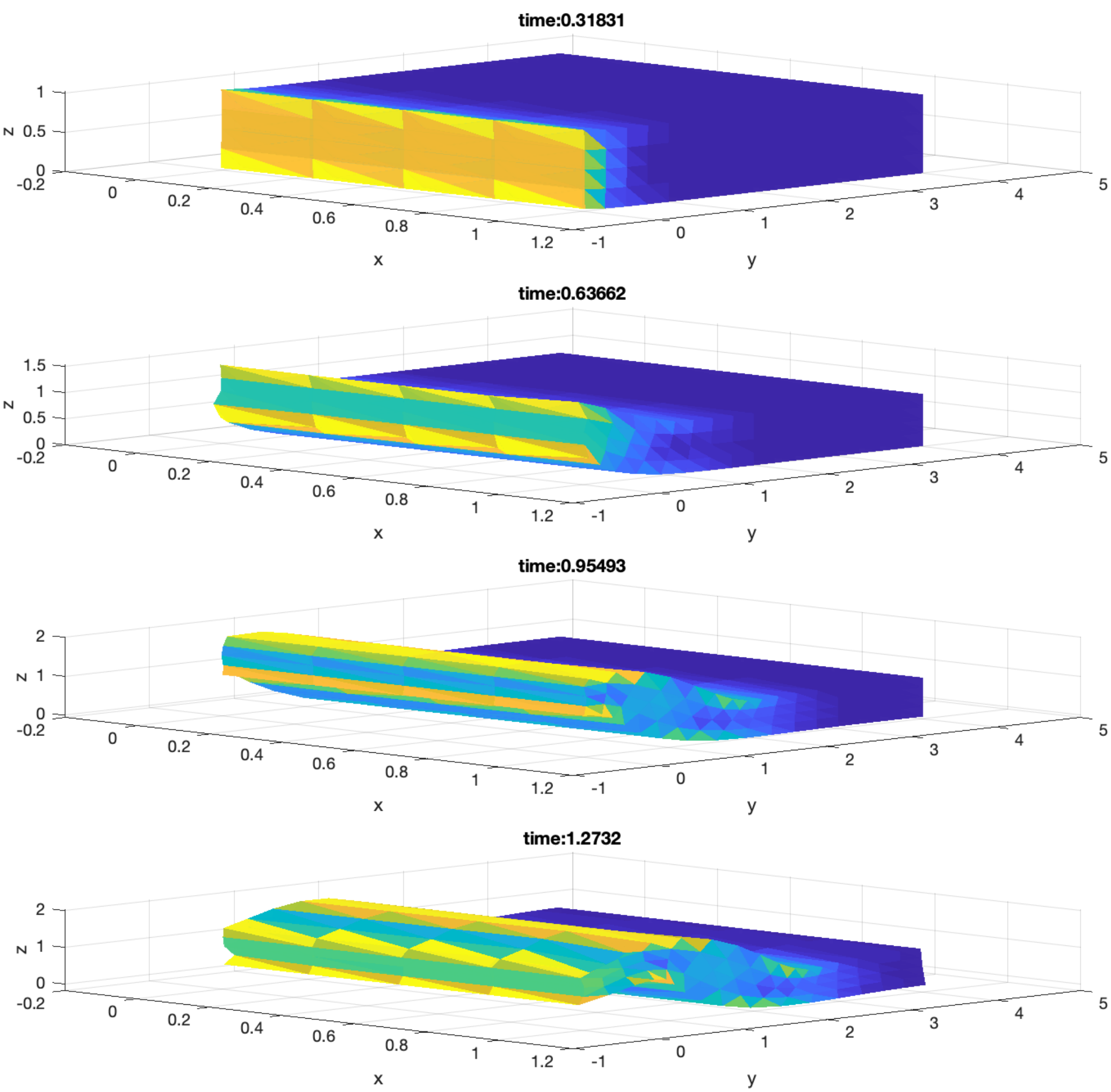

Figure 4.4: Elastic wave, part I

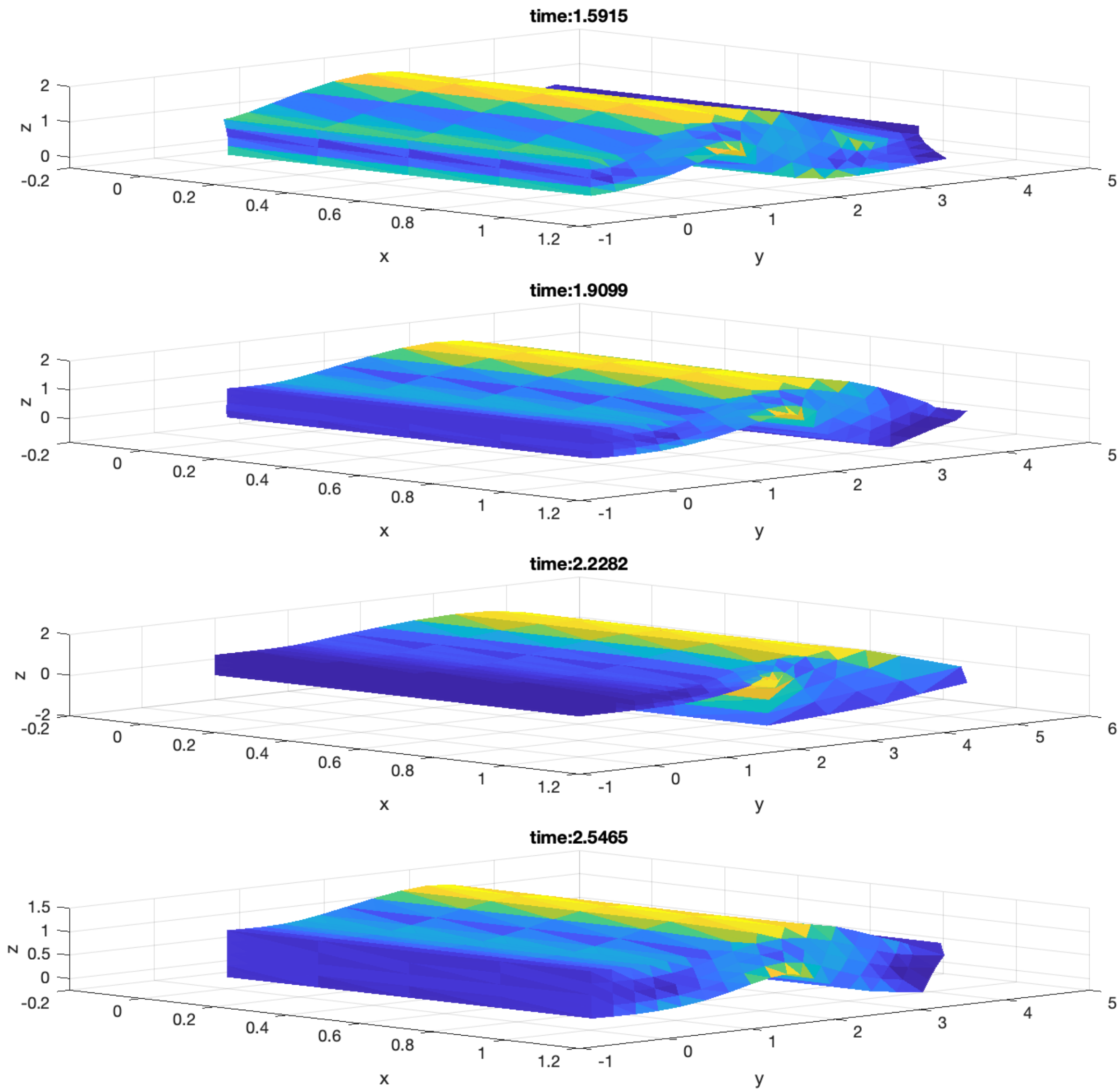

Figure 4.5: Elastic wave, part II

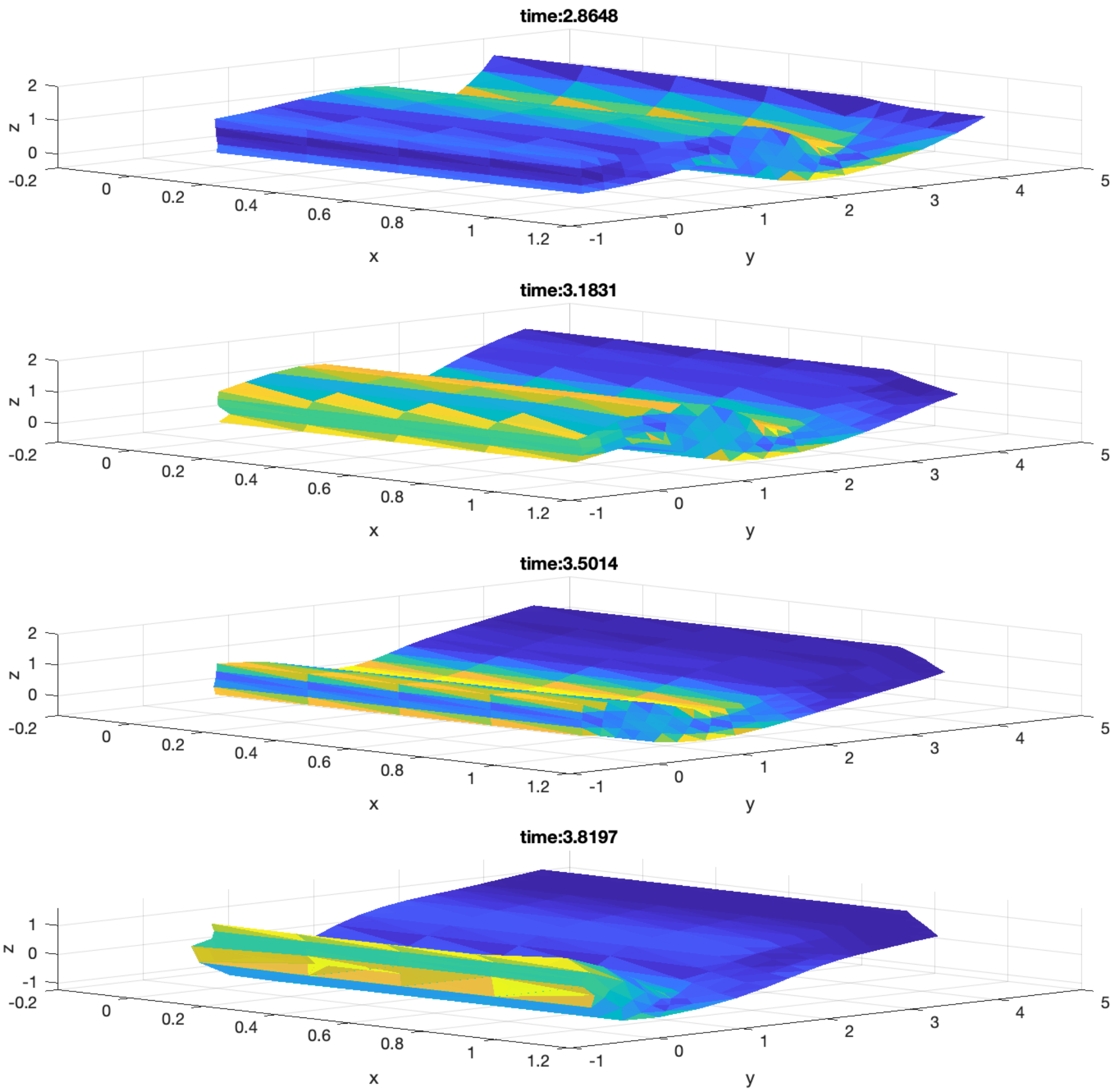

Figure 4.6: Elastic wave, part III

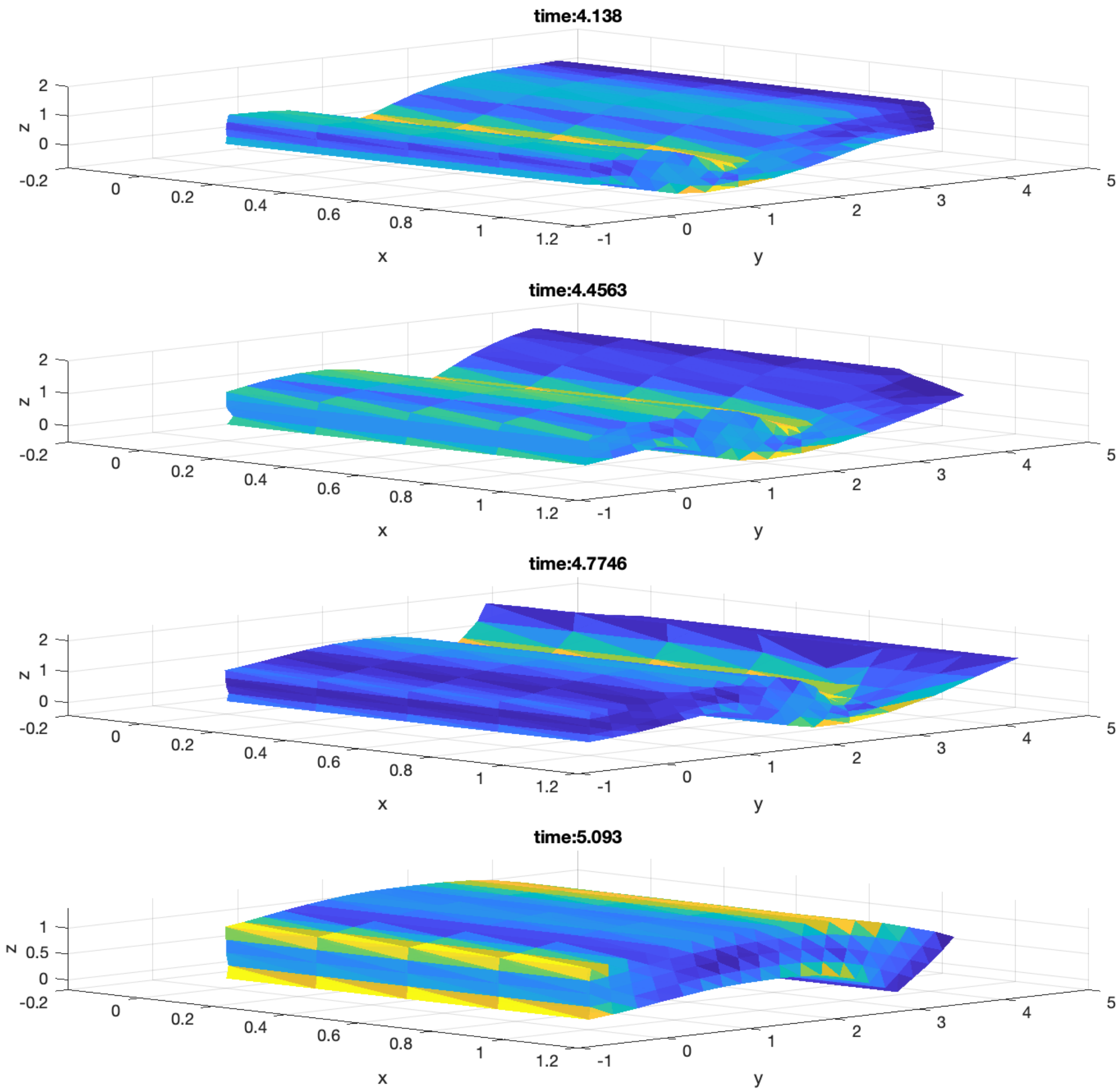

Figure 4.7: Elastic wave, part IV

Below, the head and body of a hippo, the surface of which comprise Γ_D, are lifted with a Dirichlet condition, $\mathbf{u}(\mathbf{x},t)|_{\Gamma_D} = (0, 0, 0.25 \sin^4 t)$ for $0 \le t \le \pi$ and 0 for $t \ge \pi$, and the legs (Γ_N) are subject to $\boldsymbol{\sigma}(\mathbf{x},t)\mathbf{n} = 0$ for all $t \ge 0$, hence they are free to move. The hippo mesh can be found at [44].

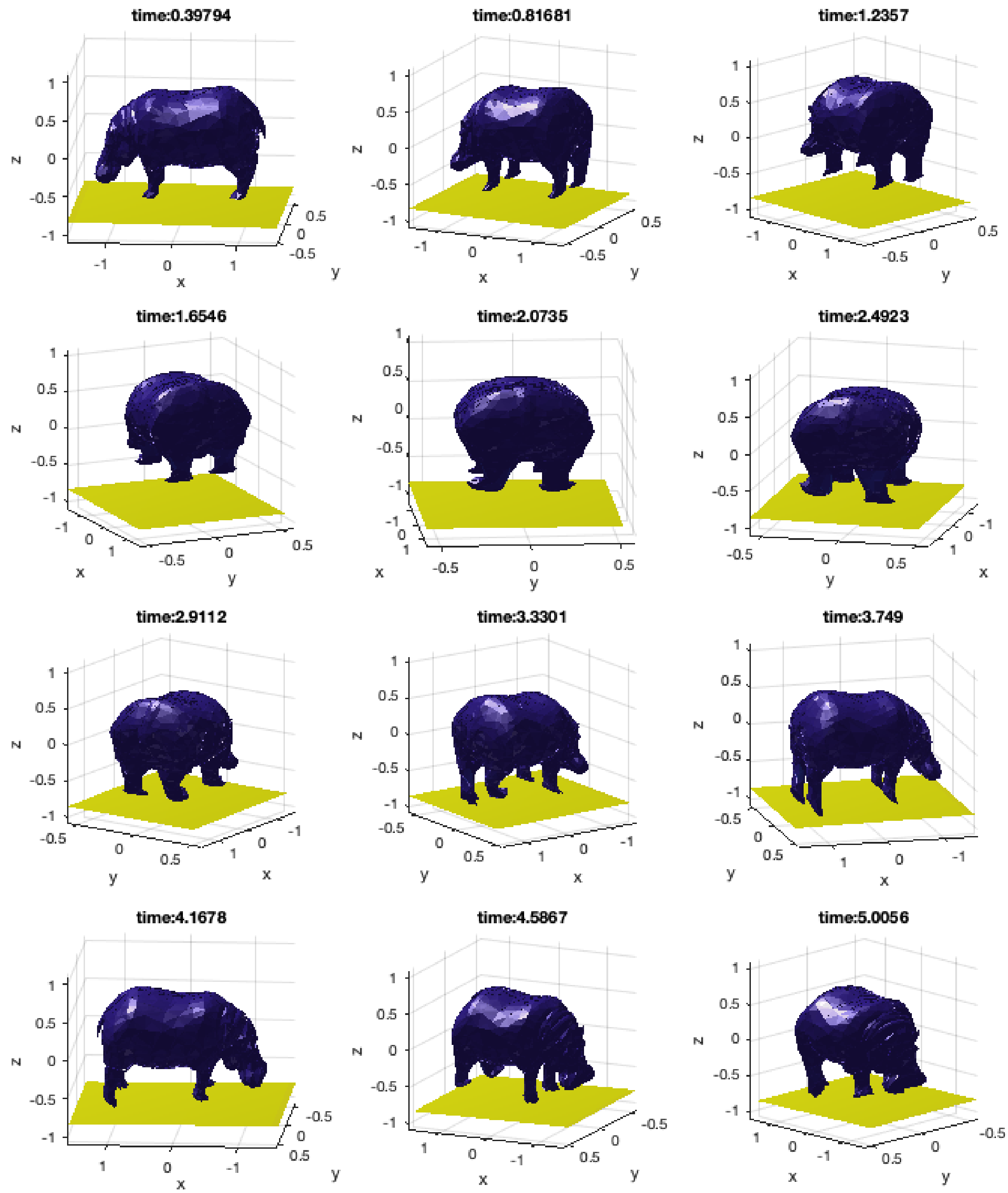

Figure 4.8: Elastic hippo

4.3 Extended HDG+ for Linear Elasticity

The following method is a simple extension of the HDG+ method using an additional variable. This method is coded as a preparation of the HDG+ method for nonlinear problems, as a way of calculating the strain directly, and as a way of dealing with the problem of anisotropy more flexibly. We consider the following differential-algebraic system, where we have introduced $\boldsymbol{\eta} : [0, \infty) \to L^2(\Omega, \mathbb{R}^{3\times 3}_{\text{sym}})$ as an additional unknown into the mix:

$$
\begin{aligned}
\mathcal{C}\boldsymbol{\eta}(t) - \boldsymbol{\sigma}(t) &= \mathbf{0}, \\
\boldsymbol{\eta}(t) - \boldsymbol{\varepsilon}(\mathbf{u}(t)) &= \mathbf{0}, \\
-\nabla \cdot \boldsymbol{\sigma}(t) + \rho\ddot{\mathbf{u}}(t) &= \mathbf{f}(t), \\
\gamma\mathbf{u}(t) &= \mathbf{g}_D(t), \\
\boldsymbol{\sigma}(t)\mathbf{n} &= \mathbf{g}_N(t).
\end{aligned}
$$

Note that the actual material law $\mathcal{C}$ and not the compliance tensor $\mathcal{A} = \mathcal{C}^{-1}$ is used in this formulation.

The HDG+ semidiscretization corresponding to these equations uses the same spaces as in Section 4.1:

$$
\begin{aligned}
\mathbb{V}_h &= \Pi_{K\in\mathcal{T}_h}\mathcal{P}_k(K; \mathbb{R}^{3\times 3}_{\text{sym}}), \\
\mathbf{W}_h &= \Pi_{K\in\mathcal{T}_h}\mathcal{P}_{k+1}(K; \mathbb{R}^3), \\
\mathbf{M}_h &= \{\boldsymbol{\mu} : \mathcal{E}_h \to \mathbb{R}^3 \ : \ \boldsymbol{\mu}|_F \in \mathcal{P}_k(F; \mathbb{R}^3), \quad \forall F \in \mathcal{E}_h\},
\end{aligned}
$$

and looks for $(\boldsymbol{\sigma}_h, \boldsymbol{\eta}_h, \mathbf{u}_h, \widehat{\mathbf{u}}_h) : [0, \infty) \to \mathbb{V}_h \times \mathbb{V}_h \times \mathbf{W}_h \times \mathbf{M}_h$ such that

$$
\begin{aligned}
(\mathcal{C}\boldsymbol{\eta}_h(t), \boldsymbol{\rho}_h)_{\mathcal{T}_h} - (\boldsymbol{\sigma}_h(t), \boldsymbol{\rho}_h)_{\mathcal{T}_h} &= 0 && \forall \boldsymbol{\rho}_h \in \mathbb{V}(\mathcal{T}_h), \\
(\boldsymbol{\eta}_h(t), \boldsymbol{\xi}_h)_{\mathcal{T}_h} + (\mathbf{u}_h(t), \nabla\cdot\boldsymbol{\xi}_h)_{\mathcal{T}_h} - \langle\widehat{\mathbf{u}}_h(t), \boldsymbol{\xi}_h\mathbf{n}\rangle_{\partial\mathcal{T}_h} &= 0 && \forall \boldsymbol{\xi}_h \in \mathbb{V}(\mathcal{T}_h), \\
-\langle\widehat{\boldsymbol{\sigma}}_h(t)\mathbf{n}, \mathbf{w}_h\rangle_{\partial\mathcal{T}_h} + (\boldsymbol{\sigma}_h, \nabla\mathbf{w}_h)_{\mathcal{T}_h} + (\rho\ddot{\mathbf{u}}_h(t), \mathbf{w}_h)_{\mathcal{T}_h} &= (\mathbf{f}(t), \mathbf{w}_h)_{\mathcal{T}_h} && \forall \mathbf{w}_h \in \mathbf{W}(\mathcal{T}_h), \\
\langle\widehat{\mathbf{u}}_h(t), \boldsymbol{\mu}_h\rangle_{\Gamma_D} &= \langle\mathbf{g}_D(t), \boldsymbol{\mu}_h\rangle_{\Gamma_D} && \forall \boldsymbol{\mu}_h \in \mathbf{M}(\mathcal{T}_h), \\
\langle\widehat{\boldsymbol{\sigma}_h}(t)\mathbf{n}, \boldsymbol{\mu}_h\rangle_{\partial\mathcal{T}_h\setminus\Gamma_D} &= \langle\mathbf{g}_N(t), \boldsymbol{\mu}_h\rangle_{\Gamma_N} && \forall \boldsymbol{\mu}_h \in \mathbf{M}(\mathcal{T}_h).
\end{aligned}
$$

The equilibrium equations and the equations associated to boundary conditions are exactly the same as those of the previous HDG+ method, with the flux function

$$\widehat{\boldsymbol{\sigma}_h}(t)\mathbf{n} = \boldsymbol{\sigma}_h(t)\mathbf{n} - \boldsymbol{\tau}(P_M\mathbf{u}_h(t) - \widehat{\mathbf{u}}_h(t)) \qquad \tau \equiv 1/h_K.$$

Proposition 4.3.1. *The method considered above is conservative, i.e.*

$$\frac{\mathrm{d}}{\mathrm{d}t}\left(\|\boldsymbol{\eta}_h(t)\|_{\mathcal{C}}^2 + \|\dot{\mathbf{u}}_h(t)\|_\rho^2 + \|P_M\mathbf{u}_h(t) - \widehat{\mathbf{u}}_h(t)\|_{\partial\mathcal{T}_h,\tau}^2\right) = 0.$$

Proof. To see that this method is conservative, suppose $\mathbf{f}(t), \dot{\mathbf{g}}_D(t)$, and $\mathbf{g}_N(t)$ vanish for all time,

$$\begin{aligned}
(\mathcal{C}\boldsymbol{\eta}_h(t), \boldsymbol{\rho}_h)_{\mathcal{T}_h} - (\boldsymbol{\sigma}_h(t), \boldsymbol{\rho}_h)_{\mathcal{T}_h} &= 0 \qquad \forall \boldsymbol{\rho}_h \in \mathbb{V}(\mathcal{T}_h),\\
(\boldsymbol{\eta}_h(t), \boldsymbol{\xi}_h)_{\mathcal{T}_h} + (\mathbf{u}_h(t), \mathrm{div}\ \boldsymbol{\xi}_h)_{\mathcal{T}_h} - \langle \widehat{\mathbf{u}}_h(t), \boldsymbol{\xi}_h\mathbf{n}\rangle_{\partial\mathcal{T}_h} &= 0 \qquad \forall \boldsymbol{\xi}_h \in \mathbb{V}(\mathcal{T}_h),\\
-(\mathrm{div}\ \boldsymbol{\sigma}_h, \mathbf{w}_h)_{\mathcal{T}_h} + (\rho\ddot{\mathbf{u}}_h(t), \mathbf{w}_h)_{\mathcal{T}_h} + \langle \boldsymbol{\tau}(\mathbf{P}_M\mathbf{u}_h - \widehat{\mathbf{u}}_h, \mathbf{w}_h\rangle_{\partial\mathcal{T}_h} &= 0 \qquad \forall \mathbf{w}_h \in \mathbf{W}(\mathcal{T}_h),\\
\langle \widehat{\mathbf{u}}_h(t), \boldsymbol{\mu}_h\rangle_{\Gamma_D} &= 0 \qquad \forall \boldsymbol{\mu}_h \in \mathbf{M}(\mathcal{T}_h),\\
\langle \widehat{\boldsymbol{\sigma}_h}(t)\mathbf{n}, \boldsymbol{\mu}_h\rangle_{\partial\mathcal{T}_h\setminus\Gamma_D} &= 0 \qquad \forall \boldsymbol{\mu}_h \in \mathbf{M}(\mathcal{T}_h).
\end{aligned}$$

Now test the first equation with $\dot{\boldsymbol{\eta}}_h(t)$, differentiate and test the second with $\boldsymbol{\sigma}_h(t)$, and test the third with $\dot{\mathbf{u}}_h(t)$:

$$\begin{aligned}
(\mathcal{C}\boldsymbol{\eta}_h(t), \dot{\boldsymbol{\eta}}_h(t))_{\mathcal{T}_h} - (\boldsymbol{\sigma}_h(t), \dot{\boldsymbol{\eta}}_h(t))_{\mathcal{T}_h} &= 0,\\
(\dot{\boldsymbol{\eta}}_h(t), \boldsymbol{\sigma}_h(t))_{\mathcal{T}_h} + (\dot{\mathbf{u}}_h(t), \mathrm{div}\ \boldsymbol{\sigma}_h(t))_{\mathcal{T}_h} - \langle \dot{\widehat{\mathbf{u}}}_h(t), \boldsymbol{\sigma}_h(t)\mathbf{n}\rangle_{\partial\mathcal{T}_h} &= 0,\\
-(\mathrm{div}\ \boldsymbol{\sigma}_h(t), \dot{\mathbf{u}}_h(t))_{\mathcal{T}_h} + (\rho\ddot{\mathbf{u}}_h(t), \dot{\mathbf{u}}_h(t))_{\mathcal{T}_h} + \langle \tau(P_M\mathbf{u}_h(t) - \widehat{\mathbf{u}}_h(t)), \dot{\mathbf{u}}_h(t)\rangle_{\partial\mathcal{T}_h} &= 0,
\end{aligned}$$

and sum to obtain

$$\frac{\mathrm{d}}{\mathrm{d}t}\left(\|\boldsymbol{\eta}_h(t)\|_{\mathcal{C}}^2 + \|\dot{\mathbf{u}}_h(t)\|_\rho^2 + \|P_M\mathbf{u}_h(t) - \widehat{\mathbf{u}}_h(t)\|_{\partial\mathcal{T}_h,\tau}^2\right) = 0.$$

□

4.4 Numerical Experiments

We take the unit cube $\Omega = [0,1]^3$ as our domain and subdivide as in (4.2). We take the same variable parameters

$$\rho = 1 + x^2 + y^2 + z^2, \qquad \lambda = 1 + 0.5(x^2 + y^2 + z^2), \qquad \mu = 8 + 0.5(x^3 + y^2 + z^2),$$

and use as an exact solution the same causal displacement field

$$\mathbf{u}(t,x,y,z) = \sin^4 t \begin{pmatrix} \cos(\pi x)\sin(\pi y)\cos(\pi z) \\ 5x^2yz + 4xy^2z + 3xyz^2 + 17 \\ \cos(2x)\cos(3y)\cos(z) \end{pmatrix} \qquad \text{for } t \geq 0$$

with the corresponding forcing function

$$\mathbf{f}(t) = -\text{div }(\lambda\nabla\mathbf{u}(t) + 2\mu\epsilon(\mathbf{u}(t))) + \rho\ddot{\mathbf{u}}(t).$$

Our spatial discretization is given by the discrete equations,

$$\begin{aligned} (\mathcal{A}\boldsymbol{\eta}_h(t), \boldsymbol{\xi})_{\mathcal{T}_h} - (\sigma_h, \boldsymbol{\xi})_{\mathcal{T}_h} &= 0, \\ (\boldsymbol{\eta}_h(t), \boldsymbol{\xi})_{\mathcal{T}_h} + (\mathbf{u}_h(t), \nabla\cdot\boldsymbol{\xi})_{\mathcal{T}_h} - \langle\widehat{\mathbf{u}}_h(t), \boldsymbol{\xi}\mathbf{n}\rangle_{\partial\mathcal{T}_h} &= 0, \\ (\boldsymbol{\sigma}_h(t), \nabla\mathbf{w})_{\mathcal{T}_h} - \langle\boldsymbol{\sigma}_h(t)\mathbf{n} - \tau(\mathbf{P}_M\mathbf{u}_h(t) - \widehat{\mathbf{u}}_h(t)), \boldsymbol{\mu}\rangle_{\partial\mathcal{T}_h} + (\rho\ddot{\mathbf{u}}_h(t), \mathbf{w})_{\partial\mathcal{T}_h} &= (\mathbf{f}(t), \mathbf{w})_{\mathcal{T}_h}, \end{aligned}$$

along with boundary and interelement balancing equations,

$$\begin{aligned} \langle\boldsymbol{\sigma}_h(t)\mathbf{n} - \tau(\mathbf{P}_M\mathbf{u}_h(t) - \widehat{\mathbf{u}}_h(t)), \boldsymbol{\mu}\rangle_{\partial\mathcal{T}_h\setminus\Gamma_D} &= \langle\mathbf{g}_N(t), \boldsymbol{\mu}\rangle_{\Gamma_N}, \\ \langle\widehat{\mathbf{u}}_h(t), \boldsymbol{\mu}\rangle_{\Gamma_D} &= \langle\mathbf{g}_D(t), \boldsymbol{\mu}\rangle_{\Gamma_D}. \end{aligned}$$

Note that the negative sign we use in the numerical flux still corresponds to the conservative case.

We again use a convolution quadrature based on the trapezoid rule for the time discretization.

In the figures below, we have $h_j = 1/j$ for $j = 1, \ldots, N$, as *these are asymptotically identical to taking h_j to be the longest edge of a tetrahedron.* We will take a fixed value of $c_t = 100$ and the final time $T = 5$. We again use a timestep

$$\delta_t = \left\lceil \frac{T}{c_t} h_j^{\frac{k+2}{2}} \right\rceil.$$

To see why, refer to Section 4.2.

In the tables below we compare h_j to the relative errors

$$e^j_{\mathbf{u}} = \frac{\|\mathbf{u}(T) - \mathbf{u}^j_h(T)\|_\Omega}{\|\mathbf{u}(T)\|_\Omega}, \qquad e^j_{\boldsymbol{\eta}} = \frac{\|\boldsymbol{\eta}(T) - \boldsymbol{\eta}^j_h(T)\|_\Omega}{\|\boldsymbol{\eta}(T)\|_\Omega}, \qquad e^j_{\boldsymbol{\sigma}} = \frac{\|\boldsymbol{\sigma}(T) - \boldsymbol{\sigma}^j_h(T)\|_\Omega}{\|\boldsymbol{\sigma}(T)\|_\Omega},$$

where $\mathbf{u}_h^j(T)$ is the computed solution on the j^{th} refinement. In the pictures below we compare $\log h_j$ to

$$\log e_{\mathbf{u}}^j, \qquad \log e_{\boldsymbol{\eta}}^j, \qquad \log e_{\boldsymbol{\sigma}}^j,$$

to observe the orders of convergence for Dirichlet, Neumann, and mixed boundary conditions at polynomial degrees $k \in \{1, 2, 3, 4\}$, respectively. We also compute

$$L_{\mathbf{u}}^j = \frac{\log e_{\mathbf{u}}^j - \log e_{\mathbf{u}}^{j-1}}{\log h_j - \log h_{j-1}} \text{ for } j = 2, \ldots, N,$$
$$L_{\boldsymbol{\eta}}^j = \frac{\log e_{\boldsymbol{\eta}}^j - \log e_{\boldsymbol{\eta}}^{j-1}}{\log h_j - \log h_{j-1}} \text{ for } j = 2, \ldots, N,$$

and

$$L_{\boldsymbol{\sigma}}^j = \frac{\log e_{\boldsymbol{\sigma}}^j - \log e_{\boldsymbol{\sigma}}^{j-1}}{\log h_j - \log h_{j-1}} \text{ for } j = 2, \ldots, N,$$

in the tables below to approximate the order of convergence.

We see that we achieve the optimal order ($\mathcal{O}(h_j^{k+2})$ for $e_{\mathbf{u}}^j$ and $\mathcal{O}(h_j^{k+1})$ for $e_{\boldsymbol{\sigma}}^j$ and $e_{\boldsymbol{\eta}}^j$). Moreover, we see that $e_{\boldsymbol{\sigma}}^j$ converges at almost exactly the same rate as $e_{\boldsymbol{\eta}}^j$.

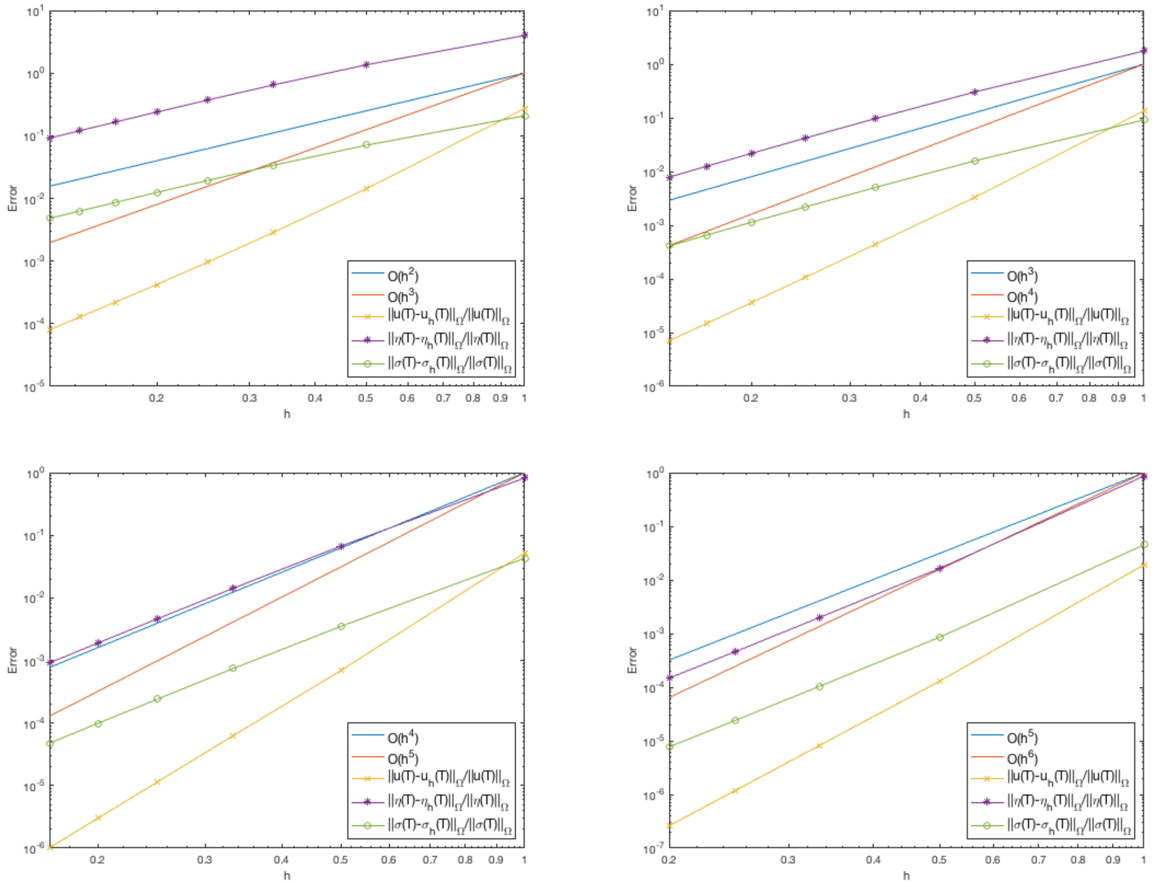

Figure 4.9: Dirichlet Conditions for the Extended Elastic Problem, Time-Dependent Case: Expected order of convergence: $\mathcal{O}(h^{k+2})$ for $\mathbf{u}_h$ and $\mathcal{O}(h^{k+1})$ for $\boldsymbol{\eta}_h$ and $\boldsymbol{\sigma}_h$. $\beta = 0.75, c = 2, \kappa/\gamma = 2$ (top-left $k = 1$, top-right $k = 2$, bottom-left $k = 3$, bottom-right $k = 4$)

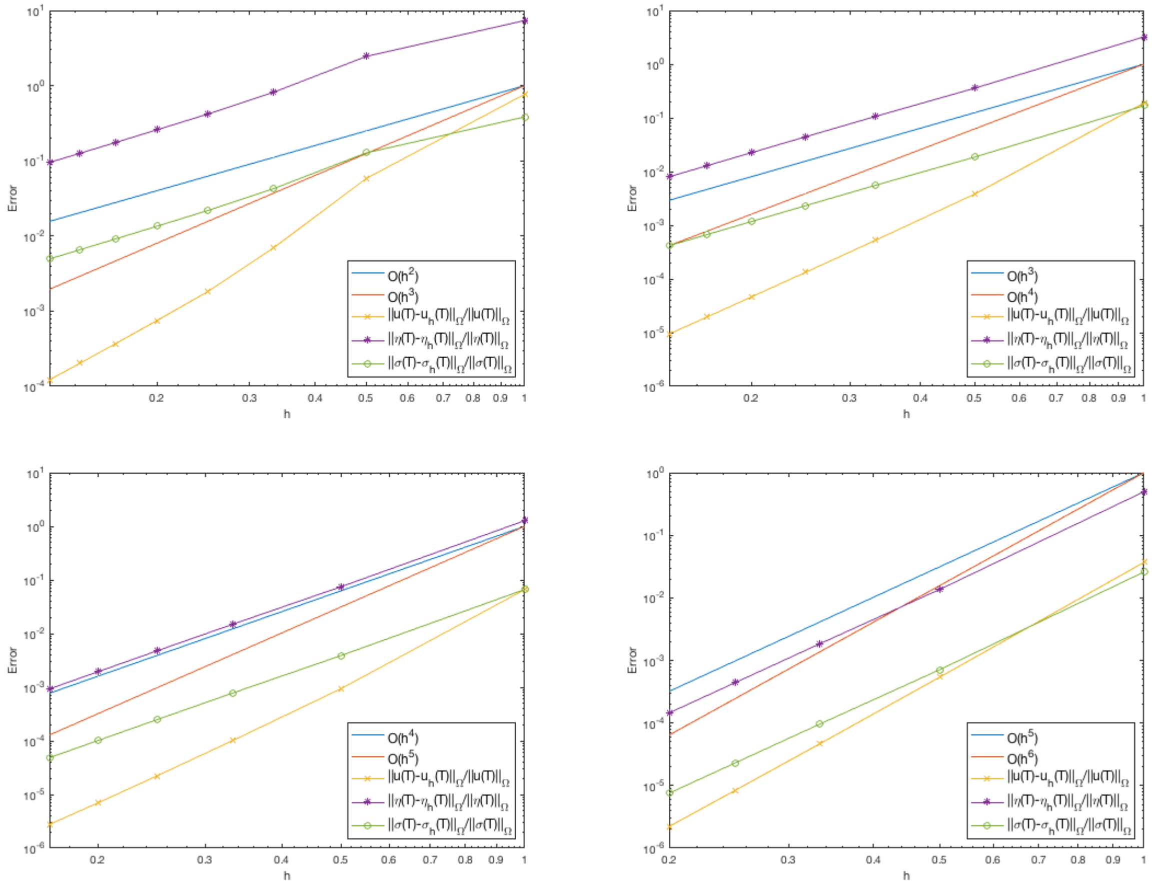

Figure 4.10: Neumann Conditions for the Extended Elastic Problem, Time-Dependent Case: Expected order of convergence: $\mathcal{O}(h^{k+2})$ for $\mathbf{u}_h$ and $\mathcal{O}(h^{k+1})$ for $\boldsymbol{\eta}_h$ and $\boldsymbol{\sigma}_h$. $\beta = 0.75, c = 2, \kappa/\gamma = 2$, (top-left $k = 1$, top-right $k = 2$, bottom-left $k = 3$,bottom-right $k = 4$)

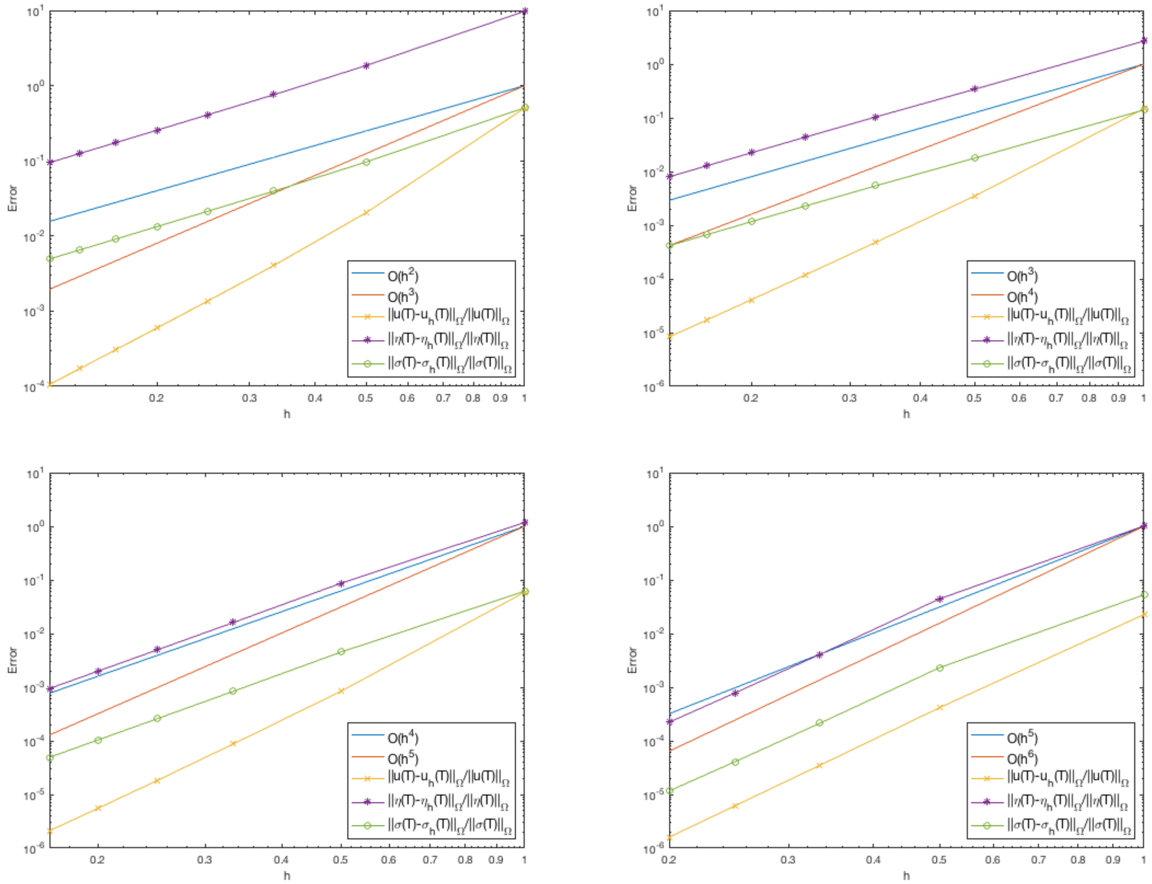

Figure 4.11: Mixed Conditions for the Extended Elastic Problem, Time-Dependent Case: Expected order of convergence: $\mathcal{O}(h^{k+2})$ for $\mathbf{u}_h$ and $\mathcal{O}(h^{k+1})$ for $\boldsymbol{\eta}_h$ and $\boldsymbol{\sigma}_h$. $\beta = 0.75, c = 2, \kappa/\gamma = 2$, (top-left $k = 1$, top-right $k = 2$, bottom-left $k = 3$, bottom-right $k = 4$))

h_j	$e^j_{\mathbf{u}}$	$e^j_{\boldsymbol{\eta}}$	$e^j_{\boldsymbol{\sigma}}$	$L^j_{\mathbf{u}}$	$L^j_{\boldsymbol{\eta}}$	$L^j_{\boldsymbol{\sigma}}$
h_1	2.73e-01	3.99e+00	2.08e-01			
h_2	1.42e-02	1.35e+00	7.07e-02	4.261878	1.55746	1.557461
h_3	2.88e-03	6.48e-01	3.38e-02	3.939888	1.820257	1.820257
h_4	9.62e-04	3.72e-01	1.94e-02	3.811022	1.928366	1.928366
h_5	4.23e-04	2.39e-01	1.25e-02	3.681268	1.986603	1.986603
h_6	2.20e-04	1.65e-01	8.61e-03	3.583031	2.021315	2.021315
h_7	1.28e-04	1.21e-01	6.29e-03	3.525734	2.041471	2.04147
h_8	8.02e-05	9.17e-02	4.78e-03	3.497459	2.052127	2.052127

Table 4.13: Time-Dependent Extended Elasticity: Dirichlet Conditions at $k = 1$

h_j	$e^j_{\mathbf{u}}$	$e^j_{\boldsymbol{\eta}}$	$e^j_{\boldsymbol{\sigma}}$	$L^j_{\mathbf{u}}$	$L^j_{\boldsymbol{\eta}}$	$L^j_{\boldsymbol{\sigma}}$
h_1	1.35e-01	1.76e+00	9.18e-02			
h_2	3.30e-03	3.04e-01	1.58e-02	5.351179	2.534917	2.534904
h_3	4.46e-04	9.76e-02	5.09e-03	4.936426	2.799807	2.799807
h_4	1.08e-04	4.22e-02	2.20e-03	4.937881	2.912835	2.912834
h_5	3.61e-05	2.17e-02	1.13e-03	4.903187	2.974129	2.974129
h_6	1.49e-05	1.26e-02	6.55e-04	4.867171	3.009933	3.00993
h_7	7.05e-06	7.87e-03	4.11e-04	4.842112	3.02971	3.02971

Table 4.14: Time-Dependent Extended Elasticity: Dirichlet Conditions at $k = 2$

h_j	$e^j_{\mathbf{u}}$	$e^j_{\boldsymbol{\eta}}$	$e^j_{\boldsymbol{\sigma}}$	$L^j_{\mathbf{u}}$	$L^j_{\boldsymbol{\eta}}$	$L^j_{\boldsymbol{\sigma}}$
h_1	5.22e-02	8.24e-01	4.30e-02			
h_2	6.88e-04	6.70e-02	3.50e-03	6.244437	3.619299	3.619302
h_3	6.28e-05	1.42e-02	7.42e-04	5.904398	3.822293	3.822295
h_4	1.13e-05	4.59e-03	2.39e-04	5.950438	3.932753	3.932745
h_5	3.00e-06	1.89e-03	9.86e-05	5.96314	3.975373	3.975365
h_6	1.01e-06	9.12e-04	4.76e-05	5.965622	3.999397	3.999441

Table 4.15: Time-Dependent Extended Elasticity: Dirichlet Conditions at $k = 3$

h_j	$e^j_{\mathbf{u}}$	$e^j_{\boldsymbol{\eta}}$	$e^j_{\boldsymbol{\sigma}}$	$L^j_{\mathbf{u}}$	$L^j_{\boldsymbol{\eta}}$	$L^j_{\boldsymbol{\sigma}}$
h_1	1.92e-02	8.64e-01	4.51e-02			
h_2	1.29e-04	1.64e-02	8.54e-04	7.215736	5.721963	5.721962
h_3	8.27e-06	2.01e-03	1.05e-04	6.777515	5.178033	5.17803
h_4	1.18e-06	4.58e-04	2.39e-05	6.771252	5.137197	5.137255
h_5	2.61e-07	1.48e-04	7.72e-06	6.75754	5.058696	5.058458

Table 4.16: Time-Dependent Extended Elasticity: Dirichlet Conditions at $k = 4$

h_j	$e^j_{\mathbf{u}}$	$e^j_{\boldsymbol{\eta}}$	$e^j_{\boldsymbol{\sigma}}$	$L^j_{\mathbf{u}}$	$L^j_{\boldsymbol{\eta}}$	$L^j_{\boldsymbol{\sigma}}$
h_1	7.68e-01	7.34e+00	3.83e-01			
h_2	5.81e-02	2.44e+00	1.28e-01	3.723071	1.586973	1.586975
h_3	6.95e-03	8.16e-01	4.26e-02	5.238639	2.704935	2.704935
h_4	1.82e-03	4.18e-01	2.18e-02	4.657562	2.323551	2.323551
h_5	7.47e-04	2.58e-01	1.35e-02	3.988641	2.166766	2.166766
h_6	3.67e-04	1.75e-01	9.11e-03	3.897815	2.14255	2.14255
h_7	2.03e-04	1.26e-01	6.56e-03	3.851873	2.124354	2.124354
h_8	1.22e-04	9.49e-02	4.95e-03	3.828342	2.110857	2.110857

Table 4.17: Time-Dependent Extended Elasticity: Neumann Conditions at $k = 1$

h_j	$e^j_{\mathbf{u}}$	$e^j_{\boldsymbol{\eta}}$	$e^j_{\boldsymbol{\sigma}}$	$L^j_{\mathbf{u}}$	$L^j_{\boldsymbol{\eta}}$	$L^j_{\boldsymbol{\sigma}}$
h_1	1.89e-01	3.22e+00	1.68e-01			
h_2	3.82e-03	3.57e-01	1.86e-02	5.630543	3.172554	3.17254
h_3	5.29e-04	1.07e-01	5.57e-03	4.87588	2.979006	2.979006
h_4	1.33e-04	4.44e-02	2.32e-03	4.795174	3.048021	3.048021
h_5	4.60e-05	2.24e-02	1.17e-03	4.76159	3.06876	3.068759
h_6	1.94e-05	1.28e-02	6.68e-04	4.729865	3.069998	3.069996
h_7	9.44e-06	7.98e-03	4.16e-04	4.677826	3.067232	3.067244

Table 4.18: Time-Dependent Extended Elasticity: Neumann Conditions at $k = 2$

h_j	$e^j_{\mathbf{u}}$	$e^j_{\boldsymbol{\eta}}$	$e^j_{\boldsymbol{\sigma}}$	$L^j_{\mathbf{u}}$	$L^j_{\boldsymbol{\eta}}$	$L^j_{\boldsymbol{\sigma}}$
h_1	6.60e-02	1.27e+00	6.65e-02			
h_2	9.34e-04	7.45e-02	3.88e-03	6.142158	4.09763	4.097633
h_3	1.03e-04	1.51e-02	7.85e-04	5.447686	3.942565	3.942566
h_4	2.22e-05	4.76e-03	2.48e-04	5.317838	4.000281	4.000287
h_5	6.96e-06	1.94e-03	1.01e-04	5.204629	4.023673	4.023668
h_6	2.76e-06	9.30e-04	4.85e-05	5.066835	4.035251	4.035289

Table 4.19: Time-Dependent Extended Elasticity: Neumann Conditions at $k = 3$

h_j	$e^j_{\mathbf{u}}$	$e^j_{\boldsymbol{\eta}}$	$e^j_{\boldsymbol{\sigma}}$	$L^j_{\mathbf{u}}$	$L^j_{\boldsymbol{\eta}}$	$L^j_{\boldsymbol{\sigma}}$
h_1	3.69e-02	4.97e-01	2.59e-02			
h_2	5.37e-04	1.36e-02	7.08e-04	6.099786	5.194337	5.194336
h_3	4.65e-05	1.84e-03	9.62e-05	6.033961	4.922191	4.922183
h_4	8.34e-06	4.39e-04	2.29e-05	5.975795	4.986759	4.986828
h_5	2.21e-06	1.45e-04	7.55e-06	5.944076	4.977906	4.977838

Table 4.20: Time-Dependent Extended Elasticity: Neumann Conditions at $k = 4$

h_j	$e^j_{\mathbf{u}}$	$e^j_{\boldsymbol{\eta}}$	$e^j_{\boldsymbol{\sigma}}$	$L^j_{\mathbf{u}}$	$L^j_{\boldsymbol{\eta}}$	$L^j_{\boldsymbol{\sigma}}$
h_1	5.04e-01	9.75e+00	5.08e-01			
h_2	2.05e-02	1.85e+00	9.66e-02	4.621784	2.396045	2.396047
h_3	4.04e-03	7.55e-01	3.94e-02	4.00516	2.213567	2.213567
h_4	1.37e-03	4.09e-01	2.14e-02	3.76347	2.125643	2.125643
h_5	5.96e-04	2.55e-01	1.33e-02	3.723121	2.123439	2.123439
h_6	3.04e-04	1.73e-01	9.04e-03	3.688181	2.114427	2.114426
h_7	1.72e-04	1.25e-01	6.53e-03	3.678222	2.108226	2.108227
h_8	1.06e-04	9.46e-02	4.94e-03	3.670764	2.102266	2.102266

Table 4.21: Time-Dependent Extended Elasticity: Mixed Conditions at $k = 1$

h_j	$e^j_{\mathbf{u}}$	$e^j_{\boldsymbol{\eta}}$	$e^j_{\boldsymbol{\sigma}}$	$L^j_{\mathbf{u}}$	$L^j_{\boldsymbol{\eta}}$	$L^j_{\boldsymbol{\sigma}}$
h_1	1.48e-01	2.69e+00	1.40e-01			
h_2	3.51e-03	3.42e-01	1.78e-02	5.401077	2.979149	2.979136
h_3	4.83e-04	1.04e-01	5.43e-03	4.893206	2.929426	2.929426
h_4	1.19e-04	4.39e-02	2.29e-03	4.854499	3.00046	3.00046
h_5	4.09e-05	2.23e-02	1.16e-03	4.800682	3.036323	3.036323
h_6	1.72e-05	1.28e-02	6.67e-04	4.756778	3.053525	3.05352
h_7	8.30e-06	7.98e-03	4.16e-04	4.726598	3.060548	3.060554

Table 4.22: Time-Dependent Extended Elasticity: Mixed Conditions at $k = 2$

h_j	$e^j_{\mathbf{u}}$	$e^j_{\boldsymbol{\eta}}$	$e^j_{\boldsymbol{\sigma}}$	$L^j_{\mathbf{u}}$	$L^j_{\boldsymbol{\eta}}$	$L^j_{\boldsymbol{\sigma}}$
h_1	5.91e-02	1.18e+00	6.16e-02			
h_2	8.40e-04	8.65e-02	4.51e-03	6.137195	3.771344	3.771348
h_3	8.74e-05	1.61e-02	8.38e-04	5.579726	4.150368	4.150368
h_4	1.82e-05	4.94e-03	2.58e-04	5.461183	4.099686	4.099688
h_5	5.51e-06	1.99e-03	1.04e-04	5.34963	4.081853	4.08184
h_6	2.11e-06	9.46e-04	4.93e-05	5.267956	4.074936	4.074983

Table 4.23: Time-Dependent Extended Elasticity: Mixed Conditions at $k = 3$

h_j	$e^j_{\mathbf{u}}$	$e^j_{\boldsymbol{\eta}}$	$e^j_{\boldsymbol{\sigma}}$	$L^j_{\mathbf{u}}$	$L^j_{\boldsymbol{\eta}}$	$L^j_{\boldsymbol{\sigma}}$
h_1	2.27e-02	1.02e+00	5.30e-02			
h_2	4.16e-04	4.44e-02	2.31e-03	5.767827	4.517999	4.517999
h_3	3.50e-05	4.08e-03	2.13e-04	6.101702	5.881931	5.881934
h_4	6.16e-06	7.83e-04	4.08e-05	6.040875	5.742611	5.742644
h_5	1.60e-06	2.22e-04	1.16e-05	6.044811	5.638637	5.638696

Table 4.24: Time-Dependent Extended Elasticity: Mixed Conditions at $k = 4$

Chapter 5

HDG+ FOR BIOT'S MODEL OF LINEAR POROELASTICITY

We first give an overview of progress made on modeling Biot's poroelasticity equations in 3D, and then propose and briefly analyze an HDG+ scheme to give both frequency-domain and time-domain approximations to the solutions of the equations.

5.1 Introduction

We turn our attention now to Biot's model of linear poroelasticity in 3D. Many people have explored this topic in various levels of detail. Linear poroelasticity as a field was created by Karl Terzaghi in 1923 to describe the 1D consolidation of clay soils [49], but the 3-dimensional model is attributed to Maurice Biot. Biot published his first work on poroelasticity in 1941 [7]. This culminated in his work, "Theory of propagation of elastic waves in a fluid-saturated porous solid, part I: low frequency range" and "part II: higher frequency range" [6]. Rice and Cleary [43] recast the problem as compressible in both fluid and solid phases, and in terms of new material parameters, such as the Poisson ratio and the bulk modulus evaluated in both drained and undrained states. An excellent overview of the history of poroelasticity, as well as the analogy between thermoelasticity and poroelasticity, can be found in Chapter 1 of [50].

More recently, Gaspar, Lisbona, and Vabishchevich present a finite difference analysis of the quasi-static version of Biot's consolidation model in 1D [20]. Yder Masson and Steven Pride model Biot's poroelastic equations across all frequencies via the finite difference approach [36]. They present an explicit time-stepping staggered-grid finite-difference scheme for solving Biot's equations in the low-frequency limit, and present numerical experiments that confirm their accuracy by comparison to exact analytical solutions for both fast compressional waves and slow waves.

Anna Naumovich writes about the quasi-static Biot poroelasticity system in her Ph.D. thesis [38]. She solves the system with a finite volume discretization that yields second-order convergence. A stabilized element-based finite volume formulation for 3D poroelastic problems can be found in [27]. Lemoine, Ou, and LeVeque [32] present an explicit time-stepping approach to modeling wave propagation with low memory overhead and wave limiters to reduce numerical artifacts in the solution.

For the more finite-element styled literature, Phillip Joseph Phillips and his advisor, Mary F. Wheeler, discuss theoretical and computational results in linear poroelasticity [40]. They use a continuous Galerkin scheme for the displacement and mixed finite elements for the pressure/pressure flux. Then, because of a locking phenomenon, they turn to discontinuous Galerkin for the displacement and mixed finite elements for the flow, and then they show that they can combine CG and mixed finite elements with an adaptive grid for the same results. Then Kolesov, Vabishchevich, and Vasilyeve [2] consider FEM approximation in space with a splitting scheme in time with an additive representation of the differentiation operator for the quasi-stationary problem (steady for motion and unsteady for temperature/pressure). In his 2015 doctoral thesis, Lorenz Berger presents a low-order FEM for poroelasticity with applications to lung modeling [4], using P0 elements for pressure and P1 for displacement. Berger, Bordas, and Kay [5] come up with a stabilized FEM for finite-strain three-field poroelasticity using Berger's low-order elements and a splitting scheme in time. Uwe Köcher and Markus Bause use DG and CG for their time discretization and mixed FEM in space for the flow problem and CG for the mechanics [29].

As for discontinuous Galerkin methods, we can consider the work of Ward, Lähivaara and Eveson. They model wave propagation in the two-dimensional case, deriving the upwind numerical flux as an exact solution for the Riemann problem including the poroelastic-elastic interface [51]. De la Puente, Dumbser, Käser and Igel build a scheme able to successfully model wave propagation in fluid-saturated porous media where anisotropy of the pore structure is allowed [15]. Ge and Ma develop and analyze a multiphysics DG method for a (fully dynamic) poroelasticity model [21], and prove that their multiphysics DG method is absolutely stable for all positive mesh sizes h. To the author's knowledge at the time of writing this, however, this is the first work on using a hybridized DG scheme, in particular combined with convolution quadrature, to model the fully dynamic Biot's system of poroelasticity in 3D.

5.2 Model Equations

The bounded domain is still denoted Ω, but now it has two different partitionings of the boundary Γ into $\Gamma_D \cup \Gamma_N$ and $\widetilde{\Gamma}_D \cup \widetilde{\Gamma}_N$. The former will still be used for displacement/stress boundary conditions, while the latter will now be used for pressure and pressure flux boundary conditions.

We will admit a compliance tensor $\mathcal{A}$ as in (3.2.2), a strongly positive density $\rho : \mathbb{R}^3 \to \mathbb{R}$, a strongly positive storativity parameter $c : \mathbb{R}^3 \to \mathbb{R}$, a constant, symmetric and uniformly positive definite matrix $\kappa \in \mathbb{R}^{3\times 3}_{\text{sym}}$ representing the hydraulic conductivity normalized by the specific weight of the fluid. In addition we will specify a Biot's constant $\beta \in [0, 1]$. We will also have forcing functions $\mathbf{f}_\mathbf{u} : [0, \infty) \to L^2(\Omega, \mathbb{R}^3)$ and $f_p : [0, \infty) \to L^2(\Omega, \mathbb{R})$, Dirichlet boundary conditions $\mathbf{g}_D : [0, \infty) \to H^{1/2}(\Gamma_D, \mathbb{R}^3)$ and $g_d : [0, \infty) \to H^{1/2}(\widetilde{\Gamma}_D, \mathbb{R})$, and Neumann conditions $\mathbf{g}_N : [0, \infty) \to L^2(\Gamma_N, \mathbb{R}^3)$ and $g_n : [0, \infty) \to L^2(\widetilde{\Gamma}_N, \mathbb{R})$.

We seek the transient displacement field $\mathbf{u} : [0, \infty) \to H^1(\Omega, \mathbb{R}^3)$, its accompanying elastic stress field $\boldsymbol{\sigma} : [0, \infty) \to H(\text{div}, \Omega; \mathbb{R}^{3\times 3}_{\text{sym}})$, and the pressure function $p : [0, \infty) \to H^1(\Omega, \mathbb{R})$ that satisfy the following equations:

$$
\begin{aligned}
\mathcal{A}\boldsymbol{\sigma}(t) &= \boldsymbol{\epsilon}(\mathbf{u}(t)) && \text{in } \Omega, && (5.2.1)\\
\rho\ddot{\mathbf{u}}(t) &= \operatorname{div}\, \boldsymbol{\sigma}(t) - \beta\nabla p(t) + \mathbf{f}_{\mathbf{u}}(t) && \text{in } \Omega, && (5.2.2)\\
\beta\nabla\cdot\dot{\mathbf{u}}(t) + c\dot{p}(t) &= \nabla\cdot(\kappa\nabla p(t)) + f_p(t) && \text{in } \Omega, && (5.2.3)\\
\mathbf{u}(t) &= \mathbf{g}_D(t) && \text{on } \Gamma_D, && (5.2.4)\\
\boldsymbol{\sigma}(t)\mathbf{n} - \beta p(t)\mathbf{n} &= \mathbf{g}_N(t) && \text{on } \Gamma_N, && (5.2.5)\\
p(t) &= g_d(t) && \text{on } \tilde{\Gamma}_D, && (5.2.6)\\
\kappa\nabla p(t)\cdot\mathbf{n} &= g_n(t) && \text{on } \tilde{\Gamma}_N, && (5.2.7)\\
\mathbf{u}(0) &= \mathbf{u}_0 && \text{in } \Omega, && (5.2.8)\\
\dot{\mathbf{u}}(0) &= \mathbf{v}_0 && \text{in } \Omega, && (5.2.9)\\
p(0) &= p_0 && \text{in } \Omega. && (5.2.10)
\end{aligned}
$$

Proposition 5.2.1. *Assume that there are no forcing terms ($\mathbf{f}_{\mathbf{u}} = \mathbf{0}, f_p = 0$ in Ω), the boundary displacement is constant in time ($\dot{\mathbf{g}}_D = \mathbf{0}$ on Γ_D), Biot stress is zero ($\mathbf{g}_N = \mathbf{0}$) on Γ_N, boundary pressure is zero ($g_d = 0$) on $\widetilde{\Gamma}_D$ and there is no pressure flux ($g_n = 0$) across $\widetilde{\Gamma}_N$. Then the system itself is dissipative, i.e., that*

$$
\frac{\mathrm{d}}{\mathrm{d}t}\left(\|\boldsymbol{\sigma}(t)\|^2_{\mathcal{A}} + \|\dot{\mathbf{u}}(t)\|^2_{\rho} + \|p(t)\|^2_c\right) \le 0.
$$

Proof. We begin by differentiating and then testing equation (5.2.1) with $\boldsymbol{\sigma}(t)$,

$$
(\mathcal{A}\dot{\boldsymbol{\sigma}}(t), \boldsymbol{\sigma}(t))_\Omega = (\boldsymbol{\epsilon}(\dot{\mathbf{u}}_h), \boldsymbol{\sigma}(t))_\Omega = (\nabla\dot{\mathbf{u}}(t), \boldsymbol{\sigma}(t))_\Omega,
$$

Next we test (5.2.2) with $\dot{\mathbf{u}}(t)$,

$$
(\rho\ddot{\mathbf{u}}(t), \dot{\mathbf{u}}(t))_\Omega = (\operatorname{div}\, \boldsymbol{\sigma}(t), \dot{\mathbf{u}}(t))_\Omega - (\beta\nabla p(t), \dot{\mathbf{u}}(t))_\Omega,
$$

or, after integrating by parts,

$$
(\rho\ddot{\mathbf{u}}(t), \dot{\mathbf{u}}(t))_\Omega = \langle\boldsymbol{\sigma}(t)\mathbf{n}, \dot{\mathbf{u}}(t)\rangle_\Gamma - (\boldsymbol{\sigma}(t), \nabla\dot{\mathbf{u}}(t))_\Omega - (\beta\nabla p(t), \dot{\mathbf{u}}(t))_\Omega.
$$

Then we test (5.2.3) with $p(t)$,

$$\beta(\nabla \cdot \dot{\mathbf{u}}(t), p(t))_\Omega + (c\dot{p}(t), p(t))_\Omega = (\nabla \cdot \kappa \nabla p(t), p(t))_\Omega.$$

After integrating by parts and dropping the boundary term due to (5.2.6) and (5.2.7), we have

$$\beta\langle \dot{\mathbf{u}}(t), p(t)\mathbf{n}\rangle_\Gamma - \beta(\dot{\mathbf{u}}(t), \nabla p(t))_\Omega + (c\dot{p}(t), p(t))_\Omega = -(\kappa \nabla p(t), \nabla p(t))_\Omega.$$

Rearranging, we have

$$\begin{aligned}
\frac{1}{2}\frac{\mathrm{d}}{\mathrm{d}t}\|\boldsymbol{\sigma}(t)\|_{\mathcal{A}}^2 - (\nabla \dot{\mathbf{u}}(t), \boldsymbol{\sigma}(t))_\Omega &= 0,\\
\frac{1}{2}\frac{\mathrm{d}}{\mathrm{d}t}\|\dot{\mathbf{u}}(t)\|_\rho^2 - \langle \boldsymbol{\sigma}(t)\mathbf{n}, \dot{\mathbf{u}}(t)\rangle_\Gamma + (\boldsymbol{\sigma}(t), \nabla \dot{\mathbf{u}}(t))_\Omega + (\beta \nabla p(t), \dot{\mathbf{u}}(t))_\Omega &= 0,\\
\langle \dot{\mathbf{u}}(t), \beta p(t)\mathbf{n}\rangle_\Gamma - (\dot{\mathbf{u}}(t), \beta \nabla p(t))_\Omega + \frac{1}{2}\frac{\mathrm{d}}{\mathrm{d}t}\|p(t)\|_c^2 + \|\nabla p(t)\|_\kappa^2 &= 0.
\end{aligned}$$

Summing, we have

$$\frac{1}{2}\frac{\mathrm{d}}{\mathrm{d}t}\|\boldsymbol{\sigma}(t)\|_{\mathcal{A}}^2 + \frac{1}{2}\frac{\mathrm{d}}{\mathrm{d}t}\|\dot{\mathbf{u}}(t)\|_\rho^2 - \langle \boldsymbol{\sigma}(t)\mathbf{n} - \beta p(t)\mathbf{n}, \dot{\mathbf{u}}(t)\rangle_\Gamma + \frac{1}{2}\frac{\mathrm{d}}{\mathrm{d}t}\|p(t)\|_c^2 + \|\nabla p(t)\|_\kappa^2 = 0,$$

or, equivalently, by dropping the boundary term due to (5.2.4) and (5.2.5),

$$\frac{\mathrm{d}}{\mathrm{d}t}\left(\|\boldsymbol{\sigma}(t)\|_{\mathcal{A}}^2 + \|\dot{\mathbf{u}}(t)\|_\rho^2 + \|p(t)\|_c^2\right) = -2\|\nabla p(t)\|_\kappa^2 \leq 0.$$

□

We now take a moment to introduce the pressure flux variable $\mathbf{q} = \kappa \nabla p$, to form the equivalent system,

$$\mathcal{A}\boldsymbol{\sigma}(t) - \boldsymbol{\epsilon}(\mathbf{u}(t)) = 0 \qquad \text{in } \Omega, \tag{5.2.11}$$

$$-\mathrm{div}\, \boldsymbol{\sigma}(t) + \rho \ddot{\mathbf{u}}(t) + \beta \nabla p(t) = \mathbf{f}_{\mathbf{u}}(t) \qquad \text{in } \Omega, \tag{5.2.12}$$

$$\kappa^{-1}\mathbf{q} - \nabla p = 0 \qquad \text{in } \Omega \tag{5.2.13}$$

$$\beta \nabla \cdot \dot{\mathbf{u}}(t) - \nabla \cdot \mathbf{q}(t) + c\dot{p}(t) = f_p(t) \qquad \text{in } \Omega, \tag{5.2.14}$$

$$\mathbf{u}(t) = \mathbf{g}_D(t) \quad \text{on } \Gamma_D, \tag{5.2.15}$$

$$\boldsymbol{\sigma}(t)\mathbf{n} - \beta p(t)\mathbf{n} = \mathbf{g}_N(t) \quad \text{on } \Gamma_N, \tag{5.2.16}$$

$$p(t) = g_d(t) \quad \text{on } \tilde{\Gamma}_D, \tag{5.2.17}$$

$$\mathbf{q}(t) \cdot \mathbf{n} = g_n(t) \quad \text{on } \tilde{\Gamma}_N, \tag{5.2.18}$$

Going through an equivalent process of differentiating and testing (5.2.11) with $\boldsymbol{\sigma}(t)$,testing (5.2.12) with $\dot{\mathbf{u}}$, testing (5.2.13) with $\mathbf{q}$, and testing (5.2.14) with p, integrating by parts and summing, we get

$$\frac{d}{dt}\left(\|\boldsymbol{\sigma}(t)\|_{\mathcal{A}}^2 + \|\dot{\mathbf{u}}(t)\|_{\rho}^2 + \|p(t)\|_c^2\right) = -2\|\mathbf{q}(t)\|_{\kappa^{-1}}^2 \le 0.$$

5.3 HDG+ semidiscretization

Next we introduce the HDG+ semidiscretization of the above system. The method involves six discrete spaces

$$\mathbb{V}_h := \{\boldsymbol{\xi} : \Omega \to \mathbb{R}^{3\times 3}_{\text{sym}} : \forall K \in \mathcal{T}_h, \boldsymbol{\xi}|_K \in \mathcal{P}_k(K; \mathbb{R}^{3\times 3}_{\text{sym}})\}, \tag{5.3.1}$$

$$\mathbf{W}_h := \{\mathbf{v} : \Omega \to \mathbb{R}^3 : \forall K \in \mathcal{T}_h, \mathbf{v}|_K \in \mathcal{P}_{k+1}(K; \mathbb{R}^3\}, \tag{5.3.2}$$

$$\mathbf{Q}_h := \{\mathbf{r} : \Omega \to \mathbb{R}^3 : \forall K \in \mathcal{T}_h, \mathbf{r}|_K \in \mathcal{P}_k(K; \mathbb{R}^3\}, \tag{5.3.3}$$

$$P_h := \{s : \Omega \to \mathbb{R} : \forall K \in \mathcal{T}_h, s|_K \in \mathcal{P}_{k+1}(K; \mathbb{R}\}, \tag{5.3.4}$$

$$\mathbf{M}_h := \{\boldsymbol{\mu} : \mathcal{E}_h \to \mathbb{R}^3 : \forall F \in \mathcal{E}_h, \boldsymbol{\mu}|_F \in \mathcal{P}_k(F, \mathbb{R}^3), \tag{5.3.5}$$

$$M_h := \{\mu : \mathcal{E}_h \to \mathbb{R} : \forall F \in \mathcal{E}_h, \mu|_F \in \mathcal{P}_k(F, \mathbb{R}), \tag{5.3.6}$$

just as in (3.2.2), where $\mathcal{P}_r(K; S)$ is the set of polynomials of total degree up to r defined on K and with values in $S \in \{\mathbb{R}^{3\times 3}_{\text{sym}}, \mathbb{R}^3, \mathbb{R}\}$, while $\mathcal{P}_k(F; \mathbb{R}^q)$ are either vector or scalar (dependent on q) polynomials on the tangential coordinates defined on the face F and of degree not greater than k. We will also use the orthogonal projectors

$$\mathbf{P}_{\mathbf{M}} : \prod_{K\in\mathcal{T}_h} L^2(\partial K, \mathbb{R}^3) \to \prod_{K\in\mathcal{T}_h} \prod_{F\in\mathcal{E}(K)} \mathcal{P}_k(F; \mathbb{R}^3)$$

and

$$P_M : \prod_{K\in\mathcal{T}_h} L^2(\partial K, \mathbb{R}) \to \prod_{K\in\mathcal{T}_h} \prod_{F\in\mathcal{E}(K)} \mathcal{P}_k(F; \mathbb{R}).$$

Note that $\mathbf{M}_h$ and M_h can be identified with subspaces of the sets of the right-hand sides. We take a shape-regular conforming tetrahedrization $\mathcal{T}_h$ of Ω and make stabilization functions

$$\boldsymbol{\tau}_{K,\mathbf{u}} : \partial K \to \mathbb{R}^{3\times 3}_{\text{sym}} \qquad \text{and} \qquad \tau_{K,p} : \partial K \to \mathbb{R}$$

such that (a) $\boldsymbol{\tau}_{K,\mathbf{u}}$ and $\tau_{K,p}$ are constant on each face and (b) there exist four positive constants C_1, C_2, C_3, and C_4 such that

$$C_1 h_K^{-1}\|\boldsymbol{\mu}\|_{\partial K}^2 \leq \langle \boldsymbol{\tau}_{K,\mathbf{u}}\boldsymbol{\mu}, \boldsymbol{\mu}\rangle_{\partial K} \leq C_2 h_K^{-1}\|\boldsymbol{\mu}\|_{\partial K}^2 \qquad \forall \boldsymbol{\mu} \in \mathbf{L}^2(\partial K), \qquad \forall K \in \mathcal{T}_h$$

$$C_3 h_K^{-1}\|\mu\|_{\partial K}^2 \leq \langle \tau_{K,p}\mu, \mu\rangle_{\partial K} \leq C_4 h_K^{-1}\|\mu\|_{\partial K}^2 \qquad \forall \mu \in L^2(\partial K), \qquad \forall K \in \mathcal{T}_h$$

where h_K is the diameter of K. The symbols $\boldsymbol{\tau}_{\mathbf{u}}$ and τ_p will be used to denote the functions defined on the set of boundaries of all elements K above, understanding that $\boldsymbol{\tau}_{\mathbf{u}}$ and τ_p may be double-valued on interior faces.

We will now look for variables

$$\begin{aligned}
\boldsymbol{\sigma}_h &: [0,\infty) \to \mathbb{V}_h,\\
\mathbf{u}_h &: [0,\infty) \to \mathbf{W}_h,\\
\mathbf{q}_h &: [0,\infty) \to \mathbf{Q}_h,\\
p_h &: [0,\infty) \to P_h,
\end{aligned}$$

and numerical traces

$$\begin{aligned}
\widehat{\mathbf{u}}_h &: [0,\infty) \to \mathbf{M}_h,\\
\widehat{p}_h &: [0,\infty) \to M_h.
\end{aligned}$$

such that for all $(\boldsymbol{\xi}_h, \mathbf{v}_h, \mathbf{r}_h, s_h) \in \mathbb{V}_h \times \mathbf{W}_h \times \mathbf{Q}_h \times P_h$ and for all $K \in \mathcal{T}_h$,

$$(\mathcal{A}\boldsymbol{\sigma}_h(t), \boldsymbol{\xi}_h)_K + (\mathbf{u}_h(t), \operatorname{div} \boldsymbol{\xi}_h)_K - \langle \widehat{\mathbf{u}}_h(t)), \boldsymbol{\xi}_h\mathbf{n}\rangle_{\partial K} = 0, \tag{5.3.7}$$

$$\begin{aligned}
&-(\operatorname{div} \boldsymbol{\sigma}_h(t), \mathbf{v}_h)_K + (\rho\ddot{\mathbf{u}}_h(t), \mathbf{v}_h)_K\\
&+\langle \boldsymbol{\tau}_{\mathbf{u}}(\mathbf{P}_M\mathbf{u}_h(t) - \widehat{\mathbf{u}}_h(t)), \mathbf{P}_M\mathbf{v}_h\rangle_{\partial K} + \beta(\nabla p_h(t), \mathbf{v}_h)_K = (\mathbf{f}_{\mathbf{u}}(t), \mathbf{v}_h)_K,
\end{aligned} \tag{5.3.8}$$

$$(\kappa^{-1}\mathbf{q}_h(t), \mathbf{r}_h)_K + (p_h(t), \nabla \cdot \mathbf{r}_h)_K - \langle \widehat{p}_h(t), \mathbf{r}_h \cdot \mathbf{n}\rangle_{\partial K} = 0, \tag{5.3.9}$$

$$\begin{aligned}
&-\beta(\dot{\mathbf{u}}_h(t), \nabla s_h)_K + \beta\langle \dot{\widehat{\mathbf{u}}}_h(t), P_M s_h\mathbf{n}\rangle_{\partial K}\\
&-(\nabla \cdot \mathbf{q}_h(t), s_h)_K + (c\dot{p}_h(t), s_h)_K + \langle \tau_p(P_M p_h(t) - \widehat{p}_h(t)), P_M s_h\rangle_{\partial K} = (f_p(t), s_h)_K.
\end{aligned} \tag{5.3.10}$$

Summing these over the various elements K, we have

$$(\mathcal{A}\boldsymbol{\sigma}_h(t), \boldsymbol{\xi}_h)_{\mathcal{T}_h} + (\mathbf{u}_h(t), \text{div } \boldsymbol{\xi}_h)_{\mathcal{T}_h} - \langle \widehat{\mathbf{u}}_h(t)), \boldsymbol{\xi}_h \mathbf{n}\rangle_{\partial\mathcal{T}_h} = 0, \tag{5.3.11}$$

$$\begin{aligned} -(\text{div } \boldsymbol{\sigma}_h(t), \mathbf{v}_h)_{\mathcal{T}_h} + (\rho\ddot{\mathbf{u}}_h(t), \mathbf{v}_h)_{\mathcal{T}_h} + \beta(\nabla p_h(t), \mathbf{v}_h)_{\mathcal{T}_h} \\ + \langle \boldsymbol{\tau}_{\mathbf{u}}(\mathbf{P}_M\mathbf{u}_h(t) - \widehat{\mathbf{u}}_h(t)), \mathbf{P}_M\mathbf{v}_h\rangle_{\partial\mathcal{T}_h} = (\mathbf{f}_{\mathbf{u}}(t), \mathbf{v}_h)_{\mathcal{T}_h}, \end{aligned} \tag{5.3.12}$$

$$(\kappa^{-1}\mathbf{q}_h(t), \mathbf{r}_h)_{\mathcal{T}_h} + (p_h(t), \nabla\cdot\mathbf{r}_h)_{\mathcal{T}_h} - \langle \widehat{p}_h(t), \mathbf{r}_h\cdot\mathbf{n}\rangle_{\partial\mathcal{T}_h} = 0, \tag{5.3.13}$$

$$\begin{aligned} -\beta(\dot{\mathbf{u}}_h(t), \nabla s_h)_{\mathcal{T}_h} + \beta\langle \dot{\widehat{\mathbf{u}}}_h(t), P_M s_h \mathbf{n}\rangle_{\partial\mathcal{T}_h} \\ -(\nabla\cdot\mathbf{q}_h(t), s_h)_{\mathcal{T}_h} + (c\dot{p}_h(t), s_h)_{\mathcal{T}_h} \\ + \langle \tau_p(P_M p_h(t) - \widehat{p}_h(t)), P_M s_h\rangle_{\partial\mathcal{T}_h} = (f_p(t), s_h)_{\mathcal{T}_h}. \end{aligned} \tag{5.3.14}$$

We now introduce boundary and equilibrium conditions as well as initial conditions:

$$\langle \widehat{\mathbf{u}}_h(t), \widehat{\mathbf{v}}_h\rangle_{\Gamma_D} = \langle \mathbf{g}_D(t), \widehat{\mathbf{v}}_h\rangle_{\Gamma_D}, \tag{5.3.15}$$

$$\langle \widehat{p}_h(t), \widehat{v}_h\rangle_{\widetilde{\Gamma}_D} = \langle g_d(t), \widehat{v}_h\rangle_{\widetilde{\Gamma}_D}, \tag{5.3.16}$$

$$\langle \boldsymbol{\sigma}_h(t)\mathbf{n} - \boldsymbol{\tau}_{\mathbf{u}}(\mathbf{P}_M\mathbf{u}_h(t) - \widehat{\mathbf{u}}_h(t)) - \beta P_M p_h(t)\mathbf{n}, \widehat{\mathbf{v}}_h\rangle_{\partial\mathcal{T}_h\setminus\Gamma_D} = \langle \mathbf{g}_N(t), \widehat{\mathbf{v}}_h\rangle_{\Gamma_N}, \tag{5.3.17}$$

$$\langle \mathbf{q}_h(t)\cdot\mathbf{n} - \tau_p(P_M p_h(t) - \widehat{p}_h(t)), \widehat{v}_h\rangle_{\partial\mathcal{T}_h\setminus\widetilde{\Gamma}_D} = \langle g_n(t), \widehat{v}_h\rangle_{\widetilde{\Gamma}_N}, \tag{5.3.18}$$

$$\mathbf{u}_h(0) = \mathbf{u}_{h,0},\ \mathbf{v}_h(0) = \mathbf{v}_{h,0},\ p(0) = p_{h,0}. \tag{5.3.19}$$

Proposition 5.3.1. *This method is also dissipative, i.e.*

$$\frac{\mathrm{d}}{\mathrm{d}t}\left(\|\boldsymbol{\sigma}_h(t)\|_{\mathcal{A}}^2 + \|\dot{\mathbf{u}}_h(t)\|_\rho^2 + \|p_h(t)\|_c^2 + \|(\mathbf{P}_M\mathbf{u}_h(t) - \widehat{\mathbf{u}}_h(t))\|_{\boldsymbol{\tau}_{\mathbf{u}}}^2\right) \le 0.$$

Proof. Let $\mathbf{f}_{\mathbf{u}}(t) = 0$, $f_p(t) = 0$, $\dot{\mathbf{g}}_D(t) = 0$, $g_d(t) = 0$, $\mathbf{g}_N(t) = 0$, and $g_n(t) = 0$. Then differentiate equation (5.3.11) and test with $\boldsymbol{\xi}_h = \boldsymbol{\sigma}_h(t)$, yielding

$$(\mathcal{A}\dot{\boldsymbol{\sigma}}_h(t), \boldsymbol{\sigma}_h(t))_{\mathcal{T}_h} + (\dot{\mathbf{u}}_h(t), \text{div } \boldsymbol{\sigma}_h(t))_{\mathcal{T}_h} - \langle \dot{\widehat{\mathbf{u}}}_h(t), \boldsymbol{\sigma}_h(t)\mathbf{n}\rangle_{\partial\mathcal{T}_h} = 0, \tag{5.3.20}$$

which, using boundary conditions (5.3.15) and (5.3.17), and the fact that $\dot{\mathbf{g}}_D = 0$ on Γ_D to replace the term

$$\begin{aligned} &\langle \dot{\widehat{\mathbf{u}}}_h(t), \boldsymbol{\sigma}_h(t)\mathbf{n}\rangle_{\partial\mathcal{T}_h} \\ &= \langle \dot{\widehat{\mathbf{u}}}_h(t), \boldsymbol{\sigma}_h(t)\mathbf{n}\rangle_{\partial\mathcal{T}_h\setminus\Gamma_D} \\ &= \langle \dot{\widehat{\mathbf{u}}}_h(t), \boldsymbol{\tau}_{\mathbf{u}}(\mathbf{P}_M\mathbf{u}_h(t) - \widehat{\mathbf{u}}_h(t)) + \beta P_M p_h(t)\mathbf{n}\rangle_{\partial\mathcal{T}_h\setminus\Gamma_D} \\ &= \langle \dot{\widehat{\mathbf{u}}}_h(t), \boldsymbol{\tau}_{\mathbf{u}}(\mathbf{P}_M\mathbf{u}_h(t) - \widehat{\mathbf{u}}_h(t)) + \beta P_M p_h(t)\mathbf{n}\rangle_{\partial\mathcal{T}_h}, \end{aligned}$$

becomes

$$\begin{aligned}(\mathcal{A}\dot{\boldsymbol{\sigma}}_h(t), \boldsymbol{\sigma}_h(t))_{\mathcal{T}_h} + (\dot{\mathbf{u}}_h(t), \operatorname{div}\, \boldsymbol{\sigma}_h(t))_{\mathcal{T}_h}& \\ -\langle \dot{\widehat{\mathbf{u}}}_h(t), \boldsymbol{\tau}_{\mathbf{u}}(\mathbf{P}_M\mathbf{u}_h(t) - \widehat{\mathbf{u}}_h(t)) + \beta P_M p_h(t)\mathbf{n}\rangle_{\partial\mathcal{T}_h} &= 0.\end{aligned} \tag{5.3.21}$$

Then we test (5.3.12) with $\mathbf{v}_h = \dot{\mathbf{u}}_h(t)$,

$$\begin{aligned}-(\operatorname{div}\, \boldsymbol{\sigma}_h(t), \dot{\mathbf{u}}_h(t))_{\mathcal{T}_h} + (\rho\ddot{\mathbf{u}}_h(t), \dot{\mathbf{u}}_h(t))_{\mathcal{T}_h} + \beta(\nabla p_h(t), \dot{\mathbf{u}}_h(t))_{\mathcal{T}_h}& \\ +\langle \boldsymbol{\tau}_{\mathbf{u}}(\mathbf{P}_M\mathbf{u}_h(t) - \widehat{\mathbf{u}}_h(t)), \mathbf{P}_M\dot{\mathbf{u}}_h(t)\rangle_{\partial\mathcal{T}_h} &= 0,\end{aligned} \tag{5.3.22}$$

and test (5.3.13) with $\mathbf{r}_h = \mathbf{q}_h(t)$,

$$(\kappa^{-1}\mathbf{q}_h(t), \mathbf{q}_h(t))_{\mathcal{T}_h} + (p_h(t), \nabla\cdot\mathbf{q}_h(t))_{\mathcal{T}_h} - \langle \widehat{p}_h(t), \mathbf{q}_h(t)\cdot\mathbf{n}\rangle_{\partial\mathcal{T}_h} = 0. \tag{5.3.23}$$

Next we use the boundary conditions (5.3.16) and (5.3.18) and the fact that $g_d = 0$ on $\widetilde{\Gamma}_D$ to replace

$$\begin{aligned}&\langle \widehat{p}_h(t), \mathbf{q}_h(t)\cdot\mathbf{n}\rangle_{\partial\mathcal{T}_h} \\ &= \langle \widehat{p}_h(t), \mathbf{q}_h(t)\cdot\mathbf{n}\rangle_{\partial\mathcal{T}_h\setminus\widetilde{\Gamma}_D} \\ &= \langle \widehat{p}_h(t), \tau_p(P_M p_h - \widehat{p}_h)\rangle_{\partial\mathcal{T}_h\setminus\widetilde{\Gamma}_D} \\ &= \langle \widehat{p}_h(t), \tau_p(P_M p_h - \widehat{p}_h)\rangle_{\partial\mathcal{T}_h},\end{aligned}$$

creating

$$(\kappa^{-1}\mathbf{q}_h(t), \mathbf{q}_h(t))_{\mathcal{T}_h} + (p_h(t), \nabla\cdot\mathbf{q}_h(t))_{\mathcal{T}_h} - \langle \widehat{p}_h(t), \tau_p(P_M p_h - \widehat{p}_h)\rangle_{\partial\mathcal{T}_h} = 0. \tag{5.3.24}$$

Now we test (5.3.14) with $s_h = p_h(t)$,

$$\begin{aligned}-\beta(\dot{\mathbf{u}}_h(t), \nabla p_h(t))_{\mathcal{T}_h} + \beta\langle \dot{\widehat{\mathbf{u}}}_h(t), P_M p_h(t)\mathbf{n}\rangle_{\partial\mathcal{T}_h} + (c\dot{p}_h(t), p_h(t))_{\mathcal{T}_h}& \\ -(\nabla\cdot\mathbf{q}_h(t), p_h(t))_{\mathcal{T}_h} + \langle \tau_p(P_M p_h(t) - \widehat{p}_h(t)), P_M p_h(t)\rangle_{\partial\mathcal{T}_h} &= 0.\end{aligned} \tag{5.3.25}$$

Summing (5.3.21), (5.3.22), (5.3.24), and (5.3.25), we get

$$\begin{aligned}\frac{1}{2}\frac{\mathrm{d}}{\mathrm{d}t}\|\boldsymbol{\sigma}_h(t)\|_{\mathcal{A}}^2 + \frac{1}{2}\frac{\mathrm{d}}{\mathrm{d}t}\|\dot{\mathbf{u}}_h(t)\|_\rho^2 + \|\mathbf{q}_h(t)\|_{\kappa^{-1}}^2 + \frac{1}{2}\frac{\mathrm{d}}{\mathrm{d}t}\|p_h(t)\|_c^2& \\ +\langle P_M p_h(t) - \widehat{p}_h(t), \tau_p(P_M p_h(t) - \widehat{p}_h(t))\rangle_{\partial\mathcal{T}_h}& \\ +\langle \boldsymbol{\tau}_{\mathbf{u}}(\mathbf{P}_M\mathbf{u}_h(t) - \widehat{\mathbf{u}}_h(t)), \mathbf{P}_M\dot{\mathbf{u}}_h(t) - \dot{\widehat{\mathbf{u}}}_h(t)\rangle_{\partial\mathcal{T}_h} &= 0.\end{aligned}$$

Combining terms, we get

$$\frac{1}{2}\frac{\mathrm{d}}{\mathrm{d}t}\|\boldsymbol{\sigma}_h(t)\|_{\mathcal{A}}^2 + \frac{1}{2}\frac{\mathrm{d}}{\mathrm{d}t}\|\dot{\mathbf{u}}_h(t)\|_{\rho}^2 + \|\mathbf{q}_h(t)\|_{\kappa^{-1}}^2 + \frac{1}{2}\frac{\mathrm{d}}{\mathrm{d}t}\|p_h(t)\|_c^2$$
$$+\|P_M p_h(t) - \widehat{p}_h(t)\|_{\tau_p}^2 + \frac{1}{2}\frac{\mathrm{d}}{\mathrm{d}t}\|(\mathbf{P}_M \mathbf{u}_h(t) - \widehat{\mathbf{u}}_h(t))\|_{\boldsymbol{\tau}_{\mathbf{u}}}^2 = 0,$$

or, better yet,

$$\frac{\mathrm{d}}{\mathrm{d}t}\left(\|\boldsymbol{\sigma}_h(t)\|_{\mathcal{A}}^2 + \|\dot{\mathbf{u}}_h(t)\|_{\rho}^2 + \|p_h(t)\|_c^2 + \|(\mathbf{P}_M \mathbf{u}_h(t) - \widehat{\mathbf{u}}_h(t))\|_{\boldsymbol{\tau}_{\mathbf{u}}}^2\right)$$
$$= -2\left(\|\mathbf{q}_h(t)\|_{\kappa^{-1}}^2 + \|P_M p_h(t) - \widehat{p}_h(t)\|_{\tau_p}^2\right) \leq 0.$$

□

5.4 Numerical Experiments in the Frequency Domain

We have prepared numerical experiments in the resolvent frequency domain to determine the viability of our method: these tests were done with a $\mathbb{V}_h, \mathbf{W}_h, \mathbf{Q}_h, P_h$ hybridizable discontinuous Galerkin scheme (see [30], [26])

First we perform frequency domain tests against the exact solution

$$\mathbf{u}_{\text{exact}} = \begin{pmatrix} \cos(\pi x)\sin(\pi y)\cos(\pi z) \\ 5\imath x^2 yz + 4xy^2 z + 3xyz^2 + 17 \\ \cos(2x)\cos(3y)\cos(z) \end{pmatrix} \qquad \text{and} \qquad p_{\text{exact}} = \sin(\pi x)\cos(\pi y)\sin(\pi z)$$

on $\Omega = [0,1]^3$ divided as in (4.2). These tests use variable Lamé parameters and mass densities

$$\mu = \frac{1}{2}(x^3 + y^2 + z^2) \qquad \text{and} \qquad \lambda = 1 + \frac{1}{2}(x^2 + y^2 + z^2),$$
$$\rho_b = x^2 + y^2 + z^2 + 1 \qquad \text{and} \qquad \rho_f = x^3 + y^4 + z^5 + 2$$

along with accompanying forcing functions

$$\mathbf{f}_{\mathbf{u}} = (-\text{div}\ \boldsymbol{\sigma}(\mathbf{u}_{\text{exact}}) + \rho_b s^2 \mathbf{u}_{\text{exact}} + \beta\nabla p_{\text{exact}})/\rho_b \text{ and}$$
$$f_p = (\beta\nabla\cdot(s\mathbf{u}_{\text{exact}}) + csp_{\text{exact}} - \nabla\cdot(\kappa\nabla p_{\text{exact}}))/(\kappa\rho_f)$$

for a wavenumber $s \in \mathbb{C}$, where $\kappa = 2$ is kept a scalar, the storativity $c = 2$ and Biot's constant $\beta = 0.75$. We use a complex wavenumber $s = .5 + .25\imath$, with a spatial discretization given by

$$(\mathcal{A}\boldsymbol{\sigma}_h, \boldsymbol{\xi}_h)_{\mathcal{T}_h} + (\mathbf{u}_h, \mathrm{div}\ \boldsymbol{\xi}_h)_{\mathcal{T}_h} - \langle \widehat{\mathbf{u}}_h, \boldsymbol{\xi}_h \mathbf{n}\rangle_{\partial\mathcal{T}_h} = 0, \tag{5.4.1}$$

$$\begin{aligned} -(\mathrm{div}\ \boldsymbol{\sigma}_h, \mathbf{v}_h)_{\mathcal{T}_h} + (\rho_b s^2 \mathbf{u}_h, \mathbf{v}_h)_{\mathcal{T}_h} + \beta(\nabla p_h, \mathbf{v}_h)_{\mathcal{T}_h} & \\ + \langle \tau_{\mathbf{u}}(\mathbf{P}_M \mathbf{u}_h - \widehat{\mathbf{u}}_h), \mathbf{P}_M \mathbf{v}_h\rangle_{\partial\mathcal{T}_h} &= (\mathbf{f}_{\mathbf{u}}, \mathbf{v}_h)_{\mathcal{T}_h}, \end{aligned} \tag{5.4.2}$$

$$(\kappa^{-1}\mathbf{q}_h, \mathbf{r}_h)_{\mathcal{T}_h} + (p_h, \nabla \cdot \mathbf{r}_h)_{\mathcal{T}_h} - \langle \widehat{p}_h, \mathbf{r}_h \cdot \mathbf{n}\rangle_{\partial\mathcal{T}_h} = 0, \tag{5.4.3}$$

$$\begin{aligned} -\beta(s\mathbf{u}_h, \nabla s_h)_{\mathcal{T}_h} + \beta\langle s\widehat{\mathbf{u}}_h, P_M s_h \mathbf{n}\rangle_{\partial\mathcal{T}_h} & \\ -(\nabla \cdot \mathbf{q}_h, s_h)_{\mathcal{T}_h} + (c\dot{p}_h, s_h)_{\mathcal{T}_h} & \\ + \langle \tau_p(P_M p_h - \widehat{p}_h), P_M s_h\rangle_{\partial\mathcal{T}_h} &= (f_p, s_h)_{\mathcal{T}_h}. \end{aligned} \tag{5.4.4}$$

$$\langle \widehat{\mathbf{u}}_h, \widehat{\mathbf{v}}_h\rangle_{\Gamma_D} = \langle \mathbf{g}_D, \widehat{\mathbf{v}}_h\rangle_{\Gamma_D}, \tag{5.4.5}$$

$$\langle \widehat{p}_h, \widehat{v}_h\rangle_{\tilde{\Gamma}_D} = \langle g_d, \widehat{v}_h\rangle_{\tilde{\Gamma}_D}, \tag{5.4.6}$$

$$\langle \boldsymbol{\sigma}_h \mathbf{n} - \tau_{\mathbf{u}}(\mathbf{P}_M \mathbf{u}_h - \widehat{\mathbf{u}}_h) - \beta P_M p_h \mathbf{n}, \widehat{\mathbf{v}}_h\rangle_{\partial\mathcal{T}_h \setminus \Gamma_D} = \langle \mathbf{g}_N, \widehat{\mathbf{v}}_h\rangle_{\Gamma_N}, \tag{5.4.7}$$

$$\langle \mathbf{q}_h \cdot \mathbf{n} - \tau_p(P_M p_h - \widehat{p}_h), \widehat{v}_h\rangle_{\partial\mathcal{T}_h \setminus \tilde{\Gamma}_D} = \langle g_n, \widehat{v}_h\rangle_{\tilde{\Gamma}_N}. \tag{5.4.8}$$

The first four pictures are results of experiments with Dirichlet conditions $\mathbf{g}_D = \mathbf{u}_{\text{exact}}$ and $g_D = p_{\text{exact}}$ for $k = 1, \ldots, 4$, and the second four use Neumann conditions, specifically $\mathbf{g}_N = \sigma(\mathbf{u}_{\text{exact}})\mathbf{n} - \beta p_{\text{exact}}\mathbf{n}$ and $g_n = \nabla p_{\text{exact}} \cdot \mathbf{n}$ for $k = 1, \ldots, 4$. The next four tests use mixed conditions, with only the sides of the cube parallel to the xz-plane subject to Neumann conditions and the rest of the faces subject to Dirichlet conditions for $k = 1, \ldots, 4$. The expected order of convergence is $\mathcal{O}(h^{k+2})$ for $\mathbf{u}_h$ and p_h and $\mathcal{O}(h^{k+1})$ for $\boldsymbol{\sigma}_h$ and $\mathbf{q}_h$.

The implementation is built from the work of Fu, Gatica, and Sayas, HDG Tools for MATLAB [18], for working with HDG in three dimensions. In the figures below, *we will again identify $h_j = 1/j$ with the maximum length of an edge of any tetrahedron of the j^{th} tetrahedrization, since they are asymptotically equivalent.*. To observe the orders of convergence for Dirichlet, Neumann, and mixed boundary conditions at polynomial degrees $k = 1, 2, 3$, and 4, respectively, we compare h_j for $j = 1, \ldots, N$ to the relative errors

$$e_{\mathbf{u}}^j = \frac{\|\mathbf{u} - \mathbf{u}_h^j\|_\Omega}{\|\mathbf{u}\|_\Omega}, \quad e_{\boldsymbol{\sigma}}^j = \frac{\|\boldsymbol{\sigma} - \boldsymbol{\sigma}_h^j\|_\Omega}{\|\boldsymbol{\sigma}\|_\Omega}, \quad e_{\mathbf{q}}^j = \frac{\|\mathbf{q} - \mathbf{q}_h^j\|_\Omega}{\|\mathbf{q}\|_\Omega}, \quad e_p^j = \frac{\|p - p_h^j\|_\Omega}{\|p\|_\Omega},$$

where N indicates the maximum number of refinements of that particular tetrahedrization. In the figures that follow, we observe $\log h_j$ compared to

$$\log e_{\mathbf{u}}^j, \qquad \log e_{\boldsymbol{\sigma}}^j, \qquad \log e_{\mathbf{q}}^j, \qquad \text{and } \log e_p^j.$$

In the tables that follow, we also observe

$$\begin{aligned} L_{\mathbf{u}}^j &= \frac{\log e_{\mathbf{u}}^j - \log e_{\mathbf{u}}^{j-1}}{\log h_j - \log h_{j-1}}, & L_{\boldsymbol{\sigma}}^j &= \frac{\log e_{\boldsymbol{\sigma}}^j - \log e_{\boldsymbol{\sigma}}^{j-1}}{\log h_j - \log h_{j-1}}, \\ L_p^j &= \frac{\log e_p^j - \log e_p^{j-1}}{\log h_j - \log h_{j-1}} \qquad \text{and} & L_{\mathbf{q}}^j &= \frac{\log e_{\mathbf{q}}^j - \log e_{\mathbf{q}}^{j-1}}{\log h_j - \log h_{j-1}} \end{aligned}$$

for $j = 2, \ldots, N$ to track the approximate orders of convergence.

We expect an order of $\mathcal{O}(h_j^{k+2})$ for $e_{\mathbf{u}}^j$ and e_p^j, and an order of $\mathcal{O}(h_j^{k+1})$ for $e_{\boldsymbol{\sigma}}^j$ and $e_{\mathbf{q}}^j$, and that is what we attain, besides for the fact that it appears that we may get $\mathcal{O}(h^{k+3})$ for $e_{\mathbf{u}}^j$.

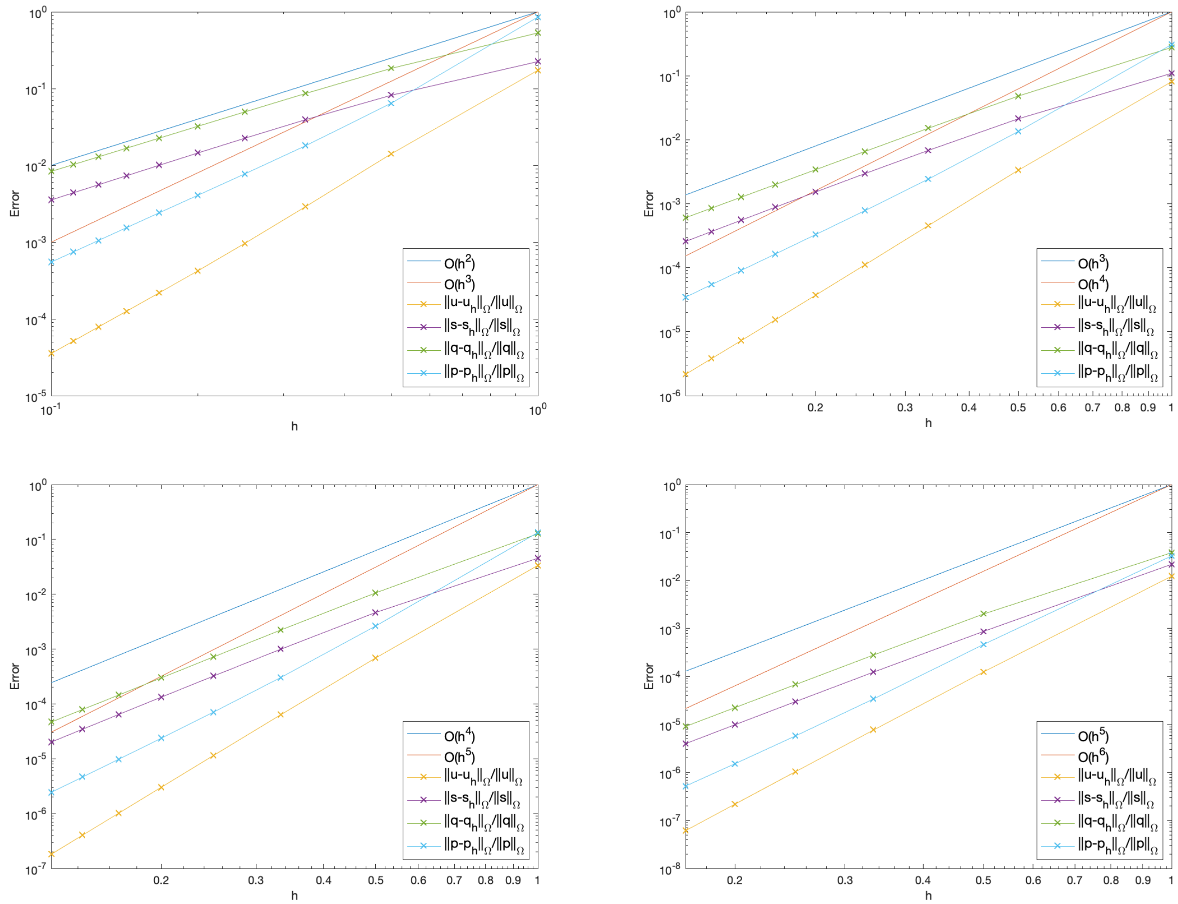

Figure 5.1: Dirichlet Conditions for the Poroelastic Problem, Frequency Domain: Expected order of convergence: $\mathcal{O}(h^{k+2})$ for $\mathbf{u}_h$ and p_h and $\mathcal{O}(h^{k+1})$ for $\boldsymbol{\sigma}_h$ and $\mathbf{q}_h$. $s = .5 + .25\imath, \beta = 0.75, c = 2, \kappa/\gamma = 2$ (top-left $k = 1$, top-right $k = 2$, mid-left $k = 3$, mid-right $k = 4$)

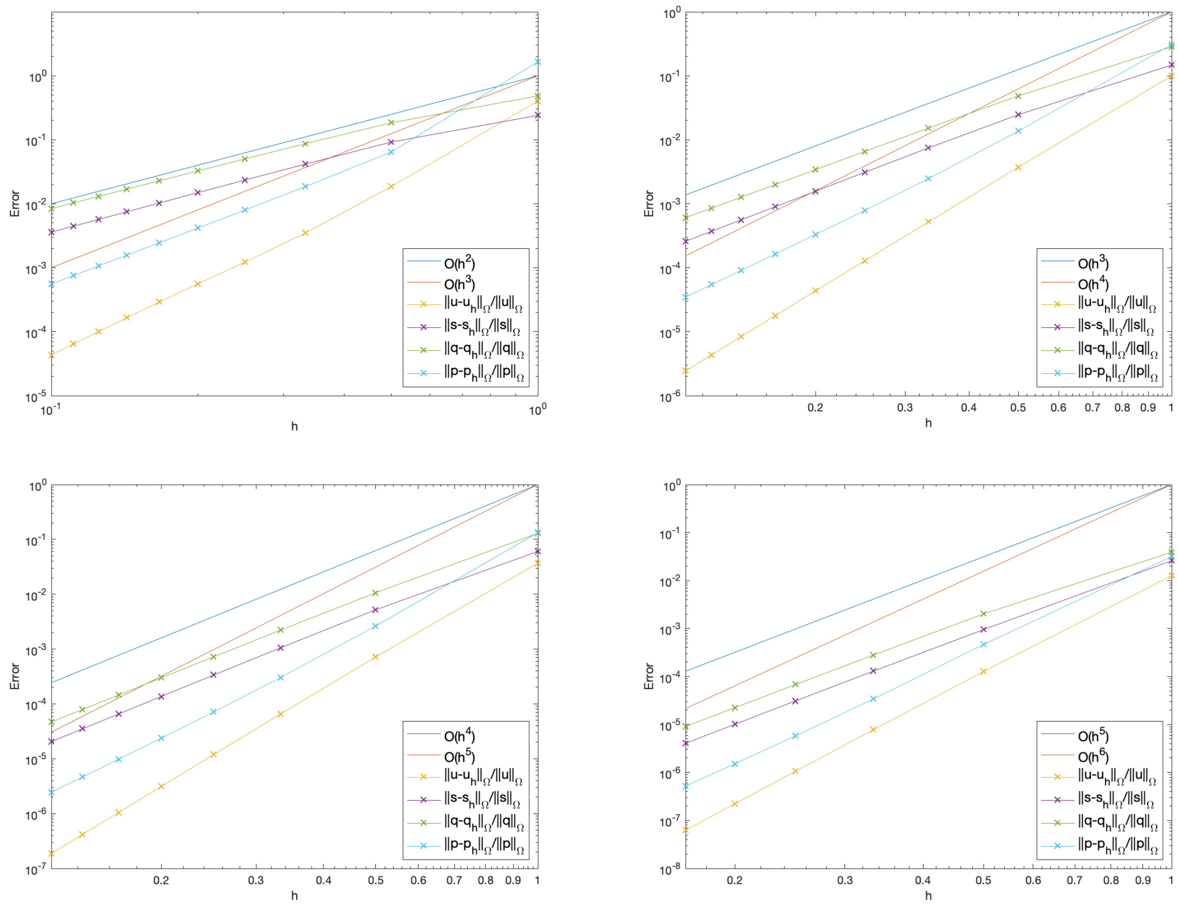

Figure 5.2: Neumann Conditions for the Poroelastic Problem, Frequency Domain: Expected order of convergence: $\mathcal{O}(h^{k+2})$ for $\mathbf{u}_h$ and p_h and $\mathcal{O}(h^{k+1})$ for $\boldsymbol{\sigma}_h$ and $\mathbf{q}_h$. $s = .5 + .25\imath, \beta = 0.75, c = 2, \kappa/\gamma = 2$ (top-left $k = 1$, top-right $k = 2$, bottom-left $k = 3$, bottom-right $k = 4$)

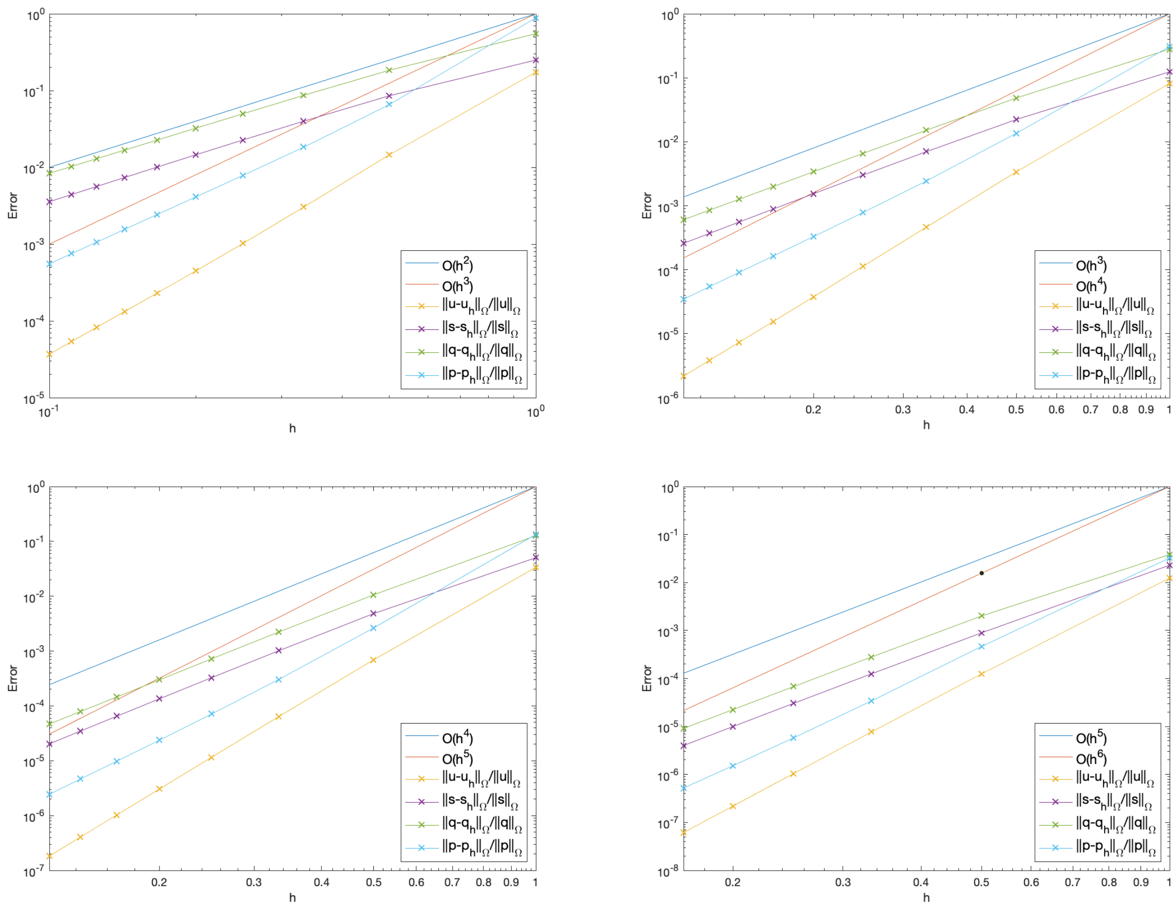

Figure 5.3: Mixed Conditions for the Poroelastic Problem, Frequency Domain: Expected order of convergence: $\mathcal{O}(h^{k+2})$ for $\mathbf{u}_h$ and p_h and $\mathcal{O}(h^{k+1})$ for $\boldsymbol{\sigma}_h$ and $\mathbf{q}_h$. $s = .5 + .25\imath, \beta = 0.75, c = 2, \kappa/\gamma = 2$ (top-left $k = 1$, top-right $k = 2$, bottom-left $k = 3$, bottom-right $k = 4$)

h_j	$e^j_{\mathbf{u}}$	$e^j_{\boldsymbol{\sigma}}$	e_p	$e^j_{\mathbf{q}}$	$L^j_{\mathbf{u}}$	$L^j_{\boldsymbol{\sigma}}$	L^j_p	$L^j_{\mathbf{q}}$
h_1	1.73e-01	2.24e-01	8.55e-01	5.30e-01				
h_2	1.42e-02	8.20e-02	6.46e-02	1.84e-01	3.61	1.45	3.73	1.53
h_3	2.90e-03	3.94e-02	1.80e-02	8.64e-02	3.91	1.81	3.15	1.86
h_4	9.66e-04	2.26e-02	7.76e-03	4.97e-02	3.83	1.93	2.93	1.92
h_5	4.22e-04	1.45e-02	4.08e-03	3.23e-02	3.71	1.99	2.88	1.94
h_6	2.19e-04	1.00e-02	2.41e-03	2.26e-02	3.61	2.02	2.88	1.95
h_7	1.26e-04	7.34e-03	1.55e-03	1.68e-02	3.56	2.03	2.88	1.95
h_8	7.86e-05	5.59e-03	1.05e-03	1.29e-02	3.55	2.04	2.89	1.95
h_9	5.17e-05	4.40e-03	7.47e-04	1.03e-02	3.56	2.04	2.9	1.95
h_{10}	3.55e-05	3.55e-03	5.50e-04	8.35e-03	3.57	2.04	2.9	1.95

Table 5.1: Frequency Domain for Poroelasticity: Dirichlet Conditions at $k = 1$

h_j	$e^j_{\mathbf{u}}$	$e^j_{\boldsymbol{\sigma}}$	e_p	$e^j_{\mathbf{q}}$	$L^j_{\mathbf{u}}$	$L^j_{\boldsymbol{\sigma}}$	L^j_p	$L^j_{\mathbf{q}}$
h_1	8.08e-02	1.09e-01	3.08e-01	2.78e-01				
h_2	3.34e-03	2.13e-02	1.35e-02	4.82e-02	4.6	2.36	4.52	2.53
h_3	4.58e-04	6.84e-03	2.44e-03	1.52e-02	4.9	2.8	4.22	2.85
h_4	1.11e-04	2.96e-03	7.79e-04	6.56e-03	4.93	2.91	3.96	2.92
h_5	3.71e-05	1.52e-03	3.29e-04	3.40e-03	4.9	2.97	3.87	2.94
h_6	1.53e-05	8.80e-04	1.63e-04	1.99e-03	4.87	3.01	3.83	2.94
h_7	7.24e-06	5.52e-04	9.07e-05	1.26e-03	4.85	3.03	3.83	2.94
h_8	3.80e-06	3.68e-04	5.44e-05	8.54e-04	4.83	3.04	3.83	2.94
h_9	2.15e-06	2.57e-04	3.46e-05	6.04e-04	4.82	3.04	3.83	2.93

Table 5.2: Frequency Domain for Poroelasticity: Dirichlet Conditions at $k = 2$

h_j	$e^j_{\mathbf{u}}$	$e^j_{\boldsymbol{\sigma}}$	e_p	$e^j_{\mathbf{q}}$	$L^j_{\mathbf{u}}$	$L^j_{\boldsymbol{\sigma}}$	L^j_p	$L^j_{\mathbf{q}}$
h_1	3.35e-02	4.54e-02	1.33e-01	1.27e-01				
h_2	6.89e-04	4.66e-03	2.63e-03	1.06e-02	5.6	3.28	5.66	3.58
h_3	6.36e-05	9.95e-04	3.03e-04	2.22e-03	5.88	3.81	5.33	3.85
h_4	1.15e-05	3.22e-04	7.09e-05	7.19e-04	5.95	3.92	5.06	3.92
h_5	3.02e-06	1.33e-04	2.37e-05	2.98e-04	5.97	3.97	4.91	3.95
h_6	1.02e-06	6.42e-05	9.78e-06	1.45e-04	5.98	4.0	4.85	3.95
h_7	4.04e-07	3.46e-05	4.65e-06	7.90e-05	5.98	4.01	4.83	3.94
h_8	1.82e-07	2.02e-05	2.44e-06	4.67e-05	5.97	4.02	4.81	3.94

Table 5.3: Frequency Domain for Poroelasticity: Dirichlet Conditions at $k = 3$

h_j	$e^j_{\mathbf{u}}$	$e^j_{\boldsymbol{\sigma}}$	e_p	$e^j_{\mathbf{q}}$	$L^j_{\mathbf{u}}$	$L^j_{\boldsymbol{\sigma}}$	L^j_p	$L^j_{\mathbf{q}}$
h_1	1.23e-02	2.18e-02	3.26e-02	3.81e-02				
h_2	1.25e-04	8.71e-04	4.66e-04	2.01e-03	6.63	4.64	6.13	4.25
h_3	7.67e-06	1.24e-04	3.41e-05	2.80e-04	6.87	4.82	6.45	4.86
h_4	1.04e-06	3.00e-05	5.78e-06	6.78e-05	6.95	4.92	6.17	4.93
h_5	2.19e-07	9.89e-06	1.52e-06	2.25e-05	6.98	4.97	5.98	4.96
h_6	6.10e-08	3.98e-06	5.20e-07	9.09e-06	7.01	5.0	5.89	4.96

Table 5.4: Frequency Domain for Poroelasticity: Dirichlet Conditions at $k = 4$

h_j	$e^j_{\mathbf{u}}$	$e^j_{\boldsymbol{\sigma}}$	e_p	$e^j_{\mathbf{q}}$	$L^j_{\mathbf{u}}$	$L^j_{\boldsymbol{\sigma}}$	L^j_p	$L^j_{\mathbf{q}}$
h_1	4.03e-01	2.41e-01	1.66e+00	4.85e-01				
h_2	1.86e-02	9.23e-02	6.45e-02	1.84e-01	4.44	1.38	4.68	1.39
h_3	3.52e-03	4.18e-02	1.86e-02	8.73e-02	4.11	1.95	3.06	1.84
h_4	1.22e-03	2.35e-02	7.97e-03	5.02e-02	3.68	2.01	2.95	1.92
h_5	5.60e-04	1.49e-02	4.17e-03	3.26e-02	3.49	2.03	2.91	1.94
h_6	2.91e-04	1.03e-02	2.46e-03	2.28e-02	3.59	2.05	2.9	1.95
h_7	1.65e-04	7.48e-03	1.57e-03	1.69e-02	3.68	2.05	2.9	1.95
h_8	1.00e-04	5.69e-03	1.06e-03	1.30e-02	3.73	2.05	2.91	1.96
h_9	6.45e-05	4.47e-03	7.56e-04	1.03e-02	3.76	2.05	2.91	1.96
h_{10}	4.33e-05	3.60e-03	5.56e-04	8.40e-03	3.78	2.05	2.92	1.96

Table 5.5: Frequency Domain for Poroelasticity: Neumann Conditions at $k = 1$

h_j	$e^j_{\mathbf{u}}$	$e^j_{\boldsymbol{\sigma}}$	e_p	$e^j_{\mathbf{q}}$	$L^j_{\mathbf{u}}$	$L^j_{\boldsymbol{\sigma}}$	L^j_p	$L^j_{\mathbf{q}}$
h_1	9.99e-02	1.47e-01	3.07e-01	2.84e-01				
h_2	3.73e-03	2.46e-02	1.36e-02	4.85e-02	4.74	2.58	4.49	2.55
h_3	5.21e-04	7.45e-03	2.46e-03	1.52e-02	4.85	2.95	4.22	2.85
h_4	1.29e-04	3.11e-03	7.86e-04	6.58e-03	4.85	3.04	3.97	2.92
h_5	4.35e-05	1.57e-03	3.31e-04	3.41e-03	4.87	3.06	3.88	2.94
h_6	1.78e-05	8.97e-04	1.64e-04	1.99e-03	4.89	3.07	3.84	2.95
h_7	8.36e-06	5.59e-04	9.09e-05	1.27e-03	4.91	3.06	3.84	2.94
h_8	4.34e-06	3.72e-04	5.44e-05	8.55e-04	4.91	3.06	3.83	2.94
h_9	2.44e-06	2.59e-04	3.47e-05	6.05e-04	4.91	3.06	3.84	2.94

Table 5.6: Frequency Domain for Poroelasticity: Neumann Conditions at $k = 2$

h_j	$e^j_{\mathbf{u}}$	$e^j_{\boldsymbol{\sigma}}$	e_p	$e^j_{\mathbf{q}}$	$L^j_{\mathbf{u}}$	$L^j_{\boldsymbol{\sigma}}$	L^j_p	$L^j_{\mathbf{q}}$
h_1	3.68e-02	6.04e-02	1.32e-01	1.29e-01				
h_2	7.18e-04	5.20e-03	2.63e-03	1.06e-02	5.68	3.54	5.65	3.6
h_3	6.59e-05	1.06e-03	3.04e-04	2.23e-03	5.89	3.93	5.32	3.85
h_4	1.19e-05	3.36e-04	7.11e-05	7.20e-04	5.96	4.0	5.05	3.93
h_5	3.13e-06	1.37e-04	2.37e-05	2.99e-04	5.98	4.02	4.92	3.95
h_6	1.05e-06	6.55e-05	9.80e-06	1.45e-04	5.99	4.03	4.85	3.95
h_7	4.17e-07	3.52e-05	4.66e-06	7.92e-05	5.99	4.04	4.83	3.94
h_8	1.88e-07	2.05e-05	2.45e-06	4.68e-05	5.97	4.05	4.82	3.94

Table 5.7: Frequency Domain for Poroelasticity: Neumann Conditions at $k = 3$

h_j	$e^j_{\mathbf{u}}$	$e^j_{\boldsymbol{\sigma}}$	e_p	$e^j_{\mathbf{q}}$	$L^j_{\mathbf{u}}$	$L^j_{\boldsymbol{\sigma}}$	L^j_p	$L^j_{\mathbf{q}}$
h_1	1.26e-02	2.59e-02	3.16e-02	3.90e-02				
h_2	1.27e-04	9.48e-04	4.65e-04	2.01e-03	6.63	4.77	6.09	4.28
h_3	7.82e-06	1.30e-04	3.41e-05	2.81e-04	6.88	4.9	6.44	4.86
h_4	1.06e-06	3.10e-05	5.79e-06	6.79e-05	6.95	4.98	6.17	4.93
h_5	2.23e-07	1.01e-05	1.52e-06	2.25e-05	6.98	5.01	5.98	4.96
h_6	6.20e-08	4.05e-06	5.20e-07	9.09e-06	7.02	5.03	5.89	4.96

Table 5.8: Frequency Domain for Poroelasticity: Neumann Conditions at $k = 4$

h_j	$e^j_{\mathbf{u}}$	$e^j_{\boldsymbol{\sigma}}$	e_p	$e^j_{\mathbf{q}}$	$L^j_{\mathbf{u}}$	$L^j_{\boldsymbol{\sigma}}$	L^j_p	$L^j_{\mathbf{q}}$
h_1	1.74e-01	2.50e-01	8.89e-01	5.51e-01				
h_2	1.46e-02	8.57e-02	6.58e-02	1.84e-01	3.58	1.54	3.76	1.58
h_3	3.04e-03	4.00e-02	1.83e-02	8.67e-02	3.87	1.88	3.15	1.86
h_4	1.02e-03	2.27e-02	7.85e-03	4.99e-02	3.79	1.96	2.94	1.92
h_5	4.47e-04	1.46e-02	4.12e-03	3.24e-02	3.69	1.99	2.89	1.94
h_6	2.31e-04	1.01e-02	2.43e-03	2.27e-02	3.62	2.01	2.89	1.95
h_7	1.33e-04	7.39e-03	1.56e-03	1.68e-02	3.59	2.03	2.89	1.95
h_8	8.22e-05	5.63e-03	1.06e-03	1.29e-02	3.59	2.03	2.9	1.95
h_9	5.38e-05	4.43e-03	7.52e-04	1.03e-02	3.59	2.04	2.9	1.95
h_{10}	3.68e-05	3.57e-03	5.53e-04	8.37e-03	3.6	2.04	2.91	1.96

Table 5.9: Frequency Domain for Poroelasticity: Mixed Conditions at $k = 1$

h_j	$e^j_{\mathbf{u}}$	$e^j_{\boldsymbol{\sigma}}$	e_p	$e^j_{\mathbf{q}}$	$L^j_{\mathbf{u}}$	$L^j_{\boldsymbol{\sigma}}$	L^j_p	$L^j_{\mathbf{q}}$
h_1	8.18e-02	1.24e-01	3.08e-01	2.80e-01				
h_2	3.39e-03	2.23e-02	1.35e-02	4.83e-02	4.59	2.48	4.51	2.54
h_3	4.64e-04	7.01e-03	2.45e-03	1.52e-02	4.9	2.85	4.22	2.85
h_4	1.13e-04	3.01e-03	7.82e-04	6.56e-03	4.93	2.94	3.97	2.92
h_5	3.77e-05	1.54e-03	3.30e-04	3.40e-03	4.9	2.99	3.87	2.94
h_6	1.55e-05	8.88e-04	1.64e-04	1.99e-03	4.88	3.02	3.84	2.94
h_7	7.33e-06	5.56e-04	9.07e-05	1.26e-03	4.86	3.04	3.83	2.94
h_8	3.84e-06	3.70e-04	5.44e-05	8.54e-04	4.84	3.05	3.83	2.94
h_9	2.17e-06	2.58e-04	3.46e-05	6.04e-04	4.83	3.05	3.83	2.93

Table 5.10: Frequency Domain for Poroelasticity: Mixed Conditions at $k = 2$

h_j	$e^j_{\mathbf{u}}$	$e^j_{\boldsymbol{\sigma}}$	e_p	$e^j_{\mathbf{q}}$	$L^j_{\mathbf{u}}$	$L^j_{\boldsymbol{\sigma}}$	L^j_p	$L^j_{\mathbf{q}}$
h_1	3.37e-02	5.04e-02	1.34e-01	1.27e-01				
h_2	6.94e-04	4.82e-03	2.64e-03	1.06e-02	5.6	3.39	5.66	3.58
h_3	6.40e-05	1.02e-03	3.04e-04	2.23e-03	5.88	3.84	5.33	3.85
h_4	1.15e-05	3.27e-04	7.10e-05	7.20e-04	5.95	3.94	5.06	3.93
h_5	3.04e-06	1.34e-04	2.37e-05	2.98e-04	5.98	3.98	4.91	3.95
h_6	1.02e-06	6.47e-05	9.79e-06	1.45e-04	5.98	4.01	4.85	3.95
h_7	4.07e-07	3.48e-05	4.65e-06	7.91e-05	5.98	4.02	4.83	3.94
h_8	1.83e-07	2.03e-05	2.44e-06	4.67e-05	5.99	4.03	4.82	3.94

Table 5.11: Frequency Domain for Poroelasticity: Mixed Conditions at $k = 3$

h_j	$e^j_{\mathbf{u}}$	$e^j_{\boldsymbol{\sigma}}$	e_p	$e^j_{\mathbf{q}}$	$L^j_{\mathbf{u}}$	$L^j_{\boldsymbol{\sigma}}$	L^j_p	$L^j_{\mathbf{q}}$
h_1	1.24e-02	2.30e-02	3.25e-02	3.84e-02				
h_2	1.25e-04	8.94e-04	4.66e-04	2.01e-03	6.63	4.68	6.13	4.25
h_3	7.70e-06	1.25e-04	3.41e-05	2.81e-04	6.87	4.84	6.45	4.86
h_4	1.04e-06	3.03e-05	5.78e-06	6.79e-05	6.95	4.94	6.17	4.93
h_5	2.20e-07	9.97e-06	1.52e-06	2.25e-05	6.97	4.98	5.98	4.96
h_6	6.10e-08	4.00e-06	5.20e-07	9.09e-06	7.04	5.01	5.89	4.96

Table 5.12: Frequency Domain for Poroelasticity: Mixed Conditions at $k = 4$

5.5 Numerical Experiments in the Time Domain

Next we perform time domain tests on $\Omega \times [0,5]$, where $\Omega = [0,1]^3$. We use the same variable parameters and mass densities as in the previous section, and test against the exact solution

$$\mathbf{u}_{\text{exact}}(t) = \sin^4(t) \begin{pmatrix} \cos(\pi x)\sin(\pi y)\cos(\pi z) \\ 5\imath x^2yz + 4xy^2z + 3xyz^2 + 17 \\ \cos(2x)\cos(3y)\cos(z) \end{pmatrix}$$

and

$$p_{\text{exact}}(t) = \sin^4(t)\sin(\pi x)\cos(\pi y)\sin(\pi z)$$

using a convolution quadrature ([34]) based on the trapezoid rule. This requires sampling the forcing and boundary data at times $t_0, \ldots, t_N$ and assembling a data matrix $G = [\mathbf{g}_n]_{n=0}^N$ given by:

$$\begin{bmatrix} \mathbf{f}_h^x(t_0), \ldots, \mathbf{f}_h^x(t_N) \\ \mathbf{f}_h^y(t_0), \ldots, \mathbf{f}_h^y(t_N) \\ \mathbf{f}_h^z(t_0), \ldots, \mathbf{f}_h^z(t_N) \\ \mathbf{f}_h^p(t_0), \ldots, \mathbf{f}_h^p(t_N) \\ \mathbf{u}_{h,D}^x(t_0), \ldots, \mathbf{u}_{h,D}^x(t_N) \\ \mathbf{u}_{h,D}^y(t_0), \ldots, \mathbf{u}_{h,D}^y(t_N) \\ \mathbf{u}_{h,D}^z(t_0), \ldots, \mathbf{u}_{h,D}^z(t_N) \\ \widetilde{\boldsymbol{\sigma}}_{h,N}^{xx}(t_0), \ldots, \widetilde{\boldsymbol{\sigma}}_{h,N}^{xx}(t_N) \\ \widetilde{\boldsymbol{\sigma}}_{h,N}^{yy}(t_0), \ldots, \widetilde{\boldsymbol{\sigma}}_{h,N}^{yy}(t_N) \\ \widetilde{\boldsymbol{\sigma}}_{h,N}^{zz}(t_0), \ldots, \widetilde{\boldsymbol{\sigma}}_{h,N}^{zz}(t_N) \\ \widetilde{\boldsymbol{\sigma}}_{h,N}^{xy}(t_0), \ldots, \widetilde{\boldsymbol{\sigma}}_{h,N}^{xy}(t_N) \\ \widetilde{\boldsymbol{\sigma}}_{h,N}^{xz}(t_0), \ldots, \widetilde{\boldsymbol{\sigma}}_{h,N}^{xz}(t_N) \\ \widetilde{\boldsymbol{\sigma}}_{h,N}^{yz}(t_0), \ldots, \widetilde{\boldsymbol{\sigma}}_{h,N}^{yz}(t_N) \\ \mathbf{p}_{h,D}(t_0), \ldots, \mathbf{p}_{h,D}(t_N) \\ \mathbf{q}_{h,N}^x(t_0), \ldots, \mathbf{q}_{h,N}^x(t_N) \\ \mathbf{q}_{h,N}^y(t_0), \ldots, \mathbf{q}_{h,N}^y(t_N) \\ \mathbf{q}_{h,N}^z(t_0), \ldots, \mathbf{q}_{h,N}^z(t_N) \end{bmatrix}$$

to feed into our CQ algorithm.

Here it should be noted that $\widetilde{\boldsymbol{\sigma}}^{*\circ}_{h,N}(t)$ above is the actual (Biot) stress felt on the Neumann faces $\widetilde{\boldsymbol{\sigma}}^{*\circ}_{h,N}(t) = \boldsymbol{\sigma}^{*\circ}_{h,N}(t) - \beta p_{h,N}(t)\delta_{*\circ}$ and:

- $\mathbf{f}^{*}_{h}(t_j)$ and $\mathbf{f}^{p}_{h}(t_j)$ are vertical length $\binom{k+3+1}{3}\times$#elements vectors of coefficients of the forcing terms $\mathbf{f}^{*}(t_j)$ and $f_p(t_j)$ projected onto our polynomial space $\mathcal{P}_{k+1}(\mathcal{T}_h)$
- $\mathbf{u}^{*}_{h,D}(t_j)$ and $p_{h,D}(t_j)$ are a vertical length $\binom{k+2}{2}\times$#Dirichlet faces vectors of the coefficients of the Dirichlet conditions projected onto $M^{\mathrm{dir}}_{h} := \prod_{F\in\Gamma_D}\mathcal{P}_k(F)$ and
- $\widetilde{\boldsymbol{\sigma}}^{*\circ}_{h,N}(t_j)$ and $\mathbf{q}^{*}_{h,N}(t_j)$ are vertical length $\binom{k+2}{2}\times$#Neumann faces vectors of the coefficients of the Neumann conditions projected onto $M^{\mathrm{neu}}_{h} := \prod_{F\in\Gamma_N}\mathcal{P}_k(F)$,

respectively, one timestep at a time, where $*$ and $\circ$ range over $\{x, y, z\}$. This uses a black box method designed in MATLAB by Hassell and Sayas [25].

The time tested is the interval $[0, T]$ (here $T = 5$) divided into timesteps

$$\delta_t = \left\lceil \frac{T}{c_t} h^{\frac{k+2}{2}} \right\rceil$$

as in (4.2).

We will also use the physical parameters, storativity c, ratio of hydraulic conductivity to unit weight of fluid $\frac{\kappa}{\gamma}$, and Biot's parameter β at

$$c = 2 \qquad \frac{\kappa}{\gamma} = 2 \qquad \beta = 0.75.$$

The spatial discretization is thus

$$
\begin{aligned}
(\mathcal{A}\boldsymbol{\sigma}_h(t), \boldsymbol{\xi}_h)_{\mathcal{T}_h} + (\mathbf{u}_h(t), \mathrm{div}\ \boldsymbol{\xi}_h)_{\mathcal{T}_h} - \langle \widehat{\mathbf{u}}_h(t)), \boldsymbol{\xi}_h \mathbf{n}\rangle_{\partial\mathcal{T}_h} &= 0,\\
-(\mathrm{div}\ \boldsymbol{\sigma}_h(t), \mathbf{v}_h)_{\mathcal{T}_h} + (\rho\ddot{\mathbf{u}}_h(t), \mathbf{v}_h)_{\mathcal{T}_h} + \beta(\nabla p_h(t), \mathbf{v}_h)_{\mathcal{T}_h} &\\
+\langle \tau_{\mathbf{u}}(\mathbf{P}_M\mathbf{u}_h(t) - \widehat{\mathbf{u}}_h(t)), \mathbf{P}_M\mathbf{v}_h\rangle_{\partial\mathcal{T}_h} &= (\rho\mathbf{f}_{\mathbf{u}}(t), \mathbf{v}_h)_{\mathcal{T}_h},\\
(\kappa^{-1}\mathbf{q}_h(t), \mathbf{r}_h)_{\mathcal{T}_h} + (p_h(t), \nabla\cdot\mathbf{r}_h)_{\mathcal{T}_h} - \langle \widehat{p}_h(t), \mathbf{r}_h\cdot\mathbf{n}\rangle_{\partial\mathcal{T}_h} &= 0,\\
-\beta(\dot{\mathbf{u}}_h(t), \nabla s_h)_{\mathcal{T}_h} + \beta\langle \dot{\widehat{\mathbf{u}}}_h(t), P_M s_h\mathbf{n}\rangle_{\partial\mathcal{T}_h} &\\
-\left(\nabla\cdot\frac{\kappa}{\gamma}\mathbf{q}_h(t), s_h\right)_{\mathcal{T}_h} + (c\dot{p}_h(t), s_h)_{\mathcal{T}_h} &\\
+\langle \tau_p(P_M p_h(t) - \widehat{p}_h(t)), P_M s_h\rangle_{\partial\mathcal{T}_h} &= \left(\frac{\kappa}{\gamma}\rho_f f_p(t), s_h\right)_{\mathcal{T}_h}.\\
\langle \widehat{\mathbf{u}}_h(t), \widehat{\mathbf{v}}_h\rangle_{\Gamma_D} &= \langle \mathbf{g}_D(t), \widehat{\mathbf{v}}_h\rangle_{\Gamma_D},\\
\langle \widehat{p}_h(t), \widehat{v}_h\rangle_{\tilde{\Gamma}_D} &= \langle g_d(t), \widehat{v}_h\rangle_{\tilde{\Gamma}_D},\\
\langle \boldsymbol{\sigma}_h(t)\mathbf{n} - \tau_{\mathbf{u}}(\mathbf{P}_M\mathbf{u}_h(t) - \widehat{\mathbf{u}}_h(t)) - \beta P_M p_h(t)\mathbf{n}, \widehat{\mathbf{v}}_h\rangle_{\partial\mathcal{T}_h\setminus\Gamma_D} &= \langle \mathbf{g}_N(t), \widehat{\mathbf{v}}_h\rangle_{\Gamma_N},\\
\langle \mathbf{q}_h(t)\cdot\mathbf{n} - \tau_p(P_M p_h(t) - \widehat{p}_h(t)), \widehat{v}_h\rangle_{\partial\mathcal{T}_h\setminus\tilde{\Gamma}_D} &= \langle g_n(t), \widehat{v}_h\rangle_{\tilde{\Gamma}_N},\\
\mathbf{u}_h(0) = 0,\ \dot{\mathbf{u}}_h(0) = 0,\ p_h(0) &= 0.
\end{aligned}
$$

The implementation is built from the work of Fu, Gatica, and Sayas, HDG Tools for MATLAB [18], for working with HDG in three dimensions, and from the work of Hassell and Sayas [25] on convolution quadrature in MATLAB.

In the tables that follow, we compare $h_j = 1/j$ for $j = 1, \ldots, N_{\max}$ (with $N_{\max}$ the maximum number of refinements for that particular experiment) to the relative errors

$$
\begin{aligned}
e^j_{\mathbf{u}} &= \frac{\|\mathbf{u}(T) - \mathbf{u}^j_h(T)\|_\Omega}{\|\mathbf{u}(T)\|_\Omega}, & & & e^j_{\boldsymbol{\sigma}} &= \frac{\|\boldsymbol{\sigma}(T) - \boldsymbol{\sigma}^j_h(T)\|_\Omega}{\|\boldsymbol{\sigma}(T)\|_\Omega},\\
e^j_{\mathbf{q}} &= \frac{\|\mathbf{q}(T) - \mathbf{q}^j_h(T)\|_\Omega}{\|\mathbf{q}(T)\|_\Omega}, & & \text{and} & e^j_p &= \frac{\|p(T) - p^j_h(T)\|_\Omega}{\|p(T)\|_\Omega},
\end{aligned}
$$

where T is the final time $T = 5$

In the figures below, we will again identify $h_j = 1/j$ with the maximum length of an edge of a tetrahedrization $\mathcal{T}_h^j$ as they are asymptotically equivalent. We compare $\log h_j$ to

$$\log e_{\mathbf{u}}^j, \log e_{\boldsymbol{\sigma}}^j, \log e_{\mathbf{q}}^j, \text{ and} \log e_p^j$$

in order to observe the orders of convergence for Dirichlet, Neumann, and mixed boundary conditions at polynomial degrees $k = 1, 2, 3$, and 4, respectively.

We also observe, for $j \geq 2$,

$$L_{\mathbf{u}}^j = \frac{\log e_{\mathbf{u}}^j - \log e_{\mathbf{u}}^{j-1}}{\log h_j - \log h_{j-1}}, \qquad L_{\boldsymbol{\sigma}}^j = \frac{\log e_{\boldsymbol{\sigma}}^j - \log e_{\boldsymbol{\sigma}}^{j-1}}{\log h_j - \log h_{j-1}},$$
$$L_p^j = \frac{\log e_p^j - \log e_p^{j-1}}{\log h_j - \log h_{j-1}}, \qquad \text{and} \qquad L_{\mathbf{q}}^j = \frac{\log e_{\mathbf{q}}^j - \log e_{\mathbf{q}}^{j-1}}{\log h_j - \log h_{j-1}},$$

in order to track the approximate orders of convergence.

We expect $\mathcal{O}(h_j^{k+2})$ convergence for $e_{\mathbf{u}}^j$ and e_p^j, and expect $\mathcal{O}(h_j^{k+1})$ convergence for $e_{\boldsymbol{\sigma}}^j$ and $e_{\mathbf{q}}^j$, and attain precisely these results.

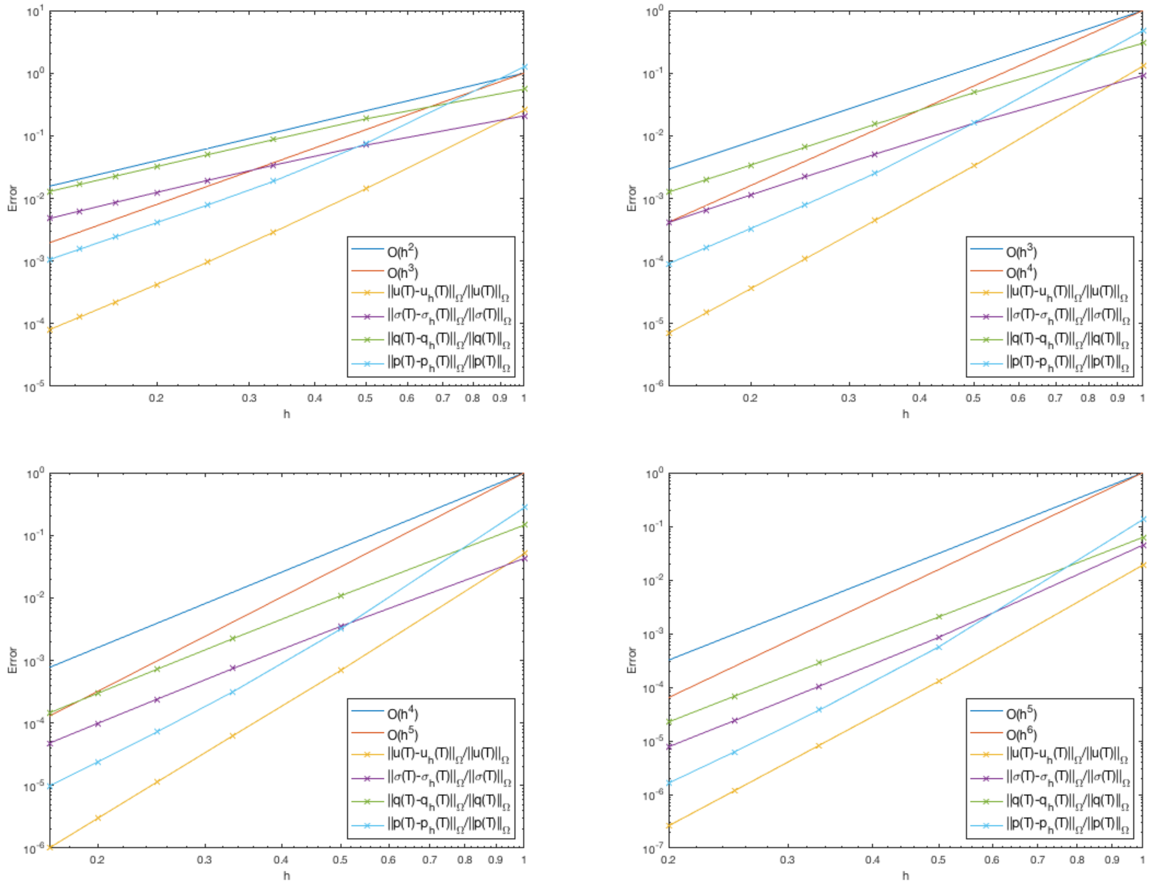

Figure 5.4: Dirichlet conditions for the Poroelastic Problem, Time-Dependent Case: Expected order of convergence: $\mathcal{O}(h^{k+2})$ for $\mathbf{u}_h$ and p_h and $\mathcal{O}(h^{k+1})$ for $\boldsymbol{\sigma}_h$ and $\mathbf{q}_h$. $\beta = 0.75, c = 2, \kappa/\gamma = 2$ (top-left $k = 1$, top-right $k = 2$, bottom-left $k = 3$, bottom-right $k = 4$)

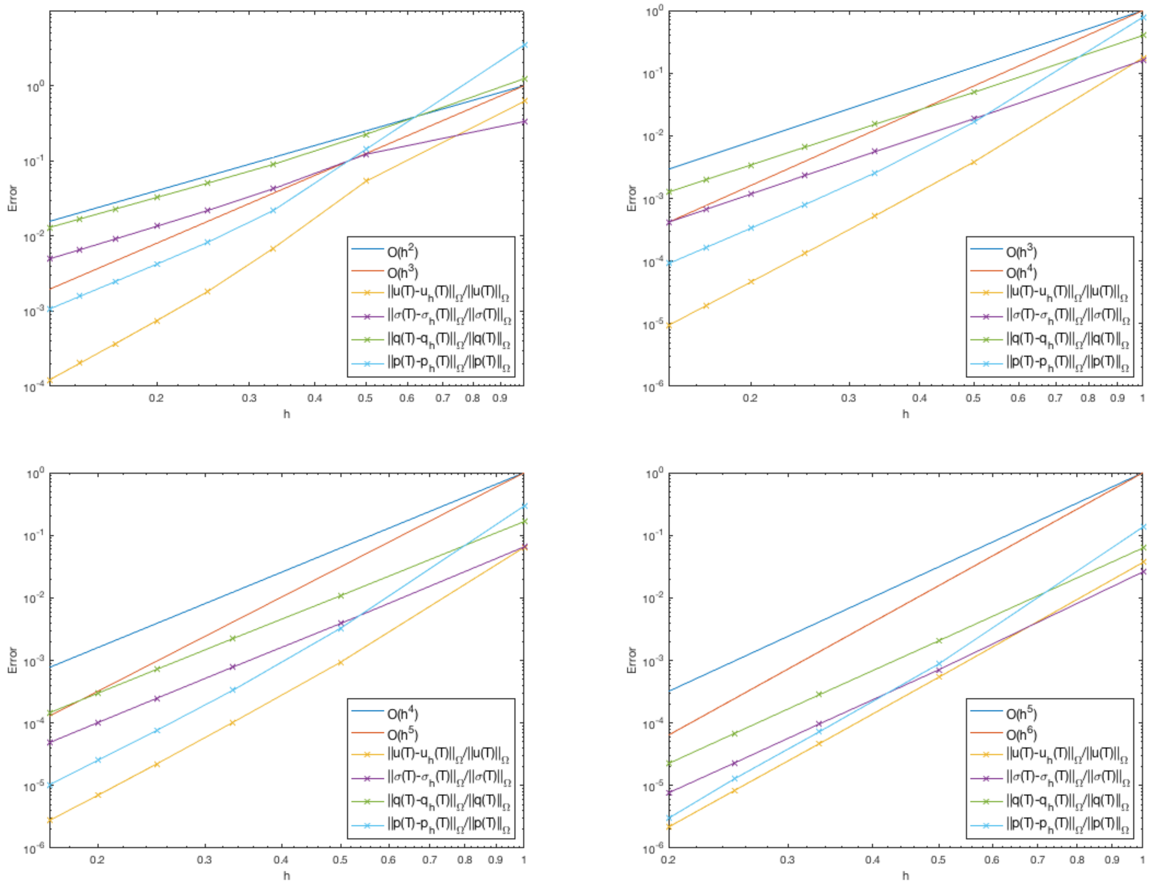

Figure 5.5: Neumann conditions for the Poroelastic Problem, Time-Dependent Case: Expected order of convergence: $\mathcal{O}(h^{k+2})$ for $\mathbf{u}_h$ and p_h and $\mathcal{O}(h^{k+1})$ for $\boldsymbol{\sigma}_h$ and $\mathbf{q}_h$. $\beta = 0.75, c = 2, \kappa/\gamma = 2$, (top-left $k = 1$, top-right $k = 2$, bottom-left $k = 3$,bottom-right $k = 4$)

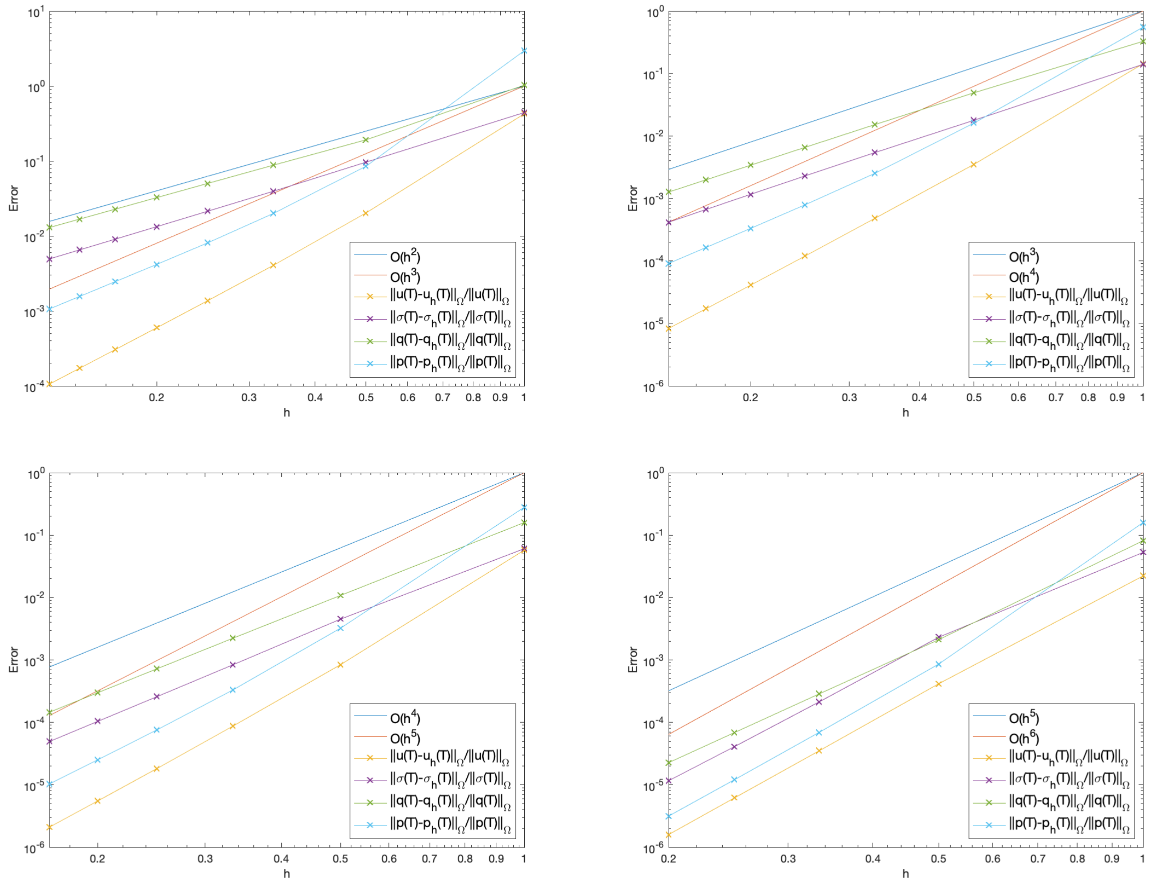

Figure 5.6: Mixed conditions for the Poroelastic Problem, Time-Dependent Case: Expected order of convergence: $\mathcal{O}(h^{k+2})$ for $\mathbf{u}_h$ and p_h and $\mathcal{O}(h^{k+1})$ for $\boldsymbol{\sigma}_h$ and $\mathbf{q}_h$. $\beta = 0.75, c = 2, \kappa/\gamma = 2$, (top-left $k = 1$, top-right $k = 2$, bottom-left $k = 3$, bottom-right $k = 4$))

h_j	$e^j_{\mathbf{u}}$	$e^j_{\boldsymbol{\sigma}}$	e^j_p	$e^j_{\mathbf{q}}$	$L^j_{\mathbf{u}}$	$L^j_{\boldsymbol{\sigma}}$	L^j_p	$L^j_{\mathbf{q}}$
h_1	2.56e-01	2.08e-01	1.26e+00	5.54e-01				
h_2	1.43e-02	7.07e-02	7.55e-02	1.86e-01	4.17	1.56	4.06	1.57
h_3	2.88e-03	3.38e-02	1.87e-02	8.66e-02	3.94	1.82	3.44	1.89
h_4	9.62e-04	1.94e-02	7.84e-03	4.97e-02	3.81	1.93	3.02	1.93
h_5	4.23e-04	1.24e-02	4.09e-03	3.22e-02	3.68	1.99	2.91	1.94
h_6	2.20e-04	8.61e-03	2.42e-03	2.26e-02	3.58	2.02	2.89	1.95
h_7	1.28e-04	6.29e-03	1.55e-03	1.67e-02	3.53	2.04	2.89	1.95
h_8	8.02e-05	4.78e-03	1.05e-03	1.29e-02	3.5	2.05	2.89	1.95

Table 5.13: Time-Dependent Poroelasticity: Dirichlet Conditions at $k = 1$

h_j	$e^j_{\mathbf{u}}$	$e^j_{\boldsymbol{\sigma}}$	e^j_p	$e^j_{\mathbf{q}}$	$L^j_{\mathbf{u}}$	$L^j_{\boldsymbol{\sigma}}$	L^j_p	$L^j_{\mathbf{q}}$
h_1	1.30e-01	9.13e-02	4.77e-01	3.00e-01				
h_2	3.31e-03	1.58e-02	1.60e-02	4.88e-02	5.29	2.53	4.9	2.62
h_3	4.46e-04	5.09e-03	2.52e-03	1.52e-02	4.94	2.8	4.56	2.88
h_4	1.08e-04	2.20e-03	7.85e-04	6.55e-03	4.94	2.91	4.05	2.93
h_5	3.61e-05	1.13e-03	3.30e-04	3.40e-03	4.9	2.97	3.89	2.94
h_6	1.49e-05	6.55e-04	1.64e-04	1.99e-03	4.87	3.01	3.84	2.95
h_7	7.05e-06	4.10e-04	9.07e-05	1.26e-03	4.84	3.03	3.83	2.94

Table 5.14: Time-Dependent Poroelasticity: Dirichlet Conditions at $k = 2$

h_j	$e_{\mathbf{u}}^j$	$e_{\boldsymbol{\sigma}}^j$	e_p^j	$e_{\mathbf{q}}^j$	$L_{\mathbf{u}}^j$	$L_{\boldsymbol{\sigma}}^j$	L_p^j	$L_{\mathbf{q}}^j$
h_1	5.08e-02	4.26e-02	2.76e-01	1.45e-01				
h_2	6.89e-04	3.50e-03	3.15e-03	1.07e-02	6.2	3.61	6.45	3.76
h_3	6.28e-05	7.42e-04	3.16e-04	2.23e-03	5.91	3.82	5.67	3.88
h_4	1.13e-05	2.39e-04	7.18e-05	7.19e-04	5.95	3.93	5.15	3.93
h_5	3.00e-06	9.85e-05	2.38e-05	2.98e-04	5.96	3.98	4.94	3.95
h_6	1.01e-06	4.75e-05	9.81e-06	1.45e-04	5.97	4.0	4.86	3.95

Table 5.15: Time-Dependent Poroelasticity: Dirichlet Conditions at $k = 3$

h_j	$e_{\mathbf{u}}^j$	$e_{\boldsymbol{\sigma}}^j$	e_p^j	$e_{\mathbf{q}}^j$	$L_{\mathbf{u}}^j$	$L_{\boldsymbol{\sigma}}^j$	L_p^j	$L_{\mathbf{q}}^j$
h_1	1.91e-02	4.47e-02	1.34e-01	6.24e-02				
h_2	1.29e-04	8.49e-04	5.64e-04	2.04e-03	7.21	5.72	7.9	4.94
h_3	8.25e-06	1.04e-04	3.73e-05	2.82e-04	6.78	5.17	6.7	4.88
h_4	1.17e-06	2.38e-05	6.22e-06	6.80e-05	6.78	5.13	6.23	4.94
h_5	2.60e-07	7.75e-06	1.63e-06	2.25e-05	6.75	5.03	6.0	4.96

Table 5.16: Time-Dependent Poroelasticity: Dirichlet Conditions at $k = 4$

h_j	$e^j_{\mathbf{u}}$	$e^j_{\boldsymbol{\sigma}}$	e^j_p	$e^j_{\mathbf{q}}$	$L^j_{\mathbf{u}}$	$L^j_{\boldsymbol{\sigma}}$	L^j_p	$L^j_{\mathbf{q}}$
h_1	6.18e-01	3.33e-01	3.49e+00	1.24e+00				
h_2	5.34e-02	1.22e-01	1.42e-01	2.25e-01	3.53	1.45	4.62	2.46
h_3	6.86e-03	4.24e-02	2.18e-02	8.97e-02	5.06	2.61	4.62	2.27
h_4	1.82e-03	2.18e-02	8.24e-03	5.04e-02	4.61	2.31	3.38	2.0
h_5	7.48e-04	1.35e-02	4.22e-03	3.25e-02	3.99	2.17	3.0	1.96
h_6	3.67e-04	9.10e-03	2.47e-03	2.28e-02	3.9	2.14	2.94	1.96
h_7	2.03e-04	6.56e-03	1.57e-03	1.68e-02	3.85	2.12	2.92	1.96
h_8	1.22e-04	4.95e-03	1.07e-03	1.30e-02	3.83	2.11	2.92	1.96

Table 5.17: Time-Dependent Poroelasticity: Neumann Conditions at $k = 1$

h_j	$e^j_{\mathbf{u}}$	$e^j_{\boldsymbol{\sigma}}$	e^j_p	$e^j_{\mathbf{q}}$	$L^j_{\mathbf{u}}$	$L^j_{\boldsymbol{\sigma}}$	L^j_p	$L^j_{\mathbf{q}}$
h_1	1.76e-01	1.61e-01	7.81e-01	4.00e-01				
h_2	3.83e-03	1.87e-02	1.65e-02	4.94e-02	5.52	3.11	5.57	3.02
h_3	5.29e-04	5.57e-03	2.56e-03	1.53e-02	4.88	2.98	4.6	2.89
h_4	1.33e-04	2.32e-03	7.94e-04	6.57e-03	4.8	3.05	4.06	2.93
h_5	4.60e-05	1.17e-03	3.32e-04	3.41e-03	4.76	3.07	3.9	2.94
h_6	1.94e-05	6.67e-04	1.65e-04	1.99e-03	4.73	3.07	3.85	2.95
h_7	9.41e-06	4.16e-04	9.10e-05	1.26e-03	4.69	3.07	3.84	2.94

Table 5.18: Time-Dependent Poroelasticity: Neumann Conditions at $k = 2$

h_j	$e^j_{\mathbf{u}}$	$e^j_{\boldsymbol{\sigma}}$	e^j_p	$e^j_{\mathbf{q}}$	$L^j_{\mathbf{u}}$	$L^j_{\boldsymbol{\sigma}}$	L^j_p	$L^j_{\mathbf{q}}$
h_1	6.42e-02	6.54e-02	2.95e-01	1.66e-01				
h_2	9.35e-04	3.88e-03	3.27e-03	1.08e-02	6.1	4.07	6.5	3.94
h_3	1.03e-04	7.85e-04	3.34e-04	2.23e-03	5.45	3.94	5.62	3.89
h_4	2.22e-05	2.48e-04	7.63e-05	7.20e-04	5.32	4.0	5.14	3.94
h_5	6.97e-06	1.01e-04	2.52e-05	2.98e-04	5.2	4.02	4.96	3.95
h_6	2.77e-06	4.85e-05	1.03e-05	1.45e-04	5.06	4.04	4.91	3.95

Table 5.19: Time-Dependent Poroelasticity: Neumann Conditions at $k = 3$

h_j	$e^j_{\mathbf{u}}$	$e^j_{\boldsymbol{\sigma}}$	e^j_p	$e^j_{\mathbf{q}}$	$L^j_{\mathbf{u}}$	$L^j_{\boldsymbol{\sigma}}$	L^j_p	$L^j_{\mathbf{q}}$
h_1	3.68e-02	2.60e-02	1.36e-01	6.28e-02				
h_2	5.38e-04	7.08e-04	8.77e-04	2.06e-03	6.1	5.2	7.28	4.93
h_3	4.66e-05	9.62e-05	7.22e-05	2.82e-04	6.03	4.92	6.16	4.9
h_4	8.32e-06	2.29e-05	1.28e-05	6.80e-05	5.98	4.98	6.02	4.95
h_5	2.17e-06	7.63e-06	3.01e-06	2.25e-05	6.02	4.93	6.49	4.96

Table 5.20: Time-Dependent Poroelasticity: Neumann Conditions at $k = 4$

h_j	$e_{\mathbf{u}}^j$	$e_{\boldsymbol{\sigma}}^j$	e_p^j	$e_{\mathbf{q}}^j$	$L_{\mathbf{u}}^j$	$L_{\boldsymbol{\sigma}}^j$	L_p^j	$L_{\mathbf{q}}^j$
h_1	4.25e-01	4.42e-01	2.95e+00	1.02e+00				
h_2	2.02e-02	9.62e-02	8.48e-02	1.91e-01	4.39	2.2	5.12	2.42
h_3	4.05e-03	3.94e-02	1.99e-02	8.78e-02	3.97	2.2	3.57	1.92
h_4	1.37e-03	2.14e-02	8.08e-03	5.01e-02	3.78	2.13	3.14	1.95
h_5	5.96e-04	1.33e-02	4.17e-03	3.24e-02	3.72	2.12	2.97	1.95
h_6	3.04e-04	9.04e-03	2.45e-03	2.27e-02	3.69	2.11	2.92	1.95
h_7	1.72e-04	6.53e-03	1.56e-03	1.68e-02	3.68	2.11	2.91	1.96
h_8	1.06e-04	4.93e-03	1.06e-03	1.29e-02	3.67	2.1	2.91	1.96

Table 5.21: Time-Dependent Poroelasticity: Mixed Conditions at $k = 1$

h_j	$e_{\mathbf{u}}^j$	$e_{\boldsymbol{\sigma}}^j$	e_p^j	$e_{\mathbf{q}}^j$	$L_{\mathbf{u}}^j$	$L_{\boldsymbol{\sigma}}^j$	L_p^j	$L_{\mathbf{q}}^j$
h_1	1.43e-01	1.40e-01	5.50e-01	3.27e-01				
h_2	3.52e-03	1.78e-02	1.61e-02	4.91e-02	5.35	2.97	5.1	2.73
h_3	4.83e-04	5.43e-03	2.53e-03	1.52e-02	4.9	2.93	4.56	2.88
h_4	1.19e-04	2.29e-03	7.90e-04	6.56e-03	4.86	3.0	4.05	2.93
h_5	4.09e-05	1.16e-03	3.31e-04	3.40e-03	4.8	3.04	3.89	2.94
h_6	1.72e-05	6.67e-04	1.64e-04	1.99e-03	4.76	3.05	3.85	2.95
h_7	8.29e-06	4.16e-04	9.10e-05	1.26e-03	4.73	3.06	3.83	2.94

Table 5.22: Time-Dependent Poroelasticity: Mixed Conditions at $k = 2$

h_j	$e^j_{\mathbf{u}}$	$e^j_{\boldsymbol{\sigma}}$	e^j_p	$e^j_{\mathbf{q}}$	$L^j_{\mathbf{u}}$	$L^j_{\boldsymbol{\sigma}}$	L^j_p	$L^j_{\mathbf{q}}$
h_1	5.73e-02	6.07e-02	2.79e-01	1.59e-01				
h_2	8.40e-04	4.51e-03	3.23e-03	1.08e-02	6.09	3.75	6.43	3.88
h_3	8.74e-05	8.38e-04	3.32e-04	2.23e-03	5.58	4.15	5.62	3.89
h_4	1.82e-05	2.58e-04	7.57e-05	7.20e-04	5.46	4.1	5.14	3.94
h_5	5.50e-06	1.04e-04	2.51e-05	2.98e-04	5.35	4.08	4.95	3.95
h_6	2.09e-06	4.93e-05	1.03e-05	1.45e-04	5.3	4.08	4.89	3.95

Table 5.23: Time-Dependent Poroelasticity: Mixed Conditions at $k = 3$

h_j	$e^j_{\mathbf{u}}$	$e^j_{\boldsymbol{\sigma}}$	e^j_p	$e^j_{\mathbf{q}}$	$L^j_{\mathbf{u}}$	$L^j_{\boldsymbol{\sigma}}$	L^j_p	$L^j_{\mathbf{q}}$
h_1	2.21e-02	5.27e-02	1.59e-01	8.11e-02				
h_2	4.15e-04	2.31e-03	8.59e-04	2.11e-03	5.74	4.51	7.53	5.26
h_3	3.50e-05	2.13e-04	6.91e-05	2.86e-04	6.1	5.88	6.22	4.94
h_4	6.15e-06	4.08e-05	1.20e-05	6.84e-05	6.04	5.74	6.08	4.97
h_5	1.59e-06	1.16e-05	3.15e-06	2.26e-05	6.06	5.63	6.01	4.97

Table 5.24: Time-Dependent Poroelasticity: Mixed Conditions at $k = 4$

We can again generate a wave by "lifting" one side of the box with a Dirichlet condition on the xz plane at $y = 0$, for example $\mathbf{u}(\mathbf{x}, t)|_{\Gamma_D} = (0, 0, \sin^4 t)$ for $t \in [0, \pi)$ and 0 for $t \in [\pi, 4\pi]$, and the rest $\boldsymbol{\sigma}\mathbf{n} = 0$ on Γ_N. Here $p = 0$ on $\widetilde{\Gamma}_D$ and $\mathbf{q} = \mathbf{0}$ on $\widetilde{\Gamma}_N$. Areas under higher pressure are plotted lighter.

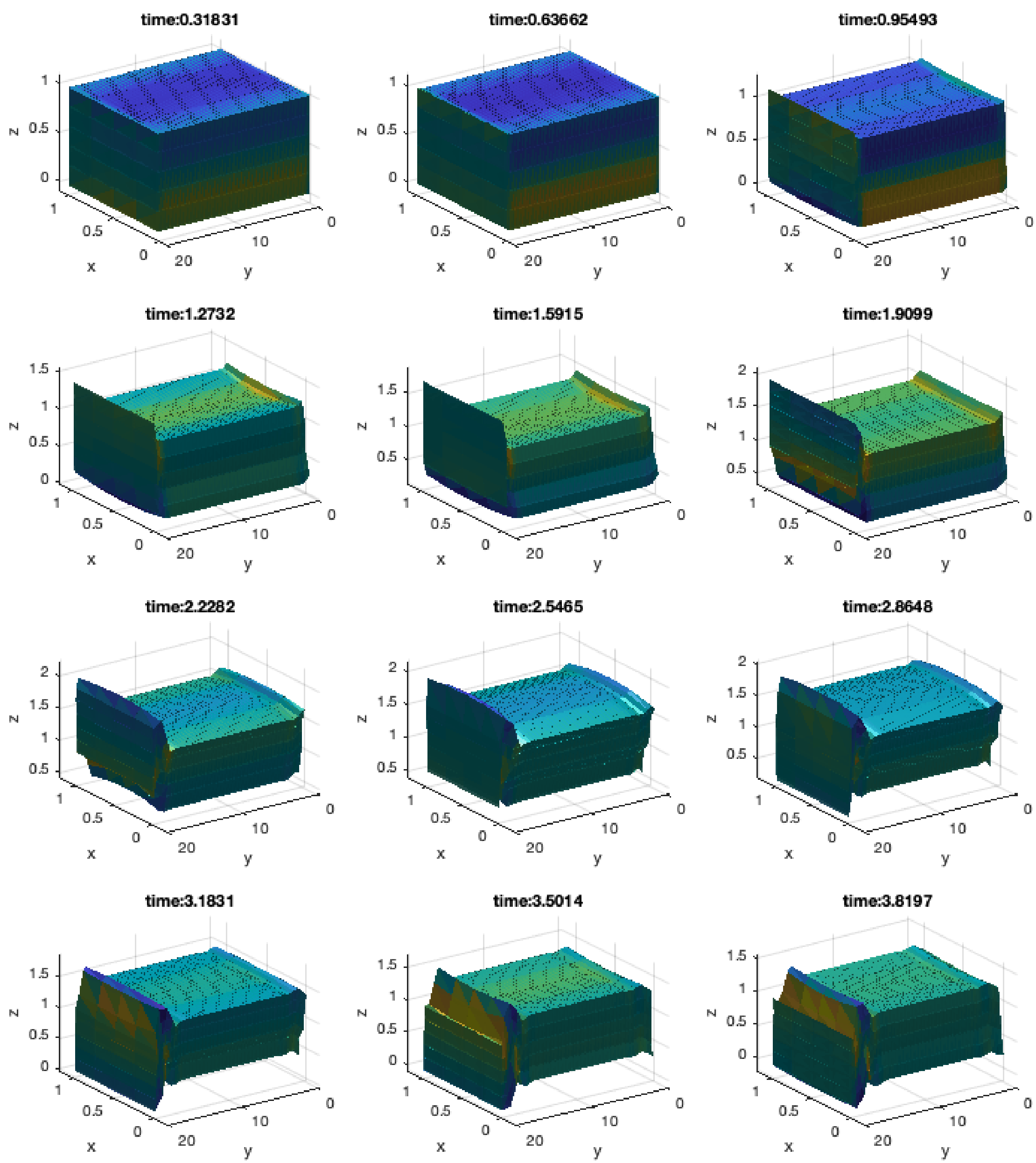

Figure 5.7: Poroelastic wave, part I

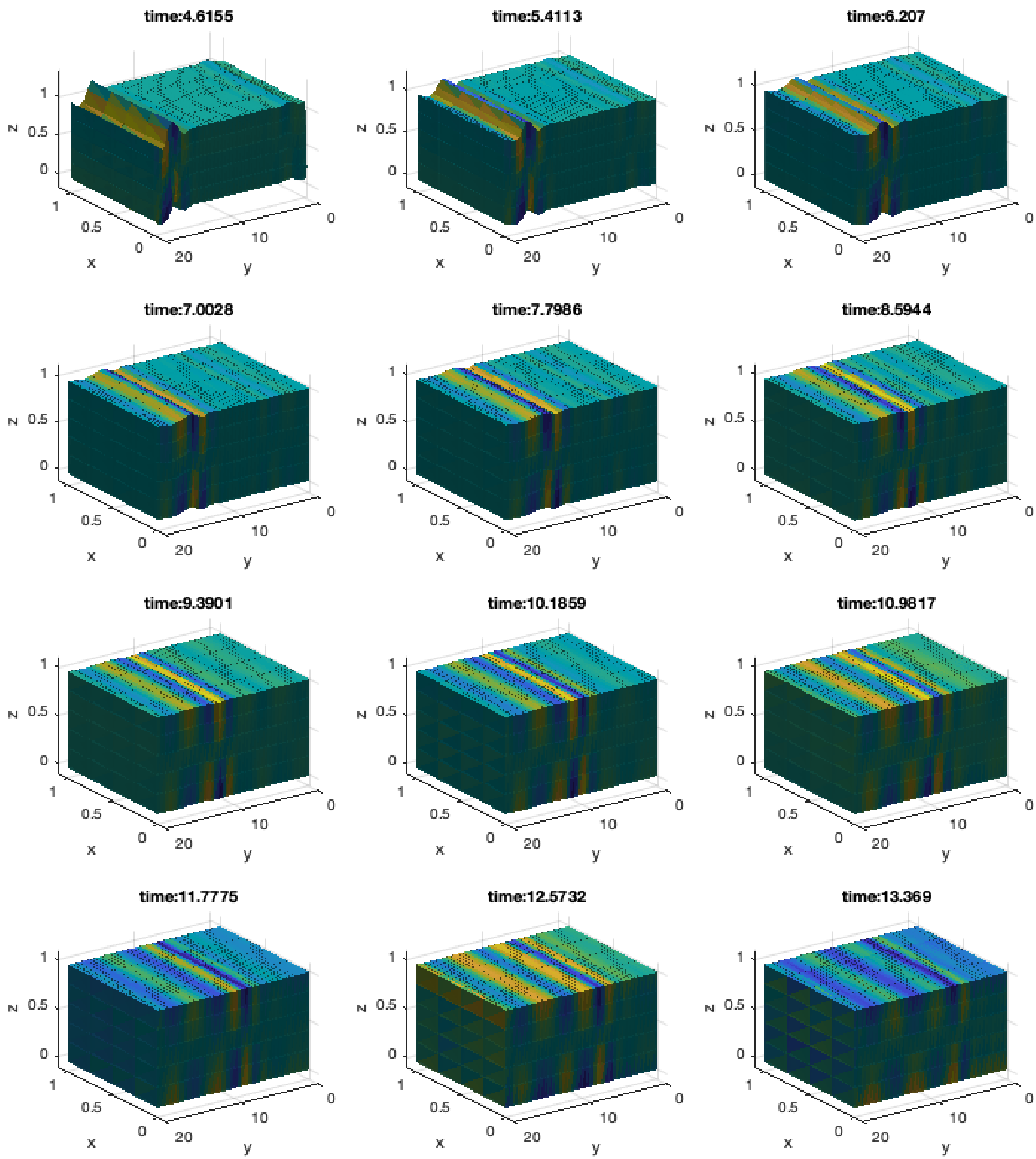

Figure 5.8: Poroelastic wave, part II

The surfaces comprising the head, shoulders, and forearms of this hippo are subject to Dirichlet conditions, namely $\mathbf{u}(x, y, z, t)|_{\Gamma_D} = [0, 0, 0.1 \sin^4 t]$ and $p(x, y, z, t)|_{\Gamma_D} = 0$ for $t \in [0, \pi]$ and 0 elsewhile, while the belly, legs and backside are subject to zero Neumann conditions for all $t \in [0, 4\pi]$. The hippo mesh can be found at [44].

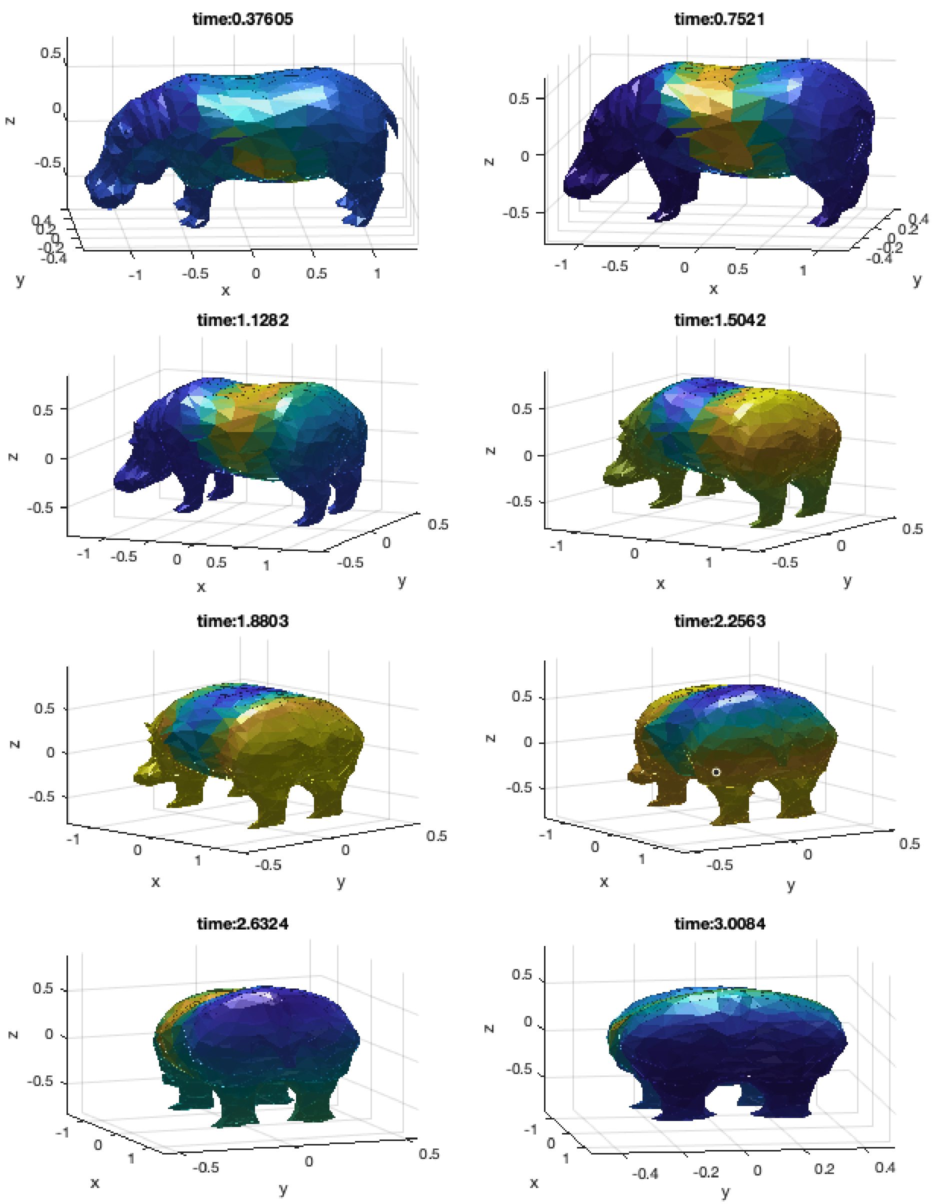

Figure 5.9: Poroelastic hippo, part I

It should be noted that, while higher pressures correspond to lighter colors, we are taking the average of the pressure at the vertices of tetrahedra to mark the colors, hence the pressure on the Dirichlet boundary looks as though it is changing, but this is just the effect of the inner vertex.

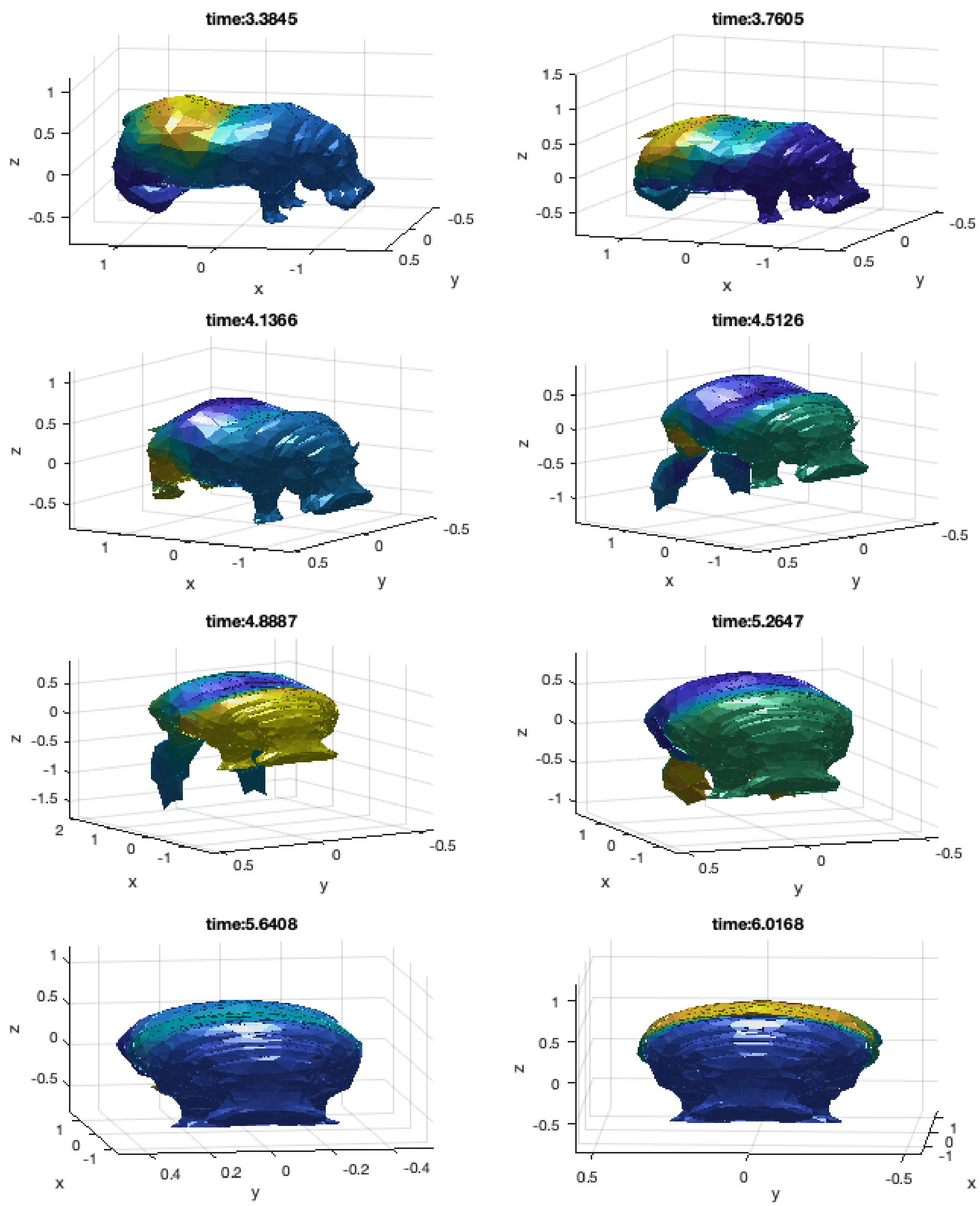

Figure 5.10: Poroelastic hippo, part II

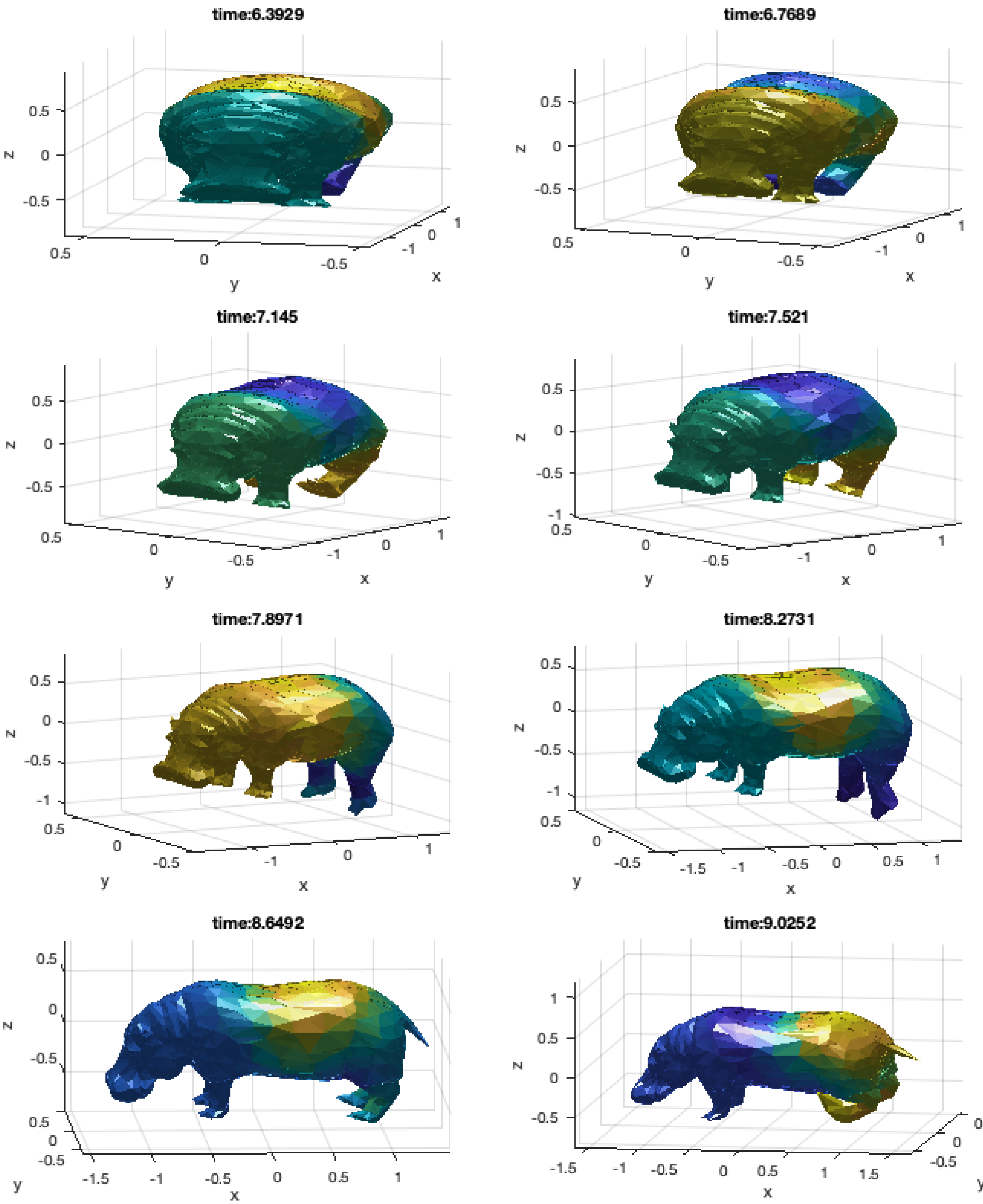

Figure 5.11: Poroelastic hippo, part III

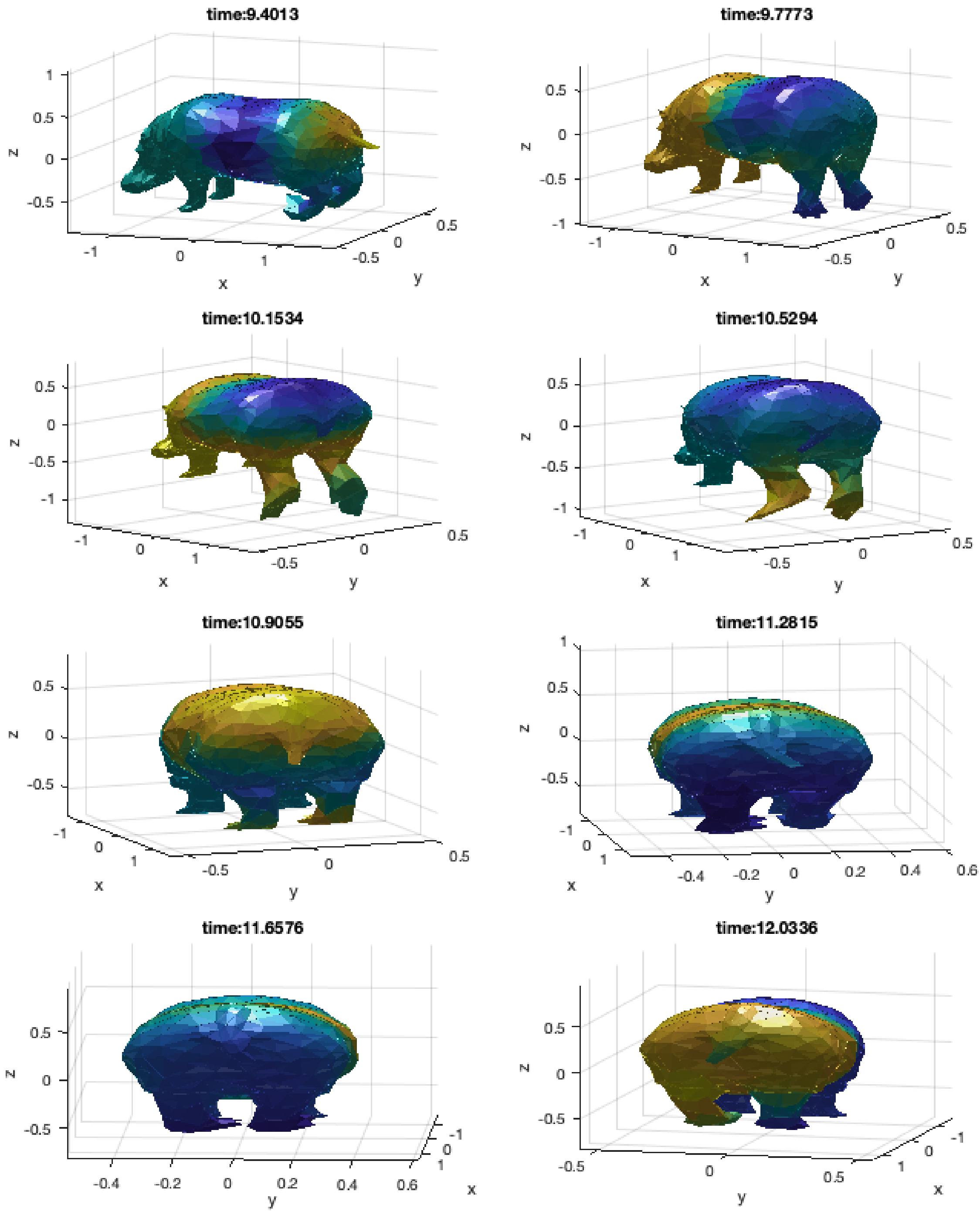

Figure 5.12: Poroelastic hippo, part IV

Chapter 6

CONCLUSIONS

We have reviewed the basics of Sobolev spaces with respect to key quantities involved in linear elasticity. Next we moved on to explain the frequency-domain case, and then the transient case. We then gave an introduction to our time-discretization method, convolution quadrature, developed by Christian Lubich [34], analyzed by Banjai and Sauter [3], and implemented in MATLAB by Hassell and Sayas [25]. The third chapter consisted of a breakdown of the HDG+ discretization for the frequency domain case and a fully rigorous analysis of the convergence of the HDG+ solution to the weak solution of the (frequency domain) elastic system. We proved that for h small enough on a shape-regular polyhedral mesh Ω, and full regularity of the exact solution, that the displacement error converges at $\mathcal{O}(h^{k+2})$ and that the error in the stress converges at $\mathcal{O}(h^{k+1})$, where h is identified with the maximum length of an edge of our tetrahedrization $\mathcal{T}_h$ and k is the polynomial degree used in the approximation.

The fourth chapter was about HDG+ for transient elasticity. The theory has been developed by Shukai Du who uses a new HDG+ projection that simplifies the static and time-harmonic analysis and makes the transient analysis quite doable–look to his coming papers for this. This left us to simply making sure that the method we used is conservative, and then performing some numerical experiments to show it is optimally convergent. We then mentioned extended HDG+ and the pros and cons of using it, namely that it is optimally convergent in displacement, stress, and strain but uses quite a bit of memory in its implementation. Fifth was HDG+ for poro/thermoelasticity. This chapter contained a short history of work on the problem, a brief analysis of the diffusive nature of the problem and of the HDG formulation, and numerical experiments to verify our convergence rates.

The projection-based analysis of HDG+ for both time-harmonic and transient Maxwell's equations and HDG+ for anisotropic and nonlinear elasticity as well remain open problems.

In closing, I would like to sincerely thank Hasan Eruslu for the reviews of convolution quadrature, and also thank Shukai Du for his support and his many insights into the nature of convergence of numerical methods, as well as Hugo Diaz-Norambuena for finding the hippo meshes. I would in particular like to thank Dr. Francisco-Javier Sayas, for both his long mentorship and his keen wit throughout the years of this Ph.D. program at the University of Delaware.

BIBLIOGRAPHY

[1] Robert Adams and John Fournier. *Sobolev Spaces*, volume 140. Elsevier, 2nd edition, June 2003.

[2] M.V. Vasilyeve A.E. Kolesov, P.N. Vabishchevich. Splitting schemes for poroelasticity and thermoelasticity problems. *Computers and Mathematics with Applications*, 67(12):2185–2198, July 2014.

[3] L. Banjai and S. Sauter. Rapid solution of the wave equation in unbounded domains. *SIAM J. Numer. Anal.*, 47(1):227–249, 2008/2009.

[4] Lorenz Berger. *A low-order finite element method for poroelasticity with applications to lung modeling*. PhD thesis, Keble College, University of Oxford, Trinity Term 2015.

[5] Lorenz Berger, Rafel Bordas, David Kay, and Simon Tavener. A stabilized finite element method for finite-strain three-field poroelasticity. *Computational Mechanics*, 60(1):51–68, July 2017.

[6] M. A. Biot. Theory of propagation of elastic waves in a fluid-saturated porous solid, part i: lower frequency range and part ii: higher frequency range. *Journal of the Acoustical Society of America*, 28:168–178 and 179–191, 1956.

[7] Maurice Biot. General theory of three-dimensional consolidation. *Journal of Applied Physics*, 12:155–164, 1941.

[8] Bernardo Cockburn, Jay Gopalakrishnan, and Johnny Guzmán. A new elasticity element made for enforcing weak stress symmetry. *Math. Comp.*, 79:1331–1349, 2010.

[9] Bernardo Cockburn, Jay Gopalakrishnan, and Raytcho Lazarov. Unified hybridization of discontinuous Galerkin, mixed, and continuous Galerkin methods for second order elliptic problem. *J. Num. Anal.*, 47(2):1319–1365, 2009.

[10] Bernardo Cockburn, Robert M. Kirby, and Spencer J. Sherwin. To CG or to HDG: A comparative study. *J. Sci. Comput.*, 51:183–212, 2010.

[11] Bernardo Cockburn and Vincent Quenneville-Bélair. Uniform-in-time superconvergence of the HDG methods for the acoustic wave equation. *Math. Comp.*, 83(285):65–85, 2014.

[12] Bernardo Cockburn and Ke Shi. Superconvergent HDG methods for linear elasticity with weakly symmetric stresses. *IMA J. Numer. Anal.*, 33:747–770, 2013.

[13] Bernardo Cockburn, S.-C. Soon, and Henryk K. Stolarski. A hybridizable discontinuous Galerkin method for linear elasticity. *Int. J. Numer. Meth. Engng.*, 80:1058–1092, 2009.

[14] Gary Cohen. *Higher-Order Numerical Methods for Transient Wave Equations*. Scientific Computation. Springer-Verlag, 2001.

[15] Josep de la Puente, Michael Dumbser, Martin Käser, and Heiner Igel. Discontinuous Galerkin methods for wave propagation in poroelastic media. *Geophysics*, 73(5):T77–T97, 2008.

[16] Shukai Du and F.-J. Sayas. New analytical tools for HDG in elasticity, with applications to elastodynamics. *In preparation*.

[17] Guosheng Fu, Bernardo Cockburn, and Henryk K. Stolarski. Analysis of an HDG method for linear elasticity. *Int. J. Numer. Meth. Engng.*, 102:551–575, 2015.

[18] Zhixing Fu, Luis F. Gatica, and Francisco-Javier Sayas. Algorithm 949: Matlab tools for HDG in three dimensions. *ACM Trans. Math. Softw.*, 41(3):20, 2015.

[19] Zhixing Fu, Norbert Heuer, and Francisco-Javier Sayas. A non-symmetric coupling of boundary elements with the Hybridizable Discontinuous Galerkin method. *Comput. Math. Appl.*, 74:2752–2768, 2017.

[20] F.J. Gaspar, F.J. Lisbona, and P.N. Vabishchevich. A finite difference analysis of Biot's consolidation model. *Applied Numerical Mathematics*, 44:487–506, 2003.

[21] Zhihao Ge and Mengxia Ma. Multiphysics discontinuous galerkin method for a poroelasticity model. *Applied Mathematics and Computation*, 301:78–94, May 2017.

[22] Vivette Girault and Pierre-Arnaud Raviart. *Finite Element Methods for Navier-Stokes*, volume 5 of *Springer Series in Computational Mathematics*. Springer-Verlag Berlin Heidelberg, 1986.

[23] Jay Gopalakrishnan, Stéphane Lanteri, Nicole Olivares, and Ronan Perussel. Stabilization in relation to wavenumber in HDG methods. *Adv. Model. and Simul. in Eng. Sci.*, page 2:13, 2015.

[24] Roland Griesmaier and Peter Monk. Error analysis for a hybridizable discontinuous Galerkin method for the Helmholtz equation. *J. Sci. Comp.*, 49:291–310, 2011.

[25] Matt Hassell and F.-J. Sayas. Convolution quadrature for wave simulations. *Numerical Simulation in Physics and Engineering*, (10.1007/978-3-319-32146-2), 2016.

[26] Allan Hungria, Daniele Prada, and F.-J. Sayas. HDG methods for elastodynamics. *Computers and Mathematics with Applications*, 74(11):2671–2690, December 2017.

[27] Herminio T. Honorio, Clovis R. Maliska, Massimiliano Ferronato, Carlo Janna. A stabilized element-based finite volume method for poroelastic problems. *J. Comput. Phys.*, 364:49–72, July 2018.

[28] Patrick Joly. Finite element methods with continuous displacement. In N. A. Kampanis, V. A. Dougalis, and J. A. Ekaterinaris, editors, *Effective Computational Methods in Wave Propagation*, chapter 10, pages 267–330. Chapman & Hall/CRC, 2008.

[29] Uwe Köcher and Markus Bause. A mixed discontinuous-continuous Galerkin time discretization for Biot's system. *arXiv:1805.00771v1*, 2018.

[30] Christophe Lehrenfeld and Joachim Schöberl. Hybrid discontinuous Galerkin methods for incompressible flow problems. *Master's Thesis - RWTH Aachen*, May 2010.

[31] Christophe Lehrenfeld and Joachim Schöberl. High order exactly divergence-free hybrid discontinuous Galerkin methods for unsteady incompressible flows. *Int. J. Numer. Meth. Engng.*, 2015.

[32] Grady I. Lemoine, M. Yvonne Ou, and Randall J. LeVeque. High-resolution finite volume modeling of wave propagation in orthotropic poroelastic media. *SIAM J. Sci. Comput.*, 35(1):B176–206, 2013.

[33] P. Lesaint and P.A. Raviart. On a finite element for solving the neutron transport equation. *Academic Press*, pages 89–145, 1974.

[34] C. Lubich. Convolution quadrature and discretized operational calculus i. *Numerische Mathematik*, (52):129–145, 1988.

[35] Christian Lubich. On the multistep time discretization of linear initial-boundary value problems and their boundary integral equations. *Numerische Mathematik*, 67(3):365–389, April 1994.

[36] Yder Masson and Steven Pride. Finite-difference modeling of Biot's poroelastic equations across all frequencies. *Geophysics, Society of Exploration Geophysicists*, 75(2):N33–N41, 2010.

[37] Peter Monk, Joachim Schöberl, and Astrid Sinwel. Hybridizing Raviart-Thomas elements for the Helmholtz equation. *Electromagnetics*, 30:146–176, 2010.

[38] Anna Naumovich. *Efficient numerical methods for the Biot poroelasticity system in multilayered domains.* PhD thesis, Universit at Kaiserslautern, 2007.

[39] N. C. Nguyen, J. Peraire, and B. Cockburn. High-order implicit hybridizable discontinuous Galerkin methods for acoustics and elastodynamics. *Journal of Computational Physics*, 230:748–769, January 2011.

[40] Phillip Joseph Phillips and Mary F. Wheeler. *Finite element methods in linear poroelasticity: theoretical and computational results.* PhD thesis, UT Austin, 2005.

[41] Weifeng Qiu, Jiguang Shen, and Ke Shi. An HDG method for linear elasticity with strong symmetric stresses. *Math. Comp.*, 87:69–93, May 2018.

[42] W.H. Reed and T.R. Hill. Triangular mesh methods for the neutron transport equation. *Tech. Report LA-UR-73-479, Los Alamos Scientific Laboratory*, 1973.

[43] James R. Rice and Michael P. Cleary. Some basic stress diffusion solutions for fluid-saturated elastic porous media with compressible constituents. *Reviews of Geophysics*, 14(2):227–241, May 1976.

[44] Szymon Rusinkiewicz, Doug DeCarlo, Adam Finkelstein, and Anothony Santella. https://gfx.cs.princeton.edu/proj/sugcon/models/, July 2003.

[45] Francisco-Javier Sayas. From Raviart-Thomas to HDG: a personal voyage. *arXiv:1307.2491*, 2013.

[46] Francisco-Javier Sayas, Matt Hassell, George Hsiao, and Constantin Bacuta. Boundary integral solvers for an evolutionary Stokes problem. *SIAM J. Numer. Anal.*, 2015.

[47] M. Stanglmeier, N. C. Nguyen, J. Peraire, and B. Cockburn. An explicit hybridizable discontinuous Galerkin method for the acoustic wave equation. *Computer Methods in Applied Mechanics and Engineering*, 300:748–769, March 2016.

[48] Junichi Takekawa, Raul Madariaga, Hitoshi Mikada, and Tada-nori Goto. Numerical simulation of seismic wave propagation produced by earthquake by using a particle method. *Geophys. J. Int.*, 2012.

[49] Karl Terzaghi. Die berechnung der durchlassigkeitzifer des tones aus dem verlauf der hydrodynamischen spannungserscheinungen. *Mathematish-naturwissenschaftliche, Klasse*, 132:125–138, 1923.

[50] Herbert F. Wang. *Theory of Linear Poroelasticity with Applications to Geomechanics and Hydrogeology.* Princeton University Press, January 2000.

[51] N.F. Dudley Ward, T. Lähivaara, and S. Eveson. A discontinuous Galerkin method for poroelastic wave propagation: The two-dimensional case. *J. Comput. Phys.*, 350:690–727, 2017.

Appendix

PERMISSIONS

Copyright Clearance Center RightsLink®

Home | Account Info | Help | LIVE CHAT

Title: HDG methods for elastodynamics

Author: Allan Hungria,Daniele Prada,Francisco-Javier Sayas

Publication: Computers & Mathematics with Applications

Publisher: Elsevier

Date: 1 December 2017

Logged in as:
Allan Hungria
LOGOUT

Please note that, as the author of this Elsevier article, you retain the right to include it in a thesis or dissertation, provided it is not published commercially. Permission is not required, but please ensure that you reference the journal as the original source. For more information on this and on your other retained rights, please visit: https://www.elsevier.com/about/our-business/policies/copyright#Author-rights

BACK | CLOSE WINDOW